SOLUTION OF ELECTROMAGNETICS PROBLEMS WITH THE EQUIVALENCE PRINCIPLE ALGORITHM

A THESIS

SUBMITTED TO THE DEPARTMENT OF ELECTRICAL AND

ELECTRONICS ENGINEERING

AND THE INSTITUTE OF ENGINEERING AND SCIENCE

OF BILKENT UNIVERSITY

IN PARTIAL FULFILLMENT OF THE REQUIREMENTS

FOR THE DEGREE OF

MASTER OF SCIENCE

By

Burak Tiryaki

September 2010

I certify that I have read this thesis and that in my opinion it is fully adequate, in scope and in quality, as a thesis for the degree of Master of Science.

Prof. Dr. Levent Gürel (Supervisor)

I certify that I have read this thesis and that in my opinion it is fully adequate, in scope and in quality, as a thesis for the degree of Master of Science.

Prof. Dr. Feza Arıkan

I certify that I have read this thesis and that in my opinion it is fully adequate, in scope and in quality, as a thesis for the degree of Master of Science.

Assoc. Prof. Vakur B. Ertürk

Approved for the Institute of Engineering and Sciences:

Prof. Dr. Levent Onural
Director of Institute of Engineering and Science

ABSTRACT

SOLUTION OF ELECTROMAGNETICS PROBLEMS WITH THE EQUIVALENCE PRINCIPLE ALGORITHM

Burak Tiryaki
M.S. in Electrical and Electronics Engineering
Supervisor: Prof. Dr. Levent Gürel
September 2010

A domain decomposition scheme based on the equivalence principle for integral equations is studied. This thesis discusses the application of the equivalence principle algorithm (EPA) in solving electromagnetics scattering problems by multiple three-dimensional perfect electric conductor (PEC) objects of arbitrary shapes. The main advantage of EPA is to improve the condition number of the system matrix. This is very important when the matrix equation is solved iteratively, e.g., with Krylov subspace methods. EPA starts solving electromagnetics problems by separating a large complex structure into basic parts, which may consist of one or more objects with arbitrary shapes. Each one is enclosed by an equivalence surface (ES). Then, the surface equivalence principle operator is used to calculate scattering via equivalent surface, and radiation from one ES to an other can be captured using the translation operators. EPA loses its accuracy if ESs are very close to each other, or if an ES is very close to PEC object. As a remedy of this problem, tangential-EPA (T-EPA) is introduced. Properties of both algorithms are investigated and discussed in detail. Accuracy and the efficiency of the methods are compared to those of the multilevel fast multipole

algorithm.

Keywords: Equivalence principle algorithm, electromagnetic scattering, domain decomposition method, iterative solution, equivalence principle, method of moments (MoM), Huygens' principle.

ÖZET

ELEKTROMANYETİK PROBLEMLERİN EŞDEĞERLİK PRENSİBİ YÖNTEMİYLE ÇÖZÜMLERİ

Burak Tiryaki
Elektrik ve Elektronik Mühendisliği Bölümü Yüksek Lisans
Tez Yöneticisi: Prof. Dr. Levent Gürel
Eylül 2010

Gelişigüzel şekilli üç boyutlu iletken yüzeyleri içeren elektromanyetik saçılım problemlerinin çözümü için eşdeğerlik prensibi algoritması (EPA) yöntemi incelenmiştir. EPA yöntemi ile elde edilen sistem matrisi, momentler metodu ve hızlı çok kutup yöntemleri gibi geleneksel yöntemlerle elde edilen sistem matrisine kısayla çok daha iyi koşullu olmaktadır. Bu da, EPA'nın en büyük avantajlarından birisidir. Bunun önemi, sistem matrisinin Krylov alt uzay yöntemleriyle iteratif olarak çözümünde ortaya çıkmaktadır. EPA elektromanyetik problemlerin çözümüne, büyük ve karmaşık geometrileri küçük ve basit geometrilere ayırarak başlar. Elde edilen yeni alt problemlerin her biri eşdeğer yüzeylerle çevrelenirler. Eşdeğer yüzeylerden meydana gelen saçılım eşdeğerlik prensibi operatörleri kullanılarak, eşdeğer yüzeyler arasındakı etkileşimler ise öteleme operatörleri kullanılarak hesaplanmaktadır. Eşdeğer yüzeyler arasındaki veya eşdeğer yüzeyle metal cisim arasındaki mesafenin çok az olması durumunda EPA ile yapılan çözümün doğruluğu azalmaktadır. Bu soruna çözüm olarak teğetsel EPA (T-EPA) yöntemi kullanılmıştır. Bu tezde, EPA ve T-EPA'nın özellikleri incelenecek ve detaylı bir şekilde tartışılacaktır. Yöntemin doğruluğu ve verimliliği çok seviyeli hızlı çok kutup yöntemiyle karşılaştırılacaktır.

Anahtar kelimeler: Eşdeğerlik prensibi algoritması, elektromanyetik saçılım, iterative çözücüler, eşdeğerlik prensibi, momentler metodu, Huygens prensibi.

ACKNOWLEDGMENTS

I would like to thank my supervisor Prof. Levent Gürel for his supervision, guidance, and suggestions throughout the development of this thesis.

I would to like to thank to Prof. Dr. Feza Arıkan and Assoc. Prof. Vakur B. Ertürk for participating in my thesis committee and for accepting to read and review this thesis.

Also, I would like to thank former and current researchers of the Bilkent University Computational Electromagnetics Research Center (BiLCEM) for their cooperation and accompaniment in my studies.

Last but not least, thanks to Seçil Kılınç for being in my life, for witnessing every moment of this process, and for motivating me all the time.

This work was supported by the Scientific and Technical Research Council of Turkey (TUBITAK) through a M.S. scholarship.

Contents

List of Figures

To My Family...

Aileme...

Chapter 1

Introduction

As a general introduction, this chapter describes the relevance of the work, the connection of the existing work and its potential with respect to future applications. We will provide historical context that describes the underlying techniques. Then, we will outline the organization of the thesis.

1.1 Historical Context

In this section, we provide historical overview of computational electromagnetics (CEM). Nowadays, CEM plays very important role in the analysis of the electromagnetic (EM) phenomena and design of EM systems. With the aid of modern computer technology and numerical algorithms many practical and real-life problems can be modelled and simulated on computers [1].

Among various computational algorithm, method of moments (MoM) is shown to be one of the most versatile and accurate techniques to solve radiation and scattering problems. Nevertheless, the method has some disadvantages. One of the major disadvantage is its high computational cost for memory and time. Due

to the limited computer capacity, this algorithm usually limited to rather small scale problems [2].

Recently, many researchers focused on developing of efficient fast solvers that basically reduce the computational cost [1]. One of the most successful techniques in this field is fast multipole algorithm (FMA) and its multilevel version multilevel fast multipole algorithm (MLFMA) [3],[4]. These fast solvers are based on iterative solution of matrix equation. Therefore, convergence of an iterative solution is important for the total efficiency of the algorithm. The disadvantage of these fast solvers is convergence of the iterative solvers.

Mainly, if the object has a complicated shape and requires discretization with elements that are very small compared with the wavelength or if the element size varies a lot, convergence of the iterative solvers will be problematic. Feeding structure of the antenna, small antennas mounted on big problems, and metamaterials can be given as examples for these cases. With first two real-life problems, some parts of the mesh are much denser than others, which will deteriorate the conditioning of the matrix system, and hence, cause iterative solvers to converge slowly or not converge at all.

Convergence of the iterative solver can be improved by choosing surface integral equation (SIE) formulation properly. Recently, several SIE formulations leading to well-conditioned matrix equation have been developed [3],[5],[6],[7]. Unfortunately, many of these SIE formulations usually lead to a lower solution accuracy [2].

Another way to improve conditioning of the system matrix is preconditioning [8]-[11]. Although effective preconditioners have been developed in recent years, the efficiency of the preconditioner is still problem. Also, preconditioners are formulation dependent. Furthermore, it is very difficult to find robust and efficient preconditioner for each problem [12].

Among various computational algorithms, the domain decomposition method (DDM) is very attractive in solving problems with high complexity. With the capability of dissociation and isolation of the solution of one region from another, DDM can be used to facilitate the parallelization of the solution, the reuse of the solution, and also to improve the conditioning of the matrix solution. DDM has been popular with the finite element method [13],[14] and finite difference method [15]-[18]. However, DDM is not popular with the integral equation method. This discrepancy comes from the difficulty of implementing DDM with integral equations. In this thesis, we will present a three-dimensional (3-D) equivalence principle algorithm (EPA) based on DDM and equivalence principle.

1.2 Outline of the Thesis

In this thesis, equivalence principle algorithm is investigated. In Chapter 2, some background information, Maxwell's equation, boundary conditions, and Huygens' principle, will be given.

In order to formulate EPA, we will use surface operators. Surface operators and their discretized form are given in Chapter 3 to understand the formulation of EPA. Then, some surface formulations for perfectly electric conductor (PEC), electric-field integral equation (EFIE), magnetic-field integral equation (MFIE), and combined-field integral equation (CFIE) will be given. Also, to discretize the formulations, all necessary tools, MoM and Rao-Wilton-Glisson (RWG) functions will be introduced.

In Chapter 4, we will start with general ideas of EPA. Then using EPA, we will formulate one-object and multi-object scattering problems. At the end of Chapter 4, numerical results will be presented.

In Chapter 5, tangential-EPA (T-EPA) will be introduced and its accuracy will be compared with EPA.

Finally, in Chapter 6, the main conclusions are drawn of the work that is reported in this thesis and recommendations are given for further development of the EPA method.

Chapter 2

Background

In the EPA approach, equivalence principle is used to formulate scattering problems in terms of equivalent source distributions. In this chapter, we present the basic theory by which those integral representation may be formulated. Maxwell's equations, boundary conditions, Huygens' principle and equivalence principle will be discussed.

2.1 Maxwell's Equations

The EM field is governed by Maxwell's equations. Together with the constitutive relations these equations describe the coupled behavior of the electric and magnetic field strengths in space and time.

Faraday's law of induction:

$$\nabla \times \boldsymbol{E}(\boldsymbol{r}, t) = -\frac{\partial \boldsymbol{B}(\boldsymbol{r}, t)}{\partial t} - \boldsymbol{M}(\boldsymbol{r}, t) \tag{2.1}$$

Ampere's circuital law with Maxwell's extension:

$$\nabla \times \boldsymbol{H}(\boldsymbol{r}, t) = \frac{\partial \boldsymbol{D}(\boldsymbol{r}, t)}{\partial t} + \boldsymbol{J}(\boldsymbol{r}, t) \tag{2.2}$$

Gauss's law:

$$\nabla \cdot \boldsymbol{D}(\boldsymbol{r}, t) = \rho_e(\boldsymbol{r}, t) \tag{2.3}$$

Gauss's Law for magnetism:

$$\nabla \cdot \boldsymbol{B}(\boldsymbol{r}, t) = \rho_m(\boldsymbol{r}, t) \tag{2.4}$$

Continuity equation:

$$\nabla \cdot \boldsymbol{J}(\boldsymbol{r}, t) = -\frac{\partial \rho_e(\boldsymbol{r}, t)}{\partial t} \tag{2.5}$$

In the Maxwell's equations, divergence equations are derivable from curl equations for time varying fields and current. Hence, there are actually only two equations with four unknown quantities $\boldsymbol{E}$, $\boldsymbol{H}$, $\boldsymbol{D}$, and $\boldsymbol{B}$, assuming that the driving sources of the system, $\boldsymbol{J}$ and $\boldsymbol{M}$, are known. The constitutive relations, which describe the material media, have to be invoked to render the above equations solvable.

Constitutive relations:

$$\boldsymbol{D}(\boldsymbol{r}, t) = \bar{\boldsymbol{\epsilon}}(\boldsymbol{r}) \cdot \boldsymbol{E}(\boldsymbol{r}, t) \tag{2.6}$$

$$\boldsymbol{B}(\boldsymbol{r}, t) = \bar{\boldsymbol{\mu}}(\boldsymbol{r}) \cdot \boldsymbol{H}(\boldsymbol{r}, t) \tag{2.7}$$

Constitutive relations for isotropic medium:

$$\boldsymbol{D}(\boldsymbol{r}, t) = \epsilon(\boldsymbol{r})\boldsymbol{E}(\boldsymbol{r}, t) \tag{2.8}$$

$$\boldsymbol{B}(\boldsymbol{r}, t) = \mu(\boldsymbol{r})\boldsymbol{H}(\boldsymbol{r}, t) \tag{2.9}$$

Constitutive relations for isotropic and homogeneous medium:

$$\boldsymbol{D}(\boldsymbol{r}, t) = \epsilon\boldsymbol{E}(\boldsymbol{r}, t) \tag{2.10}$$

$$\boldsymbol{B}(\boldsymbol{r}, t) = \mu\boldsymbol{H}(\boldsymbol{r}, t) \tag{2.11}$$

thus reducing the number of unknowns from four to two.

Linearity of Maxwell's equations allow us to use Fourier transform and simplify EM equations.

$$\boldsymbol{F}(\boldsymbol{r},t) = \frac{1}{2\pi}\int_{-\infty}^{\infty} d\omega \boldsymbol{F}(\boldsymbol{r},\omega)e^{-i\omega t} \tag{2.12}$$

Substituting (2.12) into the EM equations for the fields and currents, the equations become independent of time in the Fourier space, but the fields and currents are now functions of frequency and they are complex valued.

$$\nabla \times \boldsymbol{E}(\boldsymbol{r},\omega) = i\omega\mu\boldsymbol{H}(\boldsymbol{r},\omega) - \boldsymbol{M}(\boldsymbol{r},\omega) \tag{2.13}$$

$$\nabla \times \boldsymbol{H}(\boldsymbol{r},\omega) = -i\omega\epsilon\boldsymbol{E}(\boldsymbol{r},\omega) + \boldsymbol{J}(\boldsymbol{r},\omega) \tag{2.14}$$

$$\nabla \cdot \boldsymbol{E}(\boldsymbol{r},\omega) = \frac{1}{\epsilon}\rho_e(\boldsymbol{r},\omega) \tag{2.15}$$

$$\nabla \cdot \boldsymbol{H}(\boldsymbol{r},\omega) = \frac{1}{\mu}\rho_m(\boldsymbol{r},\omega) \tag{2.16}$$

Similarly, the continuity equation for simple medium in phasor notation can be written as

$$\nabla \cdot \boldsymbol{J}(\boldsymbol{r},\omega) = i\omega\rho_e(\boldsymbol{r},\omega) \tag{2.17}$$

2.2 Boundary Conditions

Now, we consider a piecewise smooth stationary interface ∂D, that separates two electromagnetically penetrable regions (region-1 and region-2), as depicted in Figure 2.1, where the normal $\hat{\boldsymbol{n}}$ points into region 1. At this interface, a primary impressed distribution of surface currents, $\boldsymbol{J}_S$ and $\boldsymbol{M}_S$, are taken into account. Boundary conditions are written as

$$\hat{\boldsymbol{n}} \times \Big(\boldsymbol{E}_1(\boldsymbol{r}) - \boldsymbol{E}_2(\boldsymbol{r})\Big) = -\boldsymbol{M}_S(\boldsymbol{r}) \tag{2.18}$$

$$\hat{\boldsymbol{n}} \times \Big(\boldsymbol{H}_1(\boldsymbol{r}) - \boldsymbol{H}_2(\boldsymbol{r})\Big) = \boldsymbol{J}_S(\boldsymbol{r}) \tag{2.19}$$

$$\hat{\boldsymbol{n}} \cdot \Big(\boldsymbol{D}_1(\boldsymbol{r}) - \boldsymbol{D}_2(\boldsymbol{r})\Big) = \rho_e(\boldsymbol{r}) \tag{2.20}$$

$$\hat{\boldsymbol{n}} \cdot \Big(\boldsymbol{B}_1(\boldsymbol{r}) - \boldsymbol{B}_2(\boldsymbol{r})\Big) = -\rho_m(\boldsymbol{r}) \tag{2.21}$$

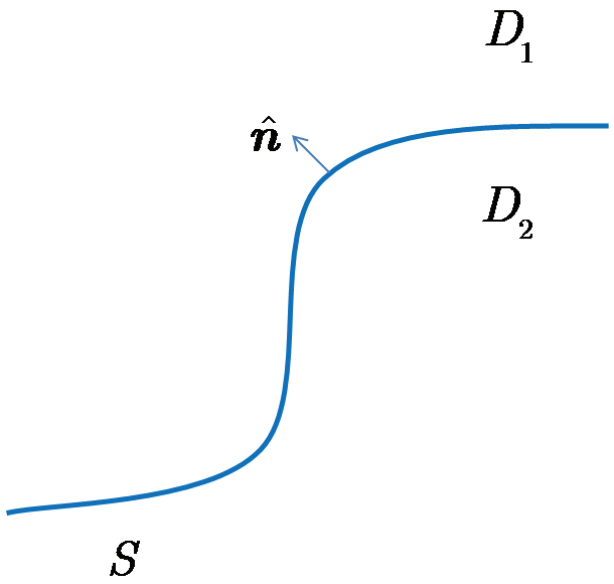

Figure 2.1: Stationary boundary surface ∂D between two adjacent domains.

By simplifying the boundary conditions for a PEC surface, we obtain

$$\hat{\boldsymbol{n}} \times \boldsymbol{E}_1(\boldsymbol{r}) = 0 \tag{2.22}$$

$$\hat{\boldsymbol{n}} \times \boldsymbol{H}_1(\boldsymbol{r}) = \boldsymbol{J}_s(\boldsymbol{r}) \tag{2.23}$$

$$\hat{\boldsymbol{n}} \cdot \boldsymbol{E}_1(\boldsymbol{r}) = \frac{1}{\epsilon}\rho_{es}(\boldsymbol{r}) \tag{2.24}$$

$$\hat{\boldsymbol{n}} \cdot \boldsymbol{H}_1(\boldsymbol{r}) = 0 \tag{2.25}$$

2.3 Surface Equivalence Theorem: Huygens' Principle

In the analysis of EM problems, sometimes it is easier to form an equivalent problem that yields the same solution within a region of interest. The surface equivalence theorem allows us to replace actual sources with equivalent sources. These fictitious sources are equivalent within the region, because they produce same fields as actual sources.

The surface equivalence theorem was introduced in 1963 by Schelkunoff [19], and it is a more rigorous formulation of Huygens' principle [20], which states [21] that "each point on a primary wavefront can be considered to be a new source of a secondary spherical wave and that a secondary wavefront can be constructed as the envelope of these secondary spherical waves."

The surface equivalence theorem is based on the uniqueness theorem, which states [22] that "a field in a lossy region is uniquely specified by the sources within the region plus the tangential components of the electric field over the boundary, or the tangential components of the magnetic field over the boundary, or the former over part of the boundary and the latter over the rest of the boundary." This theorem is also valid for lossless medium. Thus, if the tangential electric and magnetic fields are completely known over a closed surface, the fields in the source-free region can be determined.

Invoking Huygens' principle, the field inside a boundary ∂D that encloses a domain D, may be considered as being generated by an equivalent source distribution on that boundary, thereby separating that domain from its environment in an electromagnetic sense.

The associated equivalence source distribution is not unique. To this end, we introduce two distinct equivalence principles, Love's equivalence principle (LEP) and Schelkunoff's equivalence principle (SEP). LEP is based on both electric and magnetic equivalent currents. On the other hand, SEP use either electric or magnetic currents. In this thesis, we prefer to use LEP.

Before we introduce an equivalent state, we should first define the corresponding original state. An actual radiating source, which is represented by current densities $\boldsymbol{J}_1$ and $\boldsymbol{M}_1$ is as depicted in Figure 2.2. These original sources radiate and create EM fields $\boldsymbol{E}_1$ and $\boldsymbol{H}_1$ everywhere. We want to form an equivalent problem to replace the original problem. So, we choose closed surface $\mathcal{S}$ and we wish the

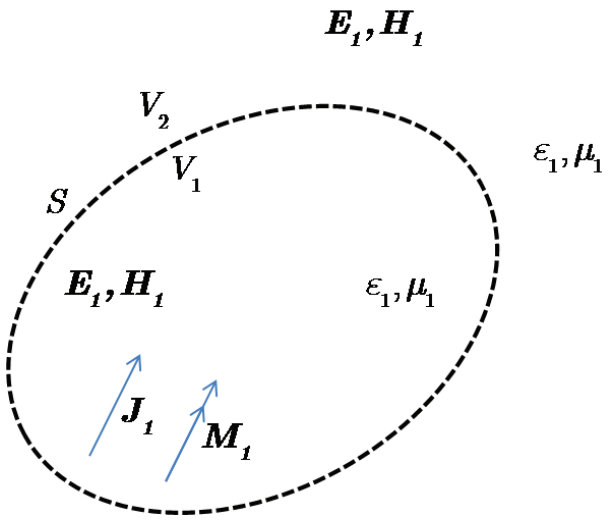

Figure 2.2: Original problem.

same fields outside the closed surface $\mathcal{S}$. The volume within $\mathcal{S}$ is denoted by V_1 and outside of $\mathcal{S}$ is denoted by V_2. An equivalent problem for Figure 2.2 is shown in Figure 2.3. In Figure 2.3, we assume that there exist fields $\boldsymbol{E}$, $\boldsymbol{H}$ inside $\mathcal{S}$, and fields $\boldsymbol{E}_1$, $\boldsymbol{H}_1$ outside of $\mathcal{S}$. For these fields to exist within and outside $\mathcal{S}$, they must satisfy the boundary conditions about the tangential electric and magnetic field components. Thus, on the imaginary surface $\mathcal{S}$, there must exist equivalent sources, such that

$$-\hat{\boldsymbol{n}} \times \Big(\boldsymbol{E}_1(\boldsymbol{r}) - \boldsymbol{E}(\boldsymbol{r})\Big) = \boldsymbol{M}_s(\boldsymbol{r}) \tag{2.26}$$

$$\hat{\boldsymbol{n}} \times \Big(\boldsymbol{H}_1(\boldsymbol{r}) - \boldsymbol{H}(\boldsymbol{r})\Big) = \boldsymbol{J}_s(\boldsymbol{r}) \tag{2.27}$$

These equivalent currents are said to be equivalent within V_2, because they will produce the original fields only outside of $\mathcal{S}$. Up to this point, we have introduced general form of equivalence theorem. We can also specialize our equivalent problem by choosing the fields inside $\mathcal{S}$, appropriately. Fields within $\mathcal{S}$, which is not the region of interest, can be anything. So, by assuming that fields within $\mathcal{S}$

are zero, equivalent currents can be rewritten as

$$-\hat{\boldsymbol{n}} \times \Big(\boldsymbol{E}_1(\boldsymbol{r})\Big) = \boldsymbol{M}_s(\boldsymbol{r}) \tag{2.28}$$

$$\hat{\boldsymbol{n}} \times \Big(\boldsymbol{H}_1(\boldsymbol{r})\Big) = \boldsymbol{J}_s(\boldsymbol{r}). \tag{2.29}$$

From these equations, we see that the equivalent currents do not generate any fields inside V_1, while they generate the correct fields in region V_2.

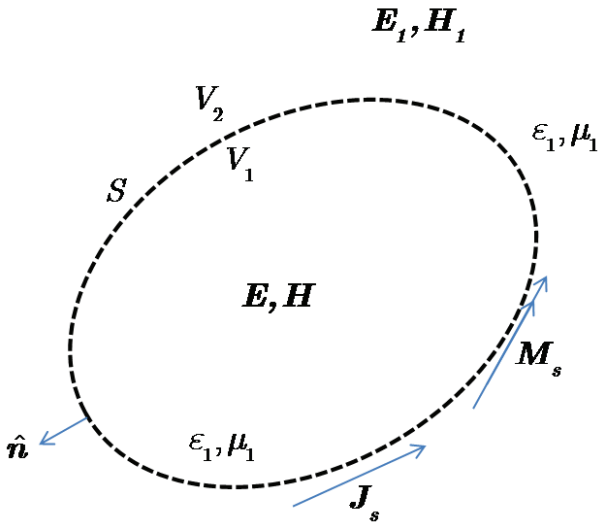

Figure 2.3: Equivalent problem.

Chapter 3

Surface Integral Equations

In this chapter, we introduce the SIEs to solve scattering and radiation problems involving 3-D PEC objects having arbitrarily shaped geometries. The SIE method is a versatile numerical technique for solving Maxwell's equations. Application of the boundary conditions leads to reduction from a 3-D domain onto its boundary.

In this chapter, we define surface operators, and then we derive EFIE, MFIE and CFIE formulations. For the numerical solution of the problems involving the continuous fields and current density, MoM is introduced. This method expands the current density in terms of known basis functions, and tests the integral equation as many times as the number of unknown coefficients. The result of this method is a linear system to be solved by a suitable technique. Finally, we also provide information about geometry modelling and meshing, triangular basis functions, and discretization of the surface operators.

3.1 Surface Operators

For surface formulations of scattering and radiation problems, three different operators are defined as

$$\mathcal{T}\{\boldsymbol{X}\}(\boldsymbol{r}) = ik \int_S d\boldsymbol{r}' \Big[\boldsymbol{X}(\boldsymbol{r}') + \frac{1}{k^2} \nabla' \cdot \boldsymbol{X}(\boldsymbol{r}') \nabla \Big] g(\boldsymbol{r}, \boldsymbol{r}') \tag{3.1}$$

$$\mathcal{K}\{\boldsymbol{X}\}(\boldsymbol{r}) = \int_S d\boldsymbol{r}' \boldsymbol{X}(\boldsymbol{r}') \times \nabla' g(\boldsymbol{r}, \boldsymbol{r}') \tag{3.2}$$

$$\mathcal{I}\{\boldsymbol{X}\}(\boldsymbol{r}) = \boldsymbol{X}(\boldsymbol{r}), \tag{3.3}$$

where $\mathcal{S}$ is the closed surface of a 3-D object with an arbitrary shape. In (3.1)–(3.3), $\boldsymbol{X}$ is either the equivalent electric current ($\boldsymbol{J}$), or the equivalent magnetic current ($\boldsymbol{M}$) on the surface, $k = \omega\sqrt{\mu\epsilon} = 2\pi/\lambda$ is the wavenumber, and $g(\boldsymbol{r}, \boldsymbol{r}')$ denotes the homogeneous-space Green's function defined in phasor notation with the $e^{-i\omega t}$ convention as

$$g(\boldsymbol{r}, \boldsymbol{r}') = \frac{\exp(ikR)}{4\pi R} \qquad \Big(R = |\boldsymbol{r} - \boldsymbol{r}'| \Big), \tag{3.4}$$

where $\boldsymbol{r}$ is observation point, $\boldsymbol{r}'$ is source point. The operator $\mathcal{K}$ is commonly separated into principal and limit values [23] as

$$\mathcal{K}\{\boldsymbol{X}\}(\boldsymbol{r}) = \mathcal{K}_{\mathcal{PV}}\{\boldsymbol{X}\}(\boldsymbol{r}) - \frac{\Omega_i}{4\pi} \mathcal{I}^{\times n}\{\boldsymbol{X}\}(\boldsymbol{r}), \tag{3.5}$$

where $0 \leq \Omega_i \leq 4\pi$ is the internal solid angle, which is nonzero when the observation point $\boldsymbol{r}$ is on the surface. In (3.5), $\mathcal{I}^{\times n}\{\boldsymbol{X}\}(\boldsymbol{r}) = \hat{\boldsymbol{n}} \times \boldsymbol{X}(\boldsymbol{r})$, where $\hat{\boldsymbol{n}}$ is the outward normal unit vector.

Using equivalent surface currents, i.e.,

$$\boldsymbol{J}(\boldsymbol{r}) = \mathcal{I}^{\times n}\{\boldsymbol{H}\}(\boldsymbol{r}) = \hat{\boldsymbol{n}} \times \boldsymbol{H}(\boldsymbol{r}) \tag{3.6}$$

$$\boldsymbol{M}(\boldsymbol{r}) = -\mathcal{I}^{\times n}\{\boldsymbol{E}\}(\boldsymbol{r}) = -\hat{\boldsymbol{n}} \times \boldsymbol{E}(\boldsymbol{r}), \tag{3.7}$$

secondary (scattered or radiated) electric and magnetic fields outside the object can be calculated [24] as

$$\boldsymbol{E}^{sec}(\boldsymbol{r}) = \eta\mathcal{T}\{\boldsymbol{J}\}(\boldsymbol{r}) - \mathcal{K}_{PV}\{\boldsymbol{M}\}(\boldsymbol{r}) + \frac{\Omega_i}{4\pi}\mathcal{I}^{\times n}\{\boldsymbol{M}\}(\boldsymbol{r}) \tag{3.8}$$

$$\boldsymbol{H}^{sec}(\boldsymbol{r}) = \frac{1}{\eta}\mathcal{T}\{\boldsymbol{M}\}(\boldsymbol{r}) + \mathcal{K}_{PV}\{\boldsymbol{J}\}(\boldsymbol{r}) - \frac{\Omega_i}{4\pi}\mathcal{I}^{\times n}\{\boldsymbol{J}\}(\boldsymbol{r}), \tag{3.9}$$

where $\eta = \sqrt{\mu/\epsilon}$ is the wave impedance.

3.2 Electric-Field Integral Equation

Scattering from a PEC object is depicted in Figure 3.1. We assume that $\boldsymbol{J}$ is a current that generates an incident field, $\boldsymbol{E}^{inc}$, that impinges on a PEC object. Then, electric current will be induced on the PEC object, which in turn radiates to generate the scattered field. Applying boundary condition about the

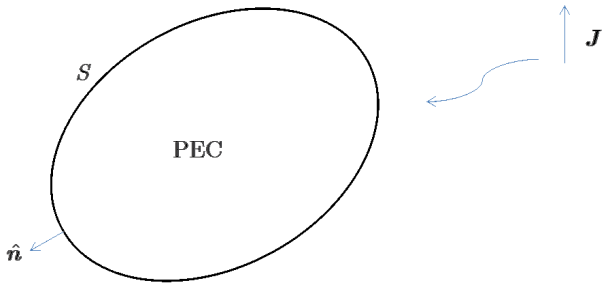

Figure 3.1: Scattering by a PEC object.

tangential component of the electric field on $\mathcal{S}$ we can derive EFIE as

$$\hat{\boldsymbol{t}} \cdot \boldsymbol{E}^{inc}(\boldsymbol{r}) + \hat{\boldsymbol{t}} \cdot \boldsymbol{E}^{sca}(\boldsymbol{r}) = 0, \tag{3.10}$$

where the observation point $\boldsymbol{r}$, is located on the surface $\mathcal{S}$. As we mentioned previously, external source or sources generate an incident field, $\boldsymbol{E}^{inc}$. The scattered electric-field, which is represented by $\boldsymbol{E}^{sca}$ can be written as

$$\boldsymbol{E}^{sca}(\boldsymbol{r}) = i\omega\mu \int_{S'} d\boldsymbol{r}' \bar{\boldsymbol{G}}(\boldsymbol{r}, \boldsymbol{r}') \cdot \boldsymbol{J}(\boldsymbol{r}'), \tag{3.11}$$

where

$$\bar{\boldsymbol{G}}(\boldsymbol{r},\boldsymbol{r}') = \left[\boldsymbol{I} - \frac{\nabla\nabla}{k^2}\right] g(\boldsymbol{r},\boldsymbol{r}'). \tag{3.12}$$

$\bar{\boldsymbol{G}}(\boldsymbol{r},\boldsymbol{r}')$ is the dyadic Green's function and $g(\boldsymbol{r},\boldsymbol{r}')$ is free-space Green's function as given in (3.4). By substituting (3.11) into (3.10), EFIE is formed as

$$\hat{\boldsymbol{t}} \cdot \int_{S'} d\boldsymbol{r}' \bar{\boldsymbol{G}}(\boldsymbol{r},\boldsymbol{r}') \cdot \boldsymbol{J}(\boldsymbol{r}') = \frac{i}{k\eta} \hat{\boldsymbol{t}} \cdot \boldsymbol{E}^{inc}(\boldsymbol{r}). \tag{3.13}$$

With the aid of surface operators, EFIE can be rewritten as

$$\hat{\boldsymbol{t}} \cdot \eta \mathcal{T}\{\boldsymbol{J}(\boldsymbol{r}')\} = -\hat{\boldsymbol{t}} \cdot \boldsymbol{E}^{inc}(\boldsymbol{r}). \tag{3.14}$$

3.3 Magnetic-Field Integral Equation

In order to derive MFIE, we follow a similar procedure with EFIE. This time we apply the boundary condition about the tangential component of the magnetic field on closed surfaces of objects as

$$\hat{\boldsymbol{n}} \times \boldsymbol{H}^{inc}(\boldsymbol{r}) + \hat{\boldsymbol{n}} \times \boldsymbol{H}^{sca}(\boldsymbol{r}) = \boldsymbol{J}(\boldsymbol{r}), \tag{3.15}$$

where the observation point $\boldsymbol{r}$, approaches the surface $\mathcal{S}$ from outside. Similar to EFIE, external source or sources generates incident field $\boldsymbol{H}^{inc}$, and $\boldsymbol{H}^{sca}$ represents the scattered field. The scattered field can be written as

$$\boldsymbol{H}^{sca}(\boldsymbol{r}) = \int_{S'} d\boldsymbol{r}' \boldsymbol{J}(\boldsymbol{r}') \times \nabla' g(\boldsymbol{r},\boldsymbol{r}'). \tag{3.16}$$

Then, (3.15) can be rewritten as

$$\boldsymbol{J}(\boldsymbol{r}) - \hat{\boldsymbol{n}} \times \int_{S'} d\boldsymbol{r}' \boldsymbol{J}(\boldsymbol{r}') \times \nabla' g(\boldsymbol{r},\boldsymbol{r}') = \hat{\boldsymbol{n}} \times \boldsymbol{H}^{inc}(\boldsymbol{r}), \tag{3.17}$$

which is the general expression for the MFIE. Finally, using $\mathcal{K}$ operator and $\mathcal{I}$ operator

$$\mathcal{I}\{\boldsymbol{J}(\boldsymbol{r})\} - \hat{\boldsymbol{n}} \times \mathcal{K}\{\boldsymbol{J}(\boldsymbol{r})\} = \hat{\boldsymbol{n}} \times \boldsymbol{H}^{inc}(\boldsymbol{r}). \tag{3.18}$$

3.4 Combined-Field Integral Equation

Both EFIE and MFIE can be used to solve scattering problems of closed objects. However, both formulations have internal resonance problems at resonance frequencies. Internal resonance problem can be avoided by using CFIE [25]. CFIE formulation is basically a linear combination of EFIE and MFIE [25], and can be written as

$$\text{CFIE} = \alpha\text{EFIE} + (1-\alpha)\text{MFIE}, \tag{3.19}$$

where α may take values between 0 and 1. Combining (3.13) and (3.17) CFIE can be written as

$$\begin{aligned}
&\alpha\left[\hat{\boldsymbol{t}}\cdot\int_{S'} d\boldsymbol{r}'\bar{\boldsymbol{G}}(\boldsymbol{r},\boldsymbol{r}')\cdot\boldsymbol{J}(\boldsymbol{r}')\right] \\
&+\frac{i}{k}(1-\alpha)\left[\boldsymbol{J}(\boldsymbol{r})-\hat{\boldsymbol{n}}\times\int_{S'} d\boldsymbol{r}'\boldsymbol{J}(\boldsymbol{r}')\times\nabla' g(\boldsymbol{r},\boldsymbol{r}')\right] \\
&=\frac{i}{k}\left[\frac{\alpha}{\eta}\hat{\boldsymbol{t}}\cdot\boldsymbol{E}^{inc}(\boldsymbol{r})+(1-\alpha)\hat{\boldsymbol{n}}\times\boldsymbol{H}^{inc}(\boldsymbol{r})\right],
\end{aligned} \tag{3.20}$$

where MFIE part is multiplied by the factor of i/k, in order to balance the equation before linear combination [29].

3.5 Method of Moments

Integral equations introduced in the previous sections can be represented in general as

$$\mathcal{L}\{\boldsymbol{f}(x)\} = \boldsymbol{g}(x), \tag{3.21}$$

where $\mathcal{L}$ is a linear operator, $\boldsymbol{g}(x)$ is known, and $\boldsymbol{f}(x)$ is to be determined. Also, $\boldsymbol{f}(x)$ and $\boldsymbol{g}(x)$ stands for the current distribution and excitation, respectively. Let $\boldsymbol{f}(x)$ be expanded in a series of functions $\boldsymbol{b_1}$, $\boldsymbol{b_2}$, $\boldsymbol{b_3}$, ... in the domain of $\mathcal{L}$, as

$$\boldsymbol{f} = \sum_{n=1}^{N} a_n \boldsymbol{b}_n, \tag{3.22}$$

where the a_n are constants. We shall call the $\boldsymbol{b}_n$ expansion functions or basis functions [26]. We use basis functions to expand the current distribution, so they should be linearly independent and they have to be chosen appropriately. Substituting (3.22) in (3.21), and using the linearity of $\mathcal{L}$, we have

$$\sum_{n=1}^{N} a_n \mathcal{L}(\boldsymbol{b}_n) = \boldsymbol{g}(x). \tag{3.23}$$

We can define the residual error as

$$\begin{aligned} R(x) &= \mathcal{L}\left\{\sum_{n=1}^{N} a_n \boldsymbol{b}_n(x)\right\} - \boldsymbol{g}(x) \\ &= \left[\sum_{n=1}^{N} a_n \mathcal{L}\{\boldsymbol{b}_n(x)\}\right] - \boldsymbol{g}(x). \end{aligned} \tag{3.24}$$

Then, our aim is to minimize the error in order to solve the problem approximately. Now, we need to define a set of weighting functions, or testing functions, $\boldsymbol{t}_1$, $\boldsymbol{t}_2$, $\boldsymbol{t}_3$, ... in the range of $\mathcal{L}$, and take the inner product of (3.23) with each $\boldsymbol{t}_m$. The result is

$$\sum_{n=1}^{N} a_n \Big\langle \boldsymbol{t}_m(\boldsymbol{r}), \mathcal{L}(\boldsymbol{f}_n) \Big\rangle = \Big\langle\ t_m(\boldsymbol{r}), \boldsymbol{g}(x) \Big\rangle \tag{3.25}$$

m = 1,2,3,.... This set of equations can be written in matrix form as

$$\bar{\boldsymbol{Z}} \cdot \boldsymbol{a} = \boldsymbol{g}. \tag{3.26}$$

$$\bar{\boldsymbol{Z}} = \begin{bmatrix} \Big\langle \boldsymbol{t}_1(\boldsymbol{r}), \mathcal{L}(\boldsymbol{f}_1) \Big\rangle & \Big\langle \boldsymbol{t}_1(\boldsymbol{r}), \mathcal{L}(\boldsymbol{f}_2) \Big\rangle & \dots \\ \Big\langle \boldsymbol{t}_2(\boldsymbol{r}), \mathcal{L}(\boldsymbol{f}_1) \Big\rangle & \Big\langle \boldsymbol{t}_2(\boldsymbol{r}), \mathcal{L}(\boldsymbol{f}_2) \Big\rangle & \dots \\ \dots & \dots & \dots \end{bmatrix} \tag{3.27}$$

$$\boldsymbol{a} = \begin{bmatrix} a_1 \\ a_2 \\ \vdots \end{bmatrix} \qquad \boldsymbol{g} = \begin{bmatrix} \Big\langle \boldsymbol{t}_1(\boldsymbol{r}), \boldsymbol{g} \Big\rangle \\ \Big\langle \boldsymbol{t}_2(\boldsymbol{r}), \boldsymbol{g} \Big\rangle \\ \vdots \end{bmatrix}. \tag{3.28}$$

We can also define an inner product as

$$\Big\langle \boldsymbol{a}(x), \boldsymbol{b}(x) \Big\rangle = \int dx \boldsymbol{a}(x) \cdot \boldsymbol{b}(x). \tag{3.29}$$

So, (3.23) can be tested for $m = 1, \ldots, N$ as

$$\int dx \boldsymbol{t}_m(x) \cdot \sum_{n=1}^{N} a_n \mathcal{L}\{\boldsymbol{b}_n(x)\} = \int dx \boldsymbol{t}_m(x) \cdot \boldsymbol{g}(x). \tag{3.30}$$

In this step, we can interchange the order of summation and integration. Then, the final equation becomes

$$\sum_{n=1}^{N} a_n \int dx \boldsymbol{t}_m(x) \cdot \mathcal{L}\{\boldsymbol{b}_n(x)\} = \int dx \boldsymbol{t}_m(x) \cdot \boldsymbol{g}(x), \tag{3.31}$$

and a linear system can be formed as

$$\sum_{n=1}^{N} a_n Z_{mn} = v_m, \tag{3.32}$$

where the matrix elements are defined as

$$Z_{mn} = \int dx \boldsymbol{t}_m(x) \cdot \mathcal{L}\{\boldsymbol{b}_n(x)\}, \tag{3.33}$$

and the vector elements are

$$v_m = \int dx \boldsymbol{t}_m(x) \cdot \boldsymbol{g}(x). \tag{3.34}$$

$\bar{\boldsymbol{Z}}$ is usually called the impedance matrix, and the vector $\boldsymbol{v}_m$ is called the excitation vector. An element of the $\bar{\boldsymbol{Z}}$ matrix at (m, n) is referred to as the interaction between the m^{th} testing and n^{th} basis functions. The method described above is called MoM [27]. If the matrix $\bar{\boldsymbol{Z}}$ is nonsingular, its inverse exists. The coefficients, $\boldsymbol{a}$, are then given in

$$\boldsymbol{a} = \bar{\boldsymbol{Z}}^{-1} \boldsymbol{v}, \tag{3.35}$$

and the solution for $\boldsymbol{f}$ is given by (3.22). This solution may be exact or approximate, depending upon the choice of the $\boldsymbol{b}_n$ and $\boldsymbol{t}_m$. The particular choice $\boldsymbol{b}_n = \boldsymbol{t}_m$ is known as the Galerkin's method.

3.6 Geometry Modelling and Meshing

Geometries to be solved need to be modelled in the computer environment. After modelling geometries, surfaces of models have to be meshed according to the

type of basis functions to be used. Figure 3.2 shows triangular meshes applied on sphere and cube models. We use triangular elements for meshing, but it is hard to model the geometry with high accuracy. To reduce the error, we have to decrease the size of elements. However, using small-sized elements lead to large number of triangles or number of unknown coefficients, N [28]. However, it becomes difficult to solve the linear system in (3.26) when N gets larger. So, to solve problem by using MoM both efficiently and accurately, the average size of the elements should be about 1/10 of the wavelength [29].

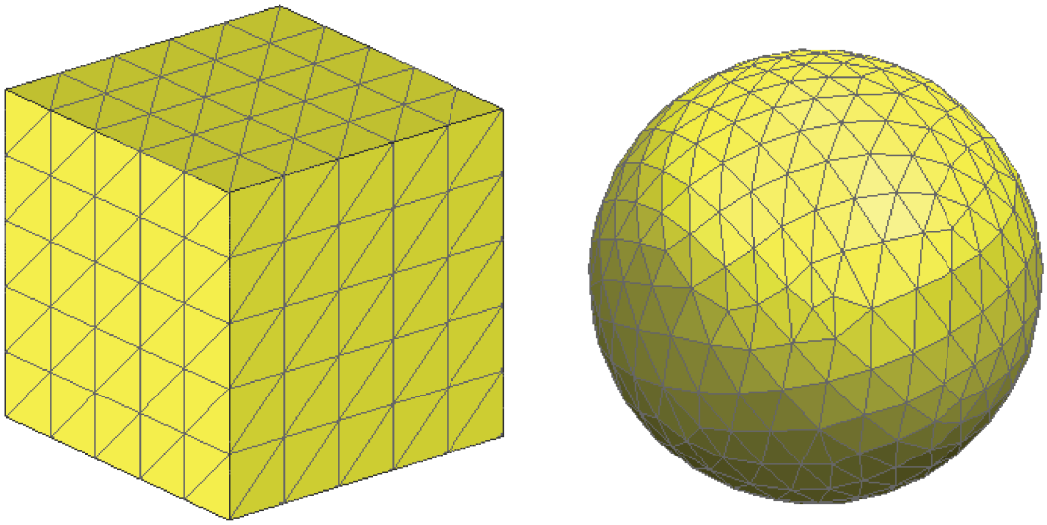

(a) (b)

Figure 3.2: Discretization by using triangular elements: (a) cube and (b) sphere.

3.7 Triangular Basis Functions

In this thesis, we work with RWG [30] functions, which are linearly varying vector functions defined on planar triangular domains. They have been used as basis and testing functions in MoM applications, because they have some useful properties. RWG functions are defined on two triangles having a common edge

of length l_n.

$$\boldsymbol{b}_n(\boldsymbol{r}) = \begin{cases} \dfrac{l_n}{2A_n^+}(\boldsymbol{r} - \boldsymbol{r}_n^+), & \boldsymbol{r} \in S_n^+ \\ \dfrac{l_n}{2A_n^-}(\boldsymbol{r}_n^- - \boldsymbol{r}), & \boldsymbol{r} \in S_n^- \\ 0, & \text{otherwise,} \end{cases} \tag{3.36}$$

where A_n^+ and A_n^- are areas of the first (S_n^+) and the second (S_n^-) triangles associated with the edge, respectively. Spatial distribution of RWG functions are shown in Figure 3.3. So, (3.36) can be rewritten for the function on the n^{th}

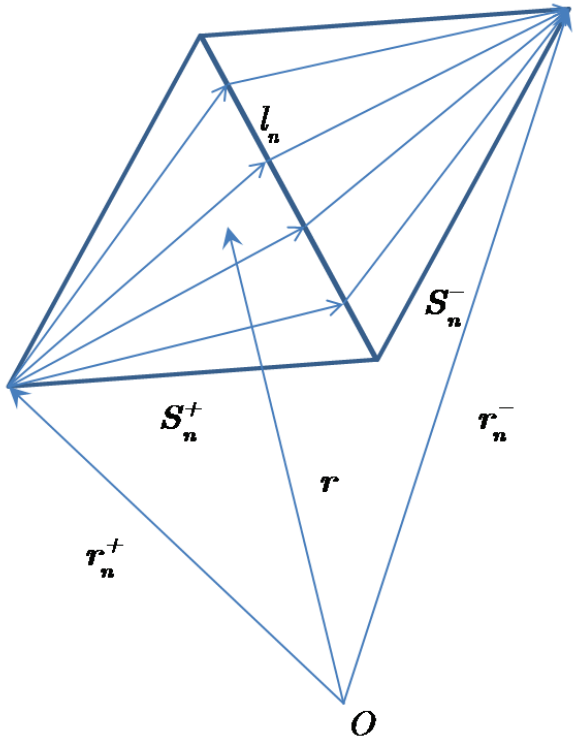

Figure 3.3: Spatial distribution of RWG functions.

triangles as

$$\boldsymbol{b}_{nb}(\boldsymbol{r}) = \pm\frac{l_{nb}}{2A_n}(\boldsymbol{r} - \boldsymbol{r}_{nb})\delta_n(\boldsymbol{r}), \tag{3.37}$$

where $\delta_n(\boldsymbol{r})$ is used to indicate that the value is one if $\boldsymbol{r}$ is inside the triangle, and zero otherwise. The alignment of the function on the triangle is represented by the index $b = 1, 2, 3$. One of the important properties of the RWG functions

is that their divergence is finite everywhere. This comes from the fact that there is no discontinuity in the current flow that is crossing the boundaries of the triangles. In general, divergence of the RWG function can be written as

$$\nabla \cdot \boldsymbol{b}_n(\boldsymbol{r}) = \begin{cases} \dfrac{l_n}{A_n^+}, & \boldsymbol{r} \in S_n^+ \\ \dfrac{l_n}{A_n^-}, & \boldsymbol{r} \in S_n^- \\ 0, & \text{otherwise.} \end{cases} \tag{3.38}$$

The total charge associated with the function becomes

$$A_n^+ \frac{l_n}{A_n^+} - A_n^- \frac{l_n}{A_n^-} = 0. \tag{3.39}$$

Implementing EFIE with MoM requires divergence operation on the current density and also requires the divergence of the testing functions. Therefore, it is suitable to use RWG functions as both the basis and the testing functions.

3.8 Discretization of Surface Operators

For numerical solutions of equivalent electric ($\boldsymbol{J}^{inc}$) and magnetic ($\boldsymbol{M}^{inc}$) currents on the equivalent surface, we discretize surfaces by using small planar triangles and employ basis functions to expand unknown surface current densities, i.e.,

$$\boldsymbol{J}^{inc}(\boldsymbol{r}) = -\hat{\boldsymbol{n}} \times \boldsymbol{H}^{inc}(\boldsymbol{r}) \approx \sum_{n=1}^{N} \boldsymbol{a}_n^J \boldsymbol{b}_n(\boldsymbol{r}) \tag{3.40}$$

$$\boldsymbol{M}^{inc}(\boldsymbol{r}) = \hat{\boldsymbol{n}} \times \boldsymbol{E}^{inc}(\boldsymbol{r}) \approx \sum_{n=1}^{N} \boldsymbol{a}_n^M \boldsymbol{b}_n(\boldsymbol{r}), \tag{3.41}$$

where $\boldsymbol{b}_n$ represents the n^{th} basis function associated with the n^{th} edge. Testing integral equations on the surface, $N \times N$ matrix equations are constructed. Elements of the system matrix correspond to interactions of basis and testing functions, while excitation vector is obtained by testing the incident fields. Matrix elements involve discretized surface operators depending on the formulation. Considering the n^{th} basis function $\boldsymbol{b}_n$ and the m^{th} testing function $\boldsymbol{t}_m$,

tangentially-tested and normally-tested $\mathcal{K}$, $\mathcal{T}$, and $\mathcal{I}$ operators are discretized as

$$\hat{\boldsymbol{t}} \cdot \mathcal{K}_{PV} = \int_{S_m} d\boldsymbol{r} \boldsymbol{t}_m(\boldsymbol{r}) \cdot \mathcal{K}_{PV}\{\boldsymbol{b}_n\}(\boldsymbol{r}) \tag{3.42}$$

$$\hat{\boldsymbol{n}} \times \mathcal{K}_{PV} = \int_{S_m} d\boldsymbol{r} \boldsymbol{t}_m(\boldsymbol{r}) \cdot \hat{\boldsymbol{n}} \times \mathcal{K}_{PV}\{\boldsymbol{b}_n\}(\boldsymbol{r}) \tag{3.43}$$

$$\hat{\boldsymbol{t}} \cdot \mathcal{T} = \int_{S_m} d\boldsymbol{r} \boldsymbol{t}_m(\boldsymbol{r}) \cdot \mathcal{T}\{\boldsymbol{b}_n\}(\boldsymbol{r}) \tag{3.44}$$

$$\hat{\boldsymbol{n}} \times \mathcal{T} = \int_{S_m} d\boldsymbol{r} \boldsymbol{t}_m(\boldsymbol{r}) \cdot \hat{\boldsymbol{n}} \times \mathcal{T}\{\boldsymbol{b}_n\}(\boldsymbol{r}) \tag{3.45}$$

$$\hat{\boldsymbol{t}} \cdot \mathcal{I} = \int_{S_m} d\boldsymbol{r} \boldsymbol{t}_m(\boldsymbol{r}) \cdot \mathcal{I}\{\boldsymbol{b}_n\}(\boldsymbol{r}) \tag{3.46}$$

$$\mathcal{I}^{\times n} = \int_{S_m} d\boldsymbol{r} \boldsymbol{t}_m(\boldsymbol{r}) \cdot \mathcal{I}\{\boldsymbol{b}_n\}(\boldsymbol{r}) \times \hat{\boldsymbol{n}}. \tag{3.47}$$

Elements of excitation vectors in (3.34) also depend on the formulation. They involve tangential and normal testing of incident electric and magnetic fields, i.e.,

$$\boldsymbol{v}_m^{E,T} = \int_{S_m} d\boldsymbol{r} \boldsymbol{t}_m(\boldsymbol{r}) \cdot \boldsymbol{E}^{inc}(\boldsymbol{r}) \tag{3.48}$$

$$\boldsymbol{v}_m^{E,N} = \int_{S_m} d\boldsymbol{r} \boldsymbol{t}_m(\boldsymbol{r}) \cdot \hat{\boldsymbol{n}} \times \boldsymbol{E}^{inc}(\boldsymbol{r}) \tag{3.49}$$

$$\boldsymbol{v}_m^{H,T} = \int_{S_m} d\boldsymbol{r} \boldsymbol{t}_m(\boldsymbol{r}) \cdot \boldsymbol{H}^{inc}(\boldsymbol{r}) \tag{3.50}$$

$$\boldsymbol{v}_m^{H,N} = \int_{S_m} d\boldsymbol{r} \boldsymbol{t}_m(\boldsymbol{r}) \cdot \hat{\boldsymbol{n}} \times \boldsymbol{H}^{inc}(\boldsymbol{r}). \tag{3.51}$$

Interaction between the m^{th} testing function $\boldsymbol{t}_m$, and the n^{th} basis function $\boldsymbol{b}_n$ need to be derived for different operators ($\mathcal{T}$, $\mathcal{K}$, and $\mathcal{I}$) and for different testing types (tangential and normal). We discretize all operators by employing RWG functions. Then, interactions modified and divided into smaller basic integrals. Let's start with tangentially-tested $\mathcal{T}$ operator.

$$\begin{aligned}\bar{\boldsymbol{T}}^T[m,n] = ik \int_{S_m} d\boldsymbol{r} \boldsymbol{t}_m(\boldsymbol{r}) \cdot \int_{S_n} d\boldsymbol{r}' g(\boldsymbol{r},\boldsymbol{r}') \boldsymbol{b}_n(\boldsymbol{r}') \\ + \frac{i}{k} \int_{S_m} d\boldsymbol{r} \boldsymbol{t}_m(\boldsymbol{r}) \cdot \int_{S_n} d\boldsymbol{r}' \nabla g(\boldsymbol{r},\boldsymbol{r}') \nabla' \cdot \boldsymbol{b}_n(\boldsymbol{r}')\end{aligned} \tag{3.52}$$

Using divergence-conforming functions, such as the RWG functions, and using identity (3.53), the interaction in (3.52) is modified as

$$\nabla \cdot (f\boldsymbol{A}) = \boldsymbol{A} \cdot \nabla f + (\nabla \cdot \boldsymbol{A}) f \tag{3.53}$$

$$
\begin{aligned}
\bar{\boldsymbol{T}}^T[m,n] &= ik\int_{S_m} d\boldsymbol{r}\boldsymbol{t}_m(\boldsymbol{r})\cdot\int_{S_n} d\boldsymbol{r}' g(\boldsymbol{r},\boldsymbol{r}')\boldsymbol{b}_n(\boldsymbol{r}') \\
&\quad + \frac{i}{k}\int_{S_m} d\boldsymbol{r}\boldsymbol{t}_m(\boldsymbol{r})\cdot\nabla\int_{S_n} d\boldsymbol{r}' g(\boldsymbol{r},\boldsymbol{r}')\nabla'\cdot\boldsymbol{b}_n(\boldsymbol{r}') \\
&= ik\int_{S_m} d\boldsymbol{r}\boldsymbol{t}_m(\boldsymbol{r})\cdot\int_{S_n} d\boldsymbol{r}' g(\boldsymbol{r},\boldsymbol{r}')\boldsymbol{b}_n(\boldsymbol{r}') \\
&\quad + \frac{i}{k}\int_{S_m} d\boldsymbol{r}\nabla\cdot\left\{\boldsymbol{t}_m(\boldsymbol{r})\int_{S_n} d\boldsymbol{r}' g(\boldsymbol{r},\boldsymbol{r}')\nabla'\cdot\boldsymbol{b}_n(\boldsymbol{r}')\right\} \\
&\quad - \frac{i}{k}\int_{S_m} d\boldsymbol{r}\nabla\cdot\boldsymbol{t}_m(\boldsymbol{r})\int_{S_n} d\boldsymbol{r}' g(\boldsymbol{r},\boldsymbol{r}')\nabla'\cdot\boldsymbol{b}_n(\boldsymbol{r}') \\
&= ik\int_{S_m} d\boldsymbol{r}\boldsymbol{t}_m(\boldsymbol{r})\cdot\int_{S_n} d\boldsymbol{r}' g(\boldsymbol{r},\boldsymbol{r}')\boldsymbol{b}_n(\boldsymbol{r}') \\
&\quad - \frac{i}{k}\int_{S_m} d\boldsymbol{r}\nabla\cdot\boldsymbol{t}_m(\boldsymbol{r})\int_{S_n} d\boldsymbol{r}' g(\boldsymbol{r},\boldsymbol{r}')\nabla'\cdot\boldsymbol{b}_n(\boldsymbol{r}'). \qquad (3.54)
\end{aligned}
$$

In the second term, we move differential operator onto the testing function [30], hence, the hyper-singularity of the $\mathcal{T}$ operator is eliminated. Then, tangentially-tested $\mathcal{T}$ operator expression can be rewritten as,

$$
\begin{aligned}
\bar{\boldsymbol{T}}^T[m,n] &= ik\Bigg[\int_{S_m} d\boldsymbol{r}\boldsymbol{t}_m(\boldsymbol{r})\cdot\int_{S_n} d\boldsymbol{r}' g(\boldsymbol{r},\boldsymbol{r}')\boldsymbol{b}_n(\boldsymbol{r}') \\
&\quad - \frac{1}{k^2}\int_{S_m} d\boldsymbol{r}\nabla\cdot\boldsymbol{t}_m(\boldsymbol{r})\int_{S_n} d\boldsymbol{r}' g(\boldsymbol{r},\boldsymbol{r}')\nabla'\cdot\boldsymbol{b}_n(\boldsymbol{r}')\Bigg]. \qquad (3.55)
\end{aligned}
$$

Inserting the RWG functions and their divergences explicitly by using (3.36) and (3.38),

$$
\begin{aligned}
\bar{\boldsymbol{T}}^T[m,n,a,b] &= ik\Bigg[\frac{l_{ma}}{2A_m}\gamma_{ma}\frac{l_{nb}}{2A_n}\gamma_{nb}\int_{S_m} d\boldsymbol{r}(\boldsymbol{r}-\boldsymbol{r}_{ma})\cdot\int_{S_n} d\boldsymbol{r}' g(\boldsymbol{r},\boldsymbol{r}')(\boldsymbol{r}'-\boldsymbol{r}_{nb}) \\
&\quad - \frac{1}{k^2}\frac{l_{ma}}{A_m}\frac{l_{nb}}{A_n}\gamma_{ma}\gamma_{nb}\int_{S_m} d\boldsymbol{r}\int_{S_n} d\boldsymbol{r}' g(\boldsymbol{r},\boldsymbol{r}')\Bigg], \qquad (3.56)
\end{aligned}
$$

then, by factoring out common terms,

$$
\begin{aligned}
\bar{\boldsymbol{T}}^T[m,n,a,b] &= ikC_{ma,nb}\Bigg[\int_{S_m} d\boldsymbol{r}(\boldsymbol{r}-\boldsymbol{r}_{ma})\cdot\int_{S_n} d\boldsymbol{r}' g(\boldsymbol{r},\boldsymbol{r}')(\boldsymbol{r}'-\boldsymbol{r}_{nb}) \\
&\quad - \frac{4}{k^2}\int_{S_m} d\boldsymbol{r}\int_{S_n} d\boldsymbol{r}' g(\boldsymbol{r},\boldsymbol{r}')\Bigg], \qquad (3.57)
\end{aligned}
$$

where n and m indicate the interaction is between n^{th} and m^{th} triangles, while a and b represent the alignment of the basis and testing functions on these triangles. The coefficient $C_{ma,nb}$ can be written as

$$
C_{ma,nb} = \frac{\gamma_{ma}l_{ma}\gamma_{nb}l_{nb}}{4A_mA_n}. \qquad (3.58)
$$

In the evaluation of these integrals, it obvious that the integrands tend to diverge as the observation point approaches the source point, due to the singularity of the Green's function. By using singularity extraction method [31], problematic inner integral can be divided into analytical and numerical parts, each of which can be evaluated without any problem [30],[32],[33]. In order to easily evaluate the analytical integrals appearing in the singularity extraction, we apply a coordinate transformation, so that the basis triangle lies on the x-y plane with one of its edges lying on the x-axis [29]. The first part of (3.57) can be written as,

$$\begin{aligned}\int_{S_m} d\boldsymbol{r}(\boldsymbol{r}-\boldsymbol{r}_{ma})\cdot\int_{S_n} d\boldsymbol{r}' g(\boldsymbol{r},\boldsymbol{r}')(\boldsymbol{r}'-\boldsymbol{r}_{nb}) &= \int_{S_m} d\boldsymbol{r}(x-x_{ma})\int_{S_n} d\boldsymbol{r}' g(\boldsymbol{r},\boldsymbol{r}')(x'-x_{nb}) \\ &+ \int_{S_m} d\boldsymbol{r}(y-y_{ma})\int_{S_n} d\boldsymbol{r}' g(\boldsymbol{r},\boldsymbol{r}')(y'-y_{nb}) \\ &+ \int_{S_m} d\boldsymbol{r}(z-z_{ma})\int_{S_n} d\boldsymbol{r}' g(\boldsymbol{r},\boldsymbol{r}')(z'-z_{nb}).\end{aligned} \tag{3.59}$$

After applying rotation such that,

$$z' \to 0, z_{nb} \to 0 \tag{3.60}$$

(3.59) becomes,

$$\begin{aligned}\int_{S_m} d\boldsymbol{r}(\boldsymbol{r}-\boldsymbol{r}_{ma})\cdot\int_{S_n} d\boldsymbol{r}' g(\boldsymbol{r},\boldsymbol{r}')(\boldsymbol{r}'-\boldsymbol{r}_{nb}) &= \int_{S_m} d\boldsymbol{r}(x-x_{ma})\int_{S_n} d\boldsymbol{r}' g(\boldsymbol{r},\boldsymbol{r}')(x'-x_{nb}) \\ &+ \int_{S_m} d\boldsymbol{r}(y-y_{ma})\int_{S_n} d\boldsymbol{r}' g(\boldsymbol{r},\boldsymbol{r}')(y'-y_{nb}).\end{aligned} \tag{3.61}$$

two scalar equations in (3.61) can be rewritten as follow:

$$\begin{aligned}\int_{S_m} d\boldsymbol{r}(x-x_{ma})\int_{S_n} d\boldsymbol{r}' g(\boldsymbol{r},\boldsymbol{r}')(x'-x_{nb}) &= \int_{S_m} d\boldsymbol{r}x\int_{S_n} d\boldsymbol{r}' g(\boldsymbol{r},\boldsymbol{r}')x' \\ &- x_{nb}\int_{S_m} d\boldsymbol{r}x\int_{S_n} d\boldsymbol{r}' g(\boldsymbol{r},\boldsymbol{r}') \\ &- x_{ma}\int_{S_m} d\boldsymbol{r}\int_{S_n} d\boldsymbol{r}' g(\boldsymbol{r},\boldsymbol{r}')x' \\ &+ x_{nb}x_{ma}\int_{S_m} d\boldsymbol{r}\int_{S_n} d\boldsymbol{r}' g(\boldsymbol{r},\boldsymbol{r}'),\end{aligned} \tag{3.62}$$

$$\int_{S_m} d\boldsymbol{r}(y-y_{ma}) \int_{S_n} d\boldsymbol{r}' g(\boldsymbol{r},\boldsymbol{r}')(y'-y_{nb}) = \int_{S_m} d\boldsymbol{r} y \int_{S_n} d\boldsymbol{r}' g(\boldsymbol{r},\boldsymbol{r}')y' - y_{nb}\int_{S_m} d\boldsymbol{r} y \int_{S_n} d\boldsymbol{r}' g(\boldsymbol{r},\boldsymbol{r}') - y_{ma}\int_{S_m} d\boldsymbol{r} \int_{S_n} d\boldsymbol{r}' g(\boldsymbol{r},\boldsymbol{r}')y' + y_{ma}y_{nb}\int_{S_m} d\boldsymbol{r} \int_{S_n} d\boldsymbol{r}' g(\boldsymbol{r},\boldsymbol{r}'). \quad (3.63)$$

Now, we can define three inner integrals as

$$I_{in1} = \int_{Sn} d\boldsymbol{r}' g(\boldsymbol{r},\boldsymbol{r}'), \quad (3.64)$$

$$I_{in2} = \int_{Sn} d\boldsymbol{r}' x' g(\boldsymbol{r},\boldsymbol{r}'), \quad (3.65)$$

$$I_{in3} = \int_{Sn} d\boldsymbol{r}' y' g(\boldsymbol{r},\boldsymbol{r}'). \quad (3.66)$$

Finally, the tangentially-tested $\mathcal{T}$ operator involves seven basic integrals, i.e.,

$$\bar{\boldsymbol{T}}^T[m,n,a,b] = ikC_{ma,nb}\Big[(x_{ma}x_{nb}+y_{ma}y_{nb}-\frac{4}{k^2})I_1 + I_2 + I_3 - x_{nb}I_4 - x_{ma}I_5 - y_{nb}I_6 - y_{ma}I_7\Big], \quad (3.67)$$

where

$$\begin{aligned} I_1 &= \int_{Sm} d\boldsymbol{r}' I_{in1}, & I_5 &= \int_{Sm} d\boldsymbol{r}' I_{in2}, \\ I_2 &= \int_{Sm} d\boldsymbol{r}' x I_{in2}, & I_6 &= \int_{Sm} d\boldsymbol{r}' y I_{in1}, \\ I_3 &= \int_{Sm} d\boldsymbol{r}' y I_{in3}, & I_7 &= \int_{Sm} d\boldsymbol{r}' I_{in3}. \\ I_4 &= \int_{Sm} d\boldsymbol{r}' x I_{in1}, \end{aligned} \quad (3.68)$$

After testing $\mathcal{T}$ operator tangentially, we divide whole interaction into basic integrals, so that we can apply similar procedures, for $\mathcal{K}$ operator. Substituting (3.36) and (3.38), into (3.42),

$$\bar{\boldsymbol{K}}^T[m,n,a,b] = \frac{\gamma_{ma}\gamma_{nb}}{4A_mA_n}\int_{S_m} d\boldsymbol{r}(\boldsymbol{r}-\boldsymbol{r}_{ma}) \cdot \int_{S_n} d\boldsymbol{r}'(\boldsymbol{r}'-\boldsymbol{r}_{nb}) \times \nabla' g(\boldsymbol{r},\boldsymbol{r}'). \quad (3.69)$$

Then, the gradient of the Green's function can be written explicitly as,

$$\nabla' g(\boldsymbol{r},\boldsymbol{r}') = \frac{e^{ikR}(1-ikR)}{4\pi R^3}(\boldsymbol{r}-\boldsymbol{r}'). \quad (3.70)$$

Using (3.70) and (3.69) becomes,

$$\bar{\boldsymbol{K}}^T[m,n,a,b] = \frac{\gamma_{ma}\gamma_{nb}}{4A_mA_n}\int_{S_m} d\boldsymbol{r}(\boldsymbol{r}-\boldsymbol{r}_{ma})\cdot\int_{S_n} d\boldsymbol{r}'(\boldsymbol{r}'-\boldsymbol{r}_{nb}) \times\frac{e^{ikR}(1-ikR)}{4\pi R^3}(\boldsymbol{r}-\boldsymbol{r}'), \tag{3.71}$$

$$\bar{\boldsymbol{K}}^T[m,n,a,b] = \frac{\gamma_{ma}\gamma_{nb}}{16\pi A_mA_n}\int_{S_m} d\boldsymbol{r}(\boldsymbol{r}-\boldsymbol{r}_{ma})\cdot\int_{S_n} d\boldsymbol{r}'(\boldsymbol{r}'-\boldsymbol{r}_{nb}) \times(\boldsymbol{r}-\boldsymbol{r}')\frac{e^{ikR}(1-ikR)}{R^3}. \tag{3.72}$$

By using identity showed in (3.73), we obtain the final form of (3.69) as

$$(\boldsymbol{r}'-\boldsymbol{r}_{nb})\times(\boldsymbol{r}-\boldsymbol{r}') = -(\boldsymbol{r}-\boldsymbol{r}_{nb})\times(\boldsymbol{r}'-\boldsymbol{r}), \tag{3.73}$$

$$\bar{\boldsymbol{K}}^T[m,n,a,b] = -\frac{\gamma_{ma}\gamma_{nb}}{16\pi A_mA_n}\int_{S_m} d\boldsymbol{r}(\boldsymbol{r}-\boldsymbol{r}_{ma})\cdot(\boldsymbol{r}-\boldsymbol{r}_{nb}) \times\int_{S_n} d\boldsymbol{r}'(\boldsymbol{r}'-\boldsymbol{r})\frac{e^{ikR}(1-ikR)}{R^3}. \tag{3.74}$$

Next, (3.74) is decomposed into three scalar equations as follows:

$$\begin{aligned}\int_{S_n} d\boldsymbol{r}'(\boldsymbol{r}'-\boldsymbol{r})\frac{e^{ikR}(1-ikR)}{R^3} &= \hat{\boldsymbol{x}}\int_{S_n} d\boldsymbol{r}'(x'-x)\frac{e^{ikR}(1-ikR)}{R^3} \\ &+ \hat{\boldsymbol{y}}\int_{S_n} d\boldsymbol{r}'(y'-y)\frac{e^{ikR}(1-ikR)}{R^3} \\ &+ \hat{\boldsymbol{z}}\int_{S_n} d\boldsymbol{r}'(z'-z)\frac{e^{ikR}(1-ikR)}{R^3}.\end{aligned} \tag{3.75}$$

Similarly, for $\mathcal{K}$ operator, applying rotation such that,

$$z' \to 0 \tag{3.76}$$

(3.75) becomes;

$$\begin{aligned}\int_{S_n} d\boldsymbol{r}'(\boldsymbol{r}'-\boldsymbol{r})\frac{e^{ikR}(1-ikR)}{R^3} &= \hat{\boldsymbol{x}}\int_{S_n} d\boldsymbol{r}'(x'-x)\frac{e^{ikR}(1-ikR)}{R^3} \\ &+ \hat{\boldsymbol{y}}\int_{S_n} d\boldsymbol{r}'(y'-y)\frac{e^{ikR}(1-ikR)}{R^3} \\ &- \hat{\boldsymbol{z}}\int_{S_n} d\boldsymbol{r}' z\frac{e^{ikR}(1-ikR)}{R^3}.\end{aligned} \tag{3.77}$$

Defining three inner integrals as

$$I_{in1} = \int_{Sn} d\boldsymbol{r}'(x' - x)\frac{e^{ikR}(1 - ikR)}{R^3}, \tag{3.78}$$

$$I_{in2} = \int_{Sn} d\boldsymbol{r}'(y' - y)\frac{e^{ikR}(1 - ikR)}{R^3}, \tag{3.79}$$

$$I_{in3} = \int_{Sn} d\boldsymbol{r}' z\frac{e^{ikR}(1 - ikR)}{R^3}, \tag{3.80}$$

and taking curl operation with some modifications we obtain

$$\begin{aligned}(\boldsymbol{r} - \boldsymbol{r}_{nb}) \times (\hat{\boldsymbol{x}}I_{in1} + \hat{\boldsymbol{y}}I_{in2} + \hat{\boldsymbol{z}}I_{in3}) = \hat{\boldsymbol{x}}\Big[&- (y - y_{nb})I_{in3} - zI_{in2})\Big] \\ &+ \hat{\boldsymbol{y}}\Big[(x - x_{nb})I_{in3} + zI_{in1})\Big] \\ &+ \hat{\boldsymbol{z}}\Big[(x - x_{nb})I_{in2} - (y - y_{nb})I_{in1})\Big],\end{aligned} \tag{3.81}$$

$$\begin{aligned}\bar{\boldsymbol{K}}^T[m, n, a, b] = -\frac{\gamma_{ma}\gamma_{nb}}{16\pi A_m A_n}\int_{S_m} d\boldsymbol{r}(x - x_{ma})\Big[&- (y - y_{nb})I_{in3} - zI_{in2})\Big] \\ &+ (y - y_{ma})\Big[(x - x_{nb})I_{in3} + zI_{in1})\Big] \\ &+ (z - z_{ma})\Big[(x - x_{nb})I_{in2} - (y - y_{nb})I_{in1})\Big].\end{aligned} \tag{3.82}$$

Finally, we end-up with the following equation

$$\begin{aligned}\bar{\boldsymbol{K}}^T[m, n, a, b] = -\frac{\gamma_{ma}\gamma_{nb}}{16\pi A_m A_n}\int_{S_m} d\boldsymbol{r}\Big[&- xyI_{in3} + xy_{nb}I_{in3} - xzI_{in2} + yx_{ma}I_{in3} \\ &- y_{nb}x_{ma}I_{in3} + zx_{ma}I_{in3} + yzI_{in1} + xyI_{in3} - yx_{nb}I_{in3} - zy_{ma}I_{in1} \\ &- xy_{ma}I_{in1} + y_{ma}x_{nb}I_{in3} + zxI_{in2} - zx_{nb}I_{in2} - xz_{ma}I_{in2} + z_{ma}x_{nb}I_{in2} \\ &- yzI_{in1} + zx_{nb}I_{in1}\Big].\end{aligned} \tag{3.83}$$

As a result, tangentially-tested $\mathcal{K}$ operator involves nine basic integrals, i.e.,

$$\begin{aligned}\bar{\boldsymbol{K}}^T[m, n, a, b] = -\frac{\gamma_{ma}\gamma_{nb}}{16\pi A_m A_n}\Big[&(y_{nb} - y_{ma})I_1 + z_{ma}I_2 - z_{ma}y_{nb}I_3 + (x_{ma} - x_{nb})I_4 \\ &- z_{ma}I_5 + z_{ma}x_{nb}I_6 + (y_{nb} - y_{ma})I_7 + (x_{ma} - x_{nb})I_8 \\ &+ (y_{ma}x_{nb} - x_{ma}y_{nb})I_9\Big],\end{aligned} \tag{3.84}$$

where

$$I_1 = \int_{Sm} d\boldsymbol{r}' z I_{in1}, \qquad I_4 = \int_{Sm} d\boldsymbol{r}' z I_{in2}, \qquad I_7 = \int_{Sm} d\boldsymbol{r}' x I_{in3},$$
$$I_2 = \int_{Sm} d\boldsymbol{r}' y I_{in1}, \qquad I_5 = \int_{Sm} d\boldsymbol{r}' x I_{in2}, \qquad I_8 = \int_{Sm} d\boldsymbol{r}' y I_{in3},$$
$$I_3 = \int_{Sm} d\boldsymbol{r}' I_{in1}, \qquad I_6 = \int_{Sm} d\boldsymbol{r}' I_{in2}, \qquad I_9 = \int_{Sm} d\boldsymbol{r}' I_{in3}. \tag{3.85}$$

The next operator is normally-tested $\mathcal{T}$ operator, which can be written as,

$$\hat{\boldsymbol{n}} \times \mathcal{T} = \int_{S_m} d\boldsymbol{r} \boldsymbol{t}_m(\boldsymbol{r}) \cdot \hat{\boldsymbol{n}} \times \mathcal{T}\{\boldsymbol{b}_n\}(\boldsymbol{r}). \tag{3.86}$$

Substituting (3.1) into (3.86)

$$\bar{\boldsymbol{T}}^N[m,n] = ik \int_{S_m} d\boldsymbol{r} \boldsymbol{t}_m(\boldsymbol{r}) \cdot \hat{\boldsymbol{n}} \times \int_{S_n} d\boldsymbol{r}' g(\boldsymbol{r},\boldsymbol{r}') \boldsymbol{b}_n(\boldsymbol{r}') + \frac{i}{k} \int_{S_m} d\boldsymbol{r} \boldsymbol{t}_m(\boldsymbol{r}) \cdot \hat{\boldsymbol{n}} \times \int_{S_n} d\boldsymbol{r}' \nabla g(\boldsymbol{r},\boldsymbol{r}') \nabla' \cdot \boldsymbol{b}_n(\boldsymbol{r}'). \tag{3.87}$$

Then, using (3.36) and (3.38) we obtain

$$\bar{\boldsymbol{T}}^N[m,n,a,b] = ik \frac{l_{ma}}{2A_m} \gamma_{ma} \frac{l_{nb}}{2A_n} \gamma_{nb} \int_{S_m} d\boldsymbol{r} (\boldsymbol{r} - \boldsymbol{r}_{ma}) \cdot \hat{\boldsymbol{n}} \times \int_{S_n} d\boldsymbol{r}' g(\boldsymbol{r},\boldsymbol{r}') (\boldsymbol{r}' - \boldsymbol{r}_{nb}) + \frac{i}{k} \int_{S_m} d\boldsymbol{r} \frac{l_{ma}}{2A_m} \gamma_{ma} (\boldsymbol{r} - \boldsymbol{r}_{ma}) \cdot \hat{\boldsymbol{n}} \times \int_{S_n} d\boldsymbol{r}' \nabla g(\boldsymbol{r},\boldsymbol{r}') \frac{l_{nb}}{A_n} \gamma_{nb}, \tag{3.88}$$

where

$$C_{ma,nb} = \frac{\gamma_{ma} l_{ma} \gamma_{nb} l_{nb}}{4 A_m A_n}. \tag{3.89}$$

Finally, we obtain,

$$\bar{\boldsymbol{T}}^N[m,n,a,b] = ikC_{ma,nb} \Bigg[\int_{S_m} d\boldsymbol{r} (\boldsymbol{r} - \boldsymbol{r}_{ma}) \cdot \hat{\boldsymbol{n}} \times \int_{S_n} d\boldsymbol{r}' g(\boldsymbol{r},\boldsymbol{r}') (\boldsymbol{r}' - \boldsymbol{r}_{nb}) + \frac{2}{k^2} \int_{S_m} d\boldsymbol{r} (\boldsymbol{r} - \boldsymbol{r}_{ma}) \cdot \hat{\boldsymbol{n}} \times \int_{S_n} d\boldsymbol{r}' \nabla g(\boldsymbol{r},\boldsymbol{r}') \Bigg]. \tag{3.90}$$

Furthermore, gradient of Green's function with respect to unprimed coordinates can be calculated as

$$\nabla g(\boldsymbol{r},\boldsymbol{r}') = \frac{e^{ikR}(1 - ikR)}{4\pi R^3} (\boldsymbol{r}' - \boldsymbol{r}). \tag{3.91}$$

Then, we obtain

$$\bar{\boldsymbol{T}}^N[m,n,a,b] = ikC_{ma,nb}\Bigg[\int_{S_m} d\boldsymbol{r}(\boldsymbol{r}-\boldsymbol{r}_{ma})\cdot\int_{S_n} d\boldsymbol{r}' g(\boldsymbol{r},\boldsymbol{r}')\hat{\boldsymbol{n}}\times(\boldsymbol{r}'-\boldsymbol{r}_{nb}) + \frac{2}{k^2}\int_{S_m} d\boldsymbol{r}(\boldsymbol{r}-\boldsymbol{r}_{ma})\cdot\hat{\boldsymbol{n}}\times\int_{S_n} d\boldsymbol{r}'\frac{e^{ikR}(1-ikR)}{4\pi R^3}(\boldsymbol{r}'-\boldsymbol{r})\Bigg]. \tag{3.92}$$

As we have done previously, we decompose (3.92) into three scalar equations,

$$\begin{aligned}\int_{S_n} d\boldsymbol{r}'(\boldsymbol{r}'-\boldsymbol{r})\frac{e^{ikR}(1-ikR)}{R^3} &= \hat{\boldsymbol{x}}\int_{S_n} d\boldsymbol{r}'(x'-x)\frac{e^{ikR}(1-ikR)}{R^3} \\ &+ \hat{\boldsymbol{y}}\int_{S_n} d\boldsymbol{r}'(y'-y)\frac{e^{ikR}(1-ikR)}{R^3} \\ &+ \hat{\boldsymbol{z}}\int_{S_n} d\boldsymbol{r}'(z'-z)\frac{e^{ikR}(1-ikR)}{R^3}.\end{aligned} \tag{3.93}$$

By applying rotation as

$$z' \to 0 \tag{3.94}$$

we obtain

$$\begin{aligned}\int_{S_n} d\boldsymbol{r}'(\boldsymbol{r}'-\boldsymbol{r})\frac{e^{ikR}(1-ikR)}{R^3} &= \hat{\boldsymbol{x}}\int_{S_m} d\boldsymbol{r}'(x'-x)\frac{e^{ikR}(1-ikR)}{R^3} \\ &+ \hat{\boldsymbol{y}}\int_{S_n} d\boldsymbol{r}'(y'-y)\frac{e^{ikR}(1-ikR)}{R^3} \\ &- \hat{\boldsymbol{z}}\int_{S_n} d\boldsymbol{r}' z\frac{e^{ikR}(1-ikR)}{R^3}.\end{aligned} \tag{3.95}$$

If we define inner integrals as

$$I_{in1} = \int_{Sn} d\boldsymbol{r}'(x'-x)\frac{e^{ikR}(1-ikR)}{R^3} \tag{3.96}$$

$$I_{in2} = \int_{Sn} d\boldsymbol{r}'(y'-y)\frac{e^{ikR}(1-ikR)}{R^3} \tag{3.97}$$

$$I_{in3} = \int_{Sn} d\boldsymbol{r}'\frac{e^{ikR}(1-ikR)}{R^3}, \tag{3.98}$$

$$\bar{\boldsymbol{T}}^N[m,n,a,b] = ikC_{ma,nb}\Bigg[\int_{S_m} d\boldsymbol{r}(\boldsymbol{r}-\boldsymbol{r}_{ma})\cdot\int_{S_n} d\boldsymbol{r}' g(\boldsymbol{r},\boldsymbol{r}')\hat{\boldsymbol{n}}\times(\boldsymbol{r}'-\boldsymbol{r}_{nb}) + \frac{2}{k^2}\int_{S_m} d\boldsymbol{r}(\boldsymbol{r}-\boldsymbol{r}_{ma})\cdot\hat{\boldsymbol{n}}\times(I_{in1}+I_{in2}+I_{in3})\Bigg], \tag{3.99}$$

and if we calculate the curl of second part and apply dot product,

$$\frac{2}{k^2}\int_{S_m} d\boldsymbol{r}(\boldsymbol{r}-\boldsymbol{r}_{ma})\cdot\hat{\boldsymbol{n}}\times(I_{in1}+I_{in2}+I_{in3})$$
$$=\frac{2}{k^2}\int_{S_m} d\boldsymbol{r}\Big[xn_yI_{in3}-xn_zI_{in2}-x_{nb}n_yI_{in3}+x_{nb}n_zI_{in2}+yn_zI_{in1}-yn_xI_{in3}$$
$$-y_{nb}n_zI_{in1}+y_{nb}n_xI_{in3}+zn_xI_{in2}-zn_yI_{in1}-z_{nb}n_xI_{in2}+z_{nb}n_yI_{in1}\Big]. \tag{3.100}$$

We apply similar procedure to the first part of the equation. Due to rotation,

$$z'\to 0, z_{nb}\to 0 \tag{3.101}$$

$$I_{in4}=\int_{Sn} d\boldsymbol{r}'\frac{e^{ikR}}{4\pi R} \tag{3.102}$$
$$I_{in5}=\int_{Sn} d\boldsymbol{r}'x'\frac{e^{ikR}}{4\pi R} \tag{3.103}$$
$$I_{in6}=\int_{Sn} d\boldsymbol{r}'y'\frac{e^{ikR}}{4\pi R}. \tag{3.104}$$

Then, we obtain

$$\int_{S_m} d\boldsymbol{r}(\boldsymbol{r}-\boldsymbol{r}_{ma})\cdot\int_{S_n} d\boldsymbol{r}'g(\boldsymbol{r},\boldsymbol{r}')\hat{\boldsymbol{n}}\times(\boldsymbol{r}'-\boldsymbol{r}_{nb})$$
$$=\int_{S_m} d\boldsymbol{r}\Big[-n_zxI_{in6}+y_{ma}n_zxI_{in4}+x_{nb}n_zI_{in6}-x_{nb}y_{ma}n_zI_{in4}+n_zyI_{in5}$$
$$-x_{ma}n_zyI_{in4}-y_{nb}n_zI_{in5}+y_{nb}x_{ma}n_zI_{in4}+zn_xI_{in6}-zy_{ma}n_xI_{in4}-zI_{in5}n_y$$
$$+zx_{ma}n_yI_{in4}-z_{nb}I_{in6}n_x+z_{nb}y_{ma}n_xI_{in4}+z_{nb}I_{in5}n_y-z_{nb}x_{ma}n_yI_{in4}\Big]. \tag{3.105}$$

By combining the first and second parts of the equation, the normally-tested $\mathcal{T}$ operator involves 19 basic integrals, i.e.,

$$\bar{\boldsymbol{T}}^N[m,n,a,b]=ikC_{ma,nb}\Bigg(\big[(y_{ma}x_{nb}n_z-x_{ma}y_{nb}n_z+z_{ma}y_{nb}n_x-z_{ma}x_{nb}n_y)I_{10}$$
$$+(z_{ma}n_y-y_{ma}n_z)I_{14}+(x_{ma}n_z-z_{ma}n_x)I_{17}+y_{nb}n_zI_{11}+n_zI_5$$
$$-x_{nb}n_zI_4-n_zI_{18}+n_xI_{19}-n_yI_{16}+(x_{nb}n_y-y_{nb}n_x)I_{13}\big]+\frac{2}{k^2}\big[n_yI_8$$
$$-n_zI_5+n_zI_2-n_xI_9+n_xI_6-n_yI_3+(z_{ma}n_y-y_{ma}n_z)I_1$$
$$+(x_{ma}n_z-z_{ma}n_x)I_4+(y_{ma}n_x-x_{ma}n_y)I_7\big]\Bigg), \tag{3.106}$$

where

$$
\begin{aligned}
I_1 &= \int_{Sm} d\boldsymbol{r}' I_{in1}, & I_8 &= \int_{Sm} d\boldsymbol{r}' x I_{in3}, & I_{15} &= \int_{Sm} d\boldsymbol{r}' y I_{in5}, \\
I_2 &= \int_{Sm} d\boldsymbol{r}' y I_{in1}, & I_9 &= \int_{Sm} d\boldsymbol{r}' y I_{in3}, & I_{16} &= \int_{Sm} d\boldsymbol{r}' z I_{in5}, \\
I_3 &= \int_{Sm} d\boldsymbol{r}' z I_{in1}, & I_{10} &= \int_{Sm} d\boldsymbol{r}' I_{in4}, & I_{17} &= \int_{Sm} d\boldsymbol{r}' I_{in6}, \\
I_4 &= \int_{Sm} d\boldsymbol{r}' 1 I_{in2}, & I_{11} &= \int_{Sm} d\boldsymbol{r}' x I_{in4}, & I_{18} &= \int_{Sm} d\boldsymbol{r}' x I_{in6}, \\
I_5 &= \int_{Sm} d\boldsymbol{r}' x I_{in2}, & I_{12} &= \int_{Sm} d\boldsymbol{r}' y I_{in4}, & I_{19} &= \int_{Sm} d\boldsymbol{r}' z I_{in6}. \\
I_6 &= \int_{Sm} d\boldsymbol{r}' z I_{in2}, & I_{13} &= \int_{Sm} d\boldsymbol{r}' z I_{in4}, & & \\
I_7 &= \int_{Sm} d\boldsymbol{r}' I_{in3}, & I_{14} &= \int_{Sm} d\boldsymbol{r}' I_{in5}, & &
\end{aligned} \tag{3.107}
$$

The next operator is normally-tested $\mathcal{K}$ operator defined as

$$
\hat{\boldsymbol{n}} \times \mathcal{K}_{PV} = \int_{S_m} d\boldsymbol{r} \boldsymbol{t}_m(\boldsymbol{r}) \cdot \hat{\boldsymbol{n}} \times \mathcal{K}_{PV}\{\boldsymbol{b}_n\}(\boldsymbol{r}) \tag{3.108}
$$

$$
\bar{\boldsymbol{K}}^N[m,n] = \int_{S_m} d\boldsymbol{r} \boldsymbol{t}_m(\boldsymbol{r}) \cdot \hat{\boldsymbol{n}} \times \int_{S_n} d\boldsymbol{r}' \boldsymbol{b}_n(\boldsymbol{r}') \times \nabla' g(\boldsymbol{r}, \boldsymbol{r}') \tag{3.109}
$$

$$
\begin{aligned}
\bar{\boldsymbol{K}}^N[m,n,a,b] = \frac{\gamma_{ma}\gamma_{nb}}{4A_m A_n} \int_{S_m} d\boldsymbol{r}(\boldsymbol{r} - \boldsymbol{r}_{ma}) \cdot \hat{\boldsymbol{n}} \times \int_{S_n} d\boldsymbol{r}'(\boldsymbol{r}' - \boldsymbol{r}_{nb}) \\
\times \frac{e^{ikR}(1-ikR)}{4\pi R^3}(\boldsymbol{r} - \boldsymbol{r}').
\end{aligned} \tag{3.110}
$$

By using identity (3.73) and (3.110) can be rewritten as

$$
\begin{aligned}
\bar{\boldsymbol{K}}^N[m,n,a,b] = \frac{\gamma_{ma}\gamma_{nb}}{16\pi A_m A_n} \int_{S_m} d\boldsymbol{r}(\boldsymbol{r} - \boldsymbol{r}_{ma}) \cdot \hat{\boldsymbol{n}} \times (\boldsymbol{r}_{nb} - \boldsymbol{r}) \\
\times \int_{S_n} d\boldsymbol{r}'(\boldsymbol{r}' - \boldsymbol{r}) \frac{e^{ikR}(1-ikR)}{R^3}.
\end{aligned} \tag{3.111}
$$

Further, by using (3.75), (4.30) and result of (3.81), calculating the curl of the resultant equation with respect to $\hat{\boldsymbol{n}}$, and finally applying the dot product we

obtain

$$\begin{aligned}\bar{\boldsymbol{K}}^N[m,n,a,b] = \frac{\gamma_{ma}\gamma_{nb}}{16\pi A_m A_n}\Big[&(n_x z_{ma} - x_{ma}n_z)I_4 + (y_{nb}n_z + y_{ma}n_z - z_{ma}n_y)I_{19} \\ &+ n_x I_{13} - (y_{ma}y_{nb}n_x + x_{ma}y_{nb}n_y)I_1 + (y_{ma}n_x + y_{nb}n_x - x_{ma}n_y)I_3 \\ &- n_x I_7 + (x_{nb}n_y + x_{ma}n_y - y_{ma}n_x)I_{10} - (x_{ma}x_{nb}n_y + y_{ma}x_{nb}n_x)I_9 \\ &- n_y I_{15} - n_x I_8 + n_z I_6 + n_z I_{14} - n_x x_{nb} I_{11} - n_y I_{16} - n_y y_{nb} I_2 \\ &+ (z_{ma}x_{nb}n_x + z_{ma}y_{nb}n_y - x_{ma}x_{nb}n_z - y_{ma}y_{nb}n_z)I_{17} - n_z I_{23} \\ &+ (n_y z_{ma} - y_{ma}n_z)I_{12} + (x_{nb}n_z + x_{ma}n_z - z_{ma}n_x)I_{18} - n_z I_{24} \\ &- (n_x x_{nb} + y_{nb}n_y)I_{20} + n_y I_{21} + n_y I_{22} n_y I_5\Big],\end{aligned} \tag{3.112}$$

where

$$\begin{aligned}
I_1 &= \int_{Sm} d\boldsymbol{r}' I_{in1}, & I_9 &= \int_{Sm} d\boldsymbol{r}' I_{in2}, & I_{17} &= \int_{Sm} d\boldsymbol{r}' I_{in3}, \\
I_2 &= \int_{Sm} d\boldsymbol{r}' x I_{in1}, & I_{10} &= \int_{Sm} d\boldsymbol{r}' x I_{in2}, & I_{18} &= \int_{Sm} d\boldsymbol{r}' x I_{in3}, \\
I_3 &= \int_{Sm} d\boldsymbol{r}' y I_{in1}, & I_{11} &= \int_{Sm} d\boldsymbol{r}' y I_{in2}, & I_{19} &= \int_{Sm} d\boldsymbol{r}' y I_{in3}, \\
I_4 &= \int_{Sm} d\boldsymbol{r}' z I_{in1}, & I_{12} &= \int_{Sm} d\boldsymbol{r}' z I_{in2}, & I_{20} &= \int_{Sm} d\boldsymbol{r}' z I_{in3}, \\
I_5 &= \int_{Sm} d\boldsymbol{r}' xy I_{in1}, & I_{13} &= \int_{Sm} d\boldsymbol{r}' xz I_{in2}, & I_{21} &= \int_{Sm} d\boldsymbol{r}' xz I_{in3}, \\
I_6 &= \int_{Sm} d\boldsymbol{r}' xz I_{in1}, & I_{14} &= \int_{Sm} d\boldsymbol{r}' yz I_{in2}, & I_{22} &= \int_{Sm} d\boldsymbol{r}' yz I_{in3}, \\
I_7 &= \int_{Sm} d\boldsymbol{r}' y^2 I_{in1}, & I_{15} &= \int_{Sm} d\boldsymbol{r}' x^2 I_{in2}, & I_{23} &= \int_{Sm} d\boldsymbol{r}' x^2 I_{in3}, \\
I_8 &= \int_{Sm} d\boldsymbol{r}' z^2 I_{in1}, & I_{16} &= \int_{Sm} d\boldsymbol{r}' y^2 I_{in2}, & I_{24} &= \int_{Sm} d\boldsymbol{r}' y^2 I_{in3}.
\end{aligned} \tag{3.113}$$

The last operator is $\mathcal{I}$ operator. In order to discretize this operator, we will start with tangentially-tested $\mathcal{I}$. By using (3.36)

$$\hat{\boldsymbol{t}} \cdot \mathcal{I} = \int_{S_m} d\boldsymbol{r} \boldsymbol{t}_m(\boldsymbol{r}) \cdot \mathcal{I}\{\boldsymbol{b}_n\}(\boldsymbol{r}) \tag{3.114}$$

$$\begin{aligned}\bar{\boldsymbol{I}}^T[n,n,a,b] &= \int_{S_n} d\boldsymbol{r} \boldsymbol{t}_n(\boldsymbol{r}) \cdot \boldsymbol{b}_n(\boldsymbol{r}) \\ &= \gamma_n \gamma_{na} \frac{l_{nb}}{2A_n} \frac{l_{na}}{2A_n} \int_{S_n} d\boldsymbol{r} (\boldsymbol{r} - \boldsymbol{r}_{nb}) \cdot (\boldsymbol{r} - \boldsymbol{r}_{na})\end{aligned} \tag{3.115}$$

The integrand of the (3.115) can be written explicitly as

$$(\boldsymbol{r}-\boldsymbol{r}_{nb})\cdot(\boldsymbol{r}-\boldsymbol{r}_{na}) = x^2+y^2+z^2 - xx_{na} - yy_{na} - zz_{na} - xx_{xb} \\ - yy_{nb} - zz_{nb} + x_{na}x_{nb} + y_{na}y_{nb} + z_{na}z_{nb}. \tag{3.116}$$

Substituting (3.116) into (3.115) we obtain

$$\bar{\boldsymbol{I}}^T[n,n,a,b] = \gamma_{nb}\gamma_{na}\frac{l_{nb}l_{na}}{4A_n^2}\int_{S_n} d\boldsymbol{r}\Big[x^2+y^2+z^2 - xx_{na} - yy_{na} - zz_{na} \\ - xx_{xb} - yy_{nb} - zz_{nb} + x_{na}x_{nb} + y_{na}y_{nb} + z_{na}z_{nb}\Big]. \tag{3.117}$$

Then, we can separate whole integral into basic integrals, such that,

$$\begin{aligned} I_1 &= \int_{Sn} d\boldsymbol{r}' x^2, & I_5 &= \int_{Sn} d\boldsymbol{r}' z^2, \\ I_2 &= \int_{Sn} d\boldsymbol{r}' x, & I_6 &= \int_{Sn} d\boldsymbol{r}' z, \\ I_3 &= \int_{Sn} d\boldsymbol{r}' y^2, & I_7 &= \int_{Sn} d\boldsymbol{r}'. \\ I_4 &= \int_{Sn} d\boldsymbol{r}' y, \end{aligned} \tag{3.118}$$

By using basic integrals, (3.114) will result,

$$\bar{\boldsymbol{I}}^T[n,n,a,b] = \gamma_{nb}\gamma_{na}\frac{l_{nb}l_{na}}{4A_n^2}\Big[I_1 - (x_{nb}+x_{na})I_2 + I_3 - (y_{nb}+y_{na})I_4 \\ + I_5 - (z_{nb}+z_{na})I_6 + (x_{na}x_{nb}+y_{na}y_{nb}+z_{na}z_{nb})I_7\Big]. \tag{3.119}$$

Finally, normally-tested $\mathcal{I}$ operator is examined.

$$\bar{\boldsymbol{I}}^N[n,n] = \int_{S_n} d\boldsymbol{r}\boldsymbol{t}_n(\boldsymbol{r})\cdot\mathcal{I}\{\boldsymbol{b}_n\}(\boldsymbol{r})\times\hat{\boldsymbol{n}}, \tag{3.120}$$

$$\bar{\boldsymbol{I}}^N[n,n,a,b] = \gamma_{nb}\gamma_{na}\frac{l_{nb}}{2A_n}\frac{l_{na}}{2A_n}\int_{S_n} d\boldsymbol{r}(\boldsymbol{r}-\boldsymbol{r}_{nb})\cdot(\boldsymbol{r}-\boldsymbol{r}_{na})\times\hat{\boldsymbol{n}},$$

where

$$(\boldsymbol{r}-\boldsymbol{r}_{nb})\cdot(\boldsymbol{r}-\boldsymbol{r}_{na})\times\hat{\boldsymbol{n}} = \Big[(xy-xy_{na}-x_{nb}y+x_{nb}y_{na})n_z - (zx-zx_{nb}-z_{na}x+z_{na}x_{nb})n_y + (zy-zy_{nb}-z_{na}y+z_{na}y_{nb})n_x - (xy-xy_{nb}-x_{na}y+x_{na}y_{nb})n_z + (yz-yz_{nb}-y_{na}z+y_{na}z_{nb})n_x - (xz-xz_{nb}-x_{na}z+x_{na}z_{nb})n_y\Big]. \tag{3.121}$$

Substituting (3.121) into (3.120) we obtain

$$\bar{\boldsymbol{I}}^N[n,n,a,b] = \gamma_{nb}\gamma_{na}\frac{l_{nb}l_{na}}{4A_n^2}\int_{S_n} d\boldsymbol{r}\Big[(x_{nb}y_{na}n_z - z_{na}x_{nb}n_y + z_{na}y_{nb}n_x + y_{na}z_{nb}n_x - x_{na}z_{nb}n_y - x_{na}y_{nb}n_z)I_1 - 2n_yI_6 + (n_x+n_y)I_5 + (x_{nb}n_y - y_{nb}n_x - y_{na}n_x + x_{na}n_y)I_4 + (z_{nb}n_y - y_{na}n_z + z_{na}n_y + y_{nb}n_x)I_2 + (x_{na}n_z - x_{nb}n_z - z_{na}n_x - z_{nb}n_x)I_3\Big], \tag{3.122}$$

where

$$I_1 = \int_{Sn} d\boldsymbol{r}', \qquad I_4 = \int_{Sn} d\boldsymbol{r}'z,$$
$$I_2 = \int_{Sn} d\boldsymbol{r}'x, \qquad I_5 = \int_{Sn} d\boldsymbol{r}'yz,$$
$$I_3 = \int_{Sn} d\boldsymbol{r}'y, \qquad I_6 = \int_{Sn} d\boldsymbol{r}'zx. \tag{3.123}$$

After discretizing operators on the left-hand-side (LHS), we discretize the possible right-hand-side (RHS) of the matrix equation as

$$\boldsymbol{v}^{E,T}[m] = \int_{S_m} d\boldsymbol{r}\boldsymbol{t}_m(\boldsymbol{r})\cdot\boldsymbol{E}^{inc}(\boldsymbol{r}) \tag{3.124}$$

$$\boldsymbol{v}^{E,N}[m] = \int_{S_m} d\boldsymbol{r}\boldsymbol{t}_m(\boldsymbol{r})\cdot\hat{\boldsymbol{n}}\times\boldsymbol{E}^{inc}(\boldsymbol{r}) \tag{3.125}$$

$$\boldsymbol{v}^{H,T}[m] = \int_{S_m} d\boldsymbol{r}\boldsymbol{t}_m(\boldsymbol{r})\cdot\boldsymbol{H}^{inc}(\boldsymbol{r}) \tag{3.126}$$

$$\boldsymbol{v}^{H,N}[m] = \int_{S_m} d\boldsymbol{r}\boldsymbol{t}_m(\boldsymbol{r})\cdot\hat{\boldsymbol{n}}\times\boldsymbol{H}^{inc}(\boldsymbol{r}). \tag{3.127}$$

Starting with (3.127) and by calculating the curl operation we obtain

$$\hat{\boldsymbol{n}} \times \boldsymbol{H}^{inc}(\boldsymbol{r}) = \hat{\boldsymbol{x}}(H_z n_y - H_y n_z) + \hat{\boldsymbol{y}}(H_x n_z - H_z n_x) + \hat{\boldsymbol{z}}(H_y n_x - H_x n_y). \tag{3.128}$$

Then, by using (3.36)

$$\boldsymbol{v}^{H,N}[m] = \int_{S_m} d\boldsymbol{r}\left(\frac{l_{ma}}{2A_m}\gamma_{ma}(\boldsymbol{r} - \boldsymbol{r}_{ma})\right) \cdot \Big(\hat{\boldsymbol{x}}(H_z n_y - H_y n_z) + \hat{\boldsymbol{y}}(H_x n_z - H_z n_x) + \hat{\boldsymbol{z}}(H_y n_x - H_x n_y)\Big), \tag{3.129}$$

and by performing dot-product in the equation,

$$\boldsymbol{v}^{H,N}[m] = \frac{l_{ma}}{2A_m}\gamma_{ma}\int_{S_m} d\boldsymbol{r}\Big[(x - x_{ma})(H_z n_y - H_y n_z) + (y - y_{ma})(H_x n_z - H_z n_x) + (z - z_{ma})(H_y n_x - H_x n_y)\Big]. \tag{3.130}$$

Next, we separate whole integral into basic integrals as

$$I_1 = \int_{Sm} d\boldsymbol{r}' x, \tag{3.131}$$

$$I_2 = \int_{Sm} d\boldsymbol{r}' y, \tag{3.132}$$

$$I_3 = \int_{Sm} d\boldsymbol{r}' z, \tag{3.133}$$

$$I_4 = \int_{Sm} d\boldsymbol{r}' 1. \tag{3.134}$$

By using these basic integrals, (3.127) can be written as

$$\boldsymbol{v}^{H,N}[m] = \frac{l_{ma}}{2A_m}\gamma_{ma}\Big[I_1(H_z n_y - H_y n_z) - x_{ma}I_4(H_z n_y - H_y n_z) + I_2(H_x n_z - H_z n_x) - y_{ma}I_4(H_x n_z - H_z n_x) + I_3(H_y n_x - H_x n_y) - z_{ma}I_4(H_y n_x - H_x n_y)\Big]. \tag{3.135}$$

If we apply same procedure for (3.125), there will be four basic integrals defined as

$$\boldsymbol{v}^{E,N}[m] = \frac{l_{ma}}{2A_m}\gamma_{ma}\Big[I_1(E_z n_y - E_y n_z) - x_{ma}I_4(E_z n_y - E_y n_z) + I_2(E_x n_z - E_z n_x) - y_{ma}I_4(E_x n_z - E_z n_x) + I_3(E_y n_x - E_x n_y) - z_{ma}I_4(E_y n_x - E_x n_y)\Big], \tag{3.136}$$

where

$$I_1 = \int_{Sm} d\boldsymbol{r}' x, \tag{3.137}$$

$$I_2 = \int_{Sm} d\boldsymbol{r}' y, \tag{3.138}$$

$$I_3 = \int_{Sm} d\boldsymbol{r}' z, \tag{3.139}$$

$$I_4 = \int_{Sm} d\boldsymbol{r}' 1. \tag{3.140}$$

Finally, tangentially tested RHSs can be discretized as follows

$$\boldsymbol{v}^{E,T}[m] = \int_{S_m} d\boldsymbol{r} \boldsymbol{t}_m(\boldsymbol{r}) \cdot \boldsymbol{E}^{inc}(\boldsymbol{r}). \tag{3.141}$$

By inserting the definition of RWG function

$$\begin{aligned}
\boldsymbol{v}^{E,T}[m] &= \frac{l_{ma}}{2A_m}\gamma_{ma} \int_{S_m} d\boldsymbol{r} \Big((\boldsymbol{r} - \boldsymbol{r}_{ma}) \cdot \boldsymbol{E}^{inc} \Big) \\
&= \frac{l_{ma}}{2A_m}\gamma_{ma} \int_{S_m} d\boldsymbol{r} \Big[(x - x_{ma})E_x + (y - y_{ma})E_y + (z - z_{ma})E_z \Big] \\
&= \frac{l_{ma}}{2A_m}\gamma_{ma} \Big[E_x I_2 + E_y I_3 + E_z I_4 - (x_{ma}E_x + y_{ma}E_y + z_{ma}E_z) I_1 \Big]
\end{aligned} \tag{3.142}$$

Here, the following basic integrals are used:

$$I_1 = \int_{Sm} d\boldsymbol{r}' 1, \tag{3.143}$$

$$I_2 = \int_{Sm} d\boldsymbol{r}' x, \tag{3.144}$$

$$I_3 = \int_{Sm} d\boldsymbol{r}' y, \tag{3.145}$$

$$I_4 = \int_{Sm} d\boldsymbol{r}' z. \tag{3.146}$$

Similar procedure can be applied to (3.126) to obtain (3.147) as

$$\begin{aligned}
\boldsymbol{v}^{H,T}[m] &= \int_{S_m} d\boldsymbol{r} \boldsymbol{t}_m(\boldsymbol{r}) \cdot \boldsymbol{H}^{inc}(\boldsymbol{r}) \\
&= \frac{l_{ma}}{2A_m}\gamma_{ma} \int_{S_m} d\boldsymbol{r} \Big((\boldsymbol{r} - \boldsymbol{r}_{ma}) \cdot \boldsymbol{H}^{inc} \Big) \\
&= \frac{l_{ma}}{2A_m}\gamma_{ma} \int_{S_m} d\boldsymbol{r} \Big[(x - x_{ma})H_x + (y - y_{ma})H_y + (z - z_{ma})H_z \Big] \\
&= \frac{l_{ma}}{2A_m}\gamma_{ma} \Big[H_x I_2 + H_y I_3 + H_z I_4 - (x_{ma}H_x + y_{ma}H_y + z_{ma}H_z) I_1 \Big]
\end{aligned} \tag{3.147}$$

by using

$$I_1 = \int_{Sm} d\boldsymbol{r}' 1, \tag{3.148}$$

$$I_2 = \int_{Sm} d\boldsymbol{r}' x, \tag{3.149}$$

$$I_3 = \int_{Sm} d\boldsymbol{r}' y, \tag{3.150}$$

$$I_4 = \int_{Sm} d\boldsymbol{r}' z. \tag{3.151}$$

Up to this point, we have discretized tangentially-tested and normally-tested $\mathcal{K}$, $\mathcal{T}$, and $\mathcal{I}$ operators. We have divided all integrals into several double basic integrals that are independent from the alignment of functions. During the calculation of interactions, we have constructed loops over triangles, instead of basis and testing functions. The basic integrals are evaluated in two steps; first inner integrals are calculated, and then, they are used in forming outer integrals. Inner integrals are performed via decomposition into numerical and analytical parts, and numerical parts are usually performed by using adaptive methods [29] employing low-order Gaussian quadratures [34].

Chapter 4

Equivalence Principle Algorithm

MoM solutions of SIEs are the preferred numerical technique to solve radiation and scattering problems. Nevertheless, its high computational cost for memory and time, restricts this method to rather small-scale problems.

Development of fast solvers, FMA and MLFMA, and modern computing technology makes electrically large problems solvable. Unfortunately, these methods also have drawbacks. One of them occurs when we try to solve the problem by using EFIE formulation. A reliable solution cannot be found if the discretization becomes very fine in terms of subdivisions per wavelength. This serious problem is called "low-frequency breakdown" [35],[36]. Another problem occurs when the structure has a complicated shape, means structure has small details on it. In this case, some part of the mesh are much denser than the others. Two examples of these cases are shown in Figure 4.1 and 4.2.

Both problems deteriorate the system matrix, and hence, cause the system matrix to become ill-conditioned. If the matrix equation is solved iteratively, e.g., with Krylov subspace methods, iterative solvers converge slowly or not converge at all. Convergence of the iterative solver can be improved by choosing SIE formulation properly. Recently, several SIE formulations leading to well-conditioned matrix

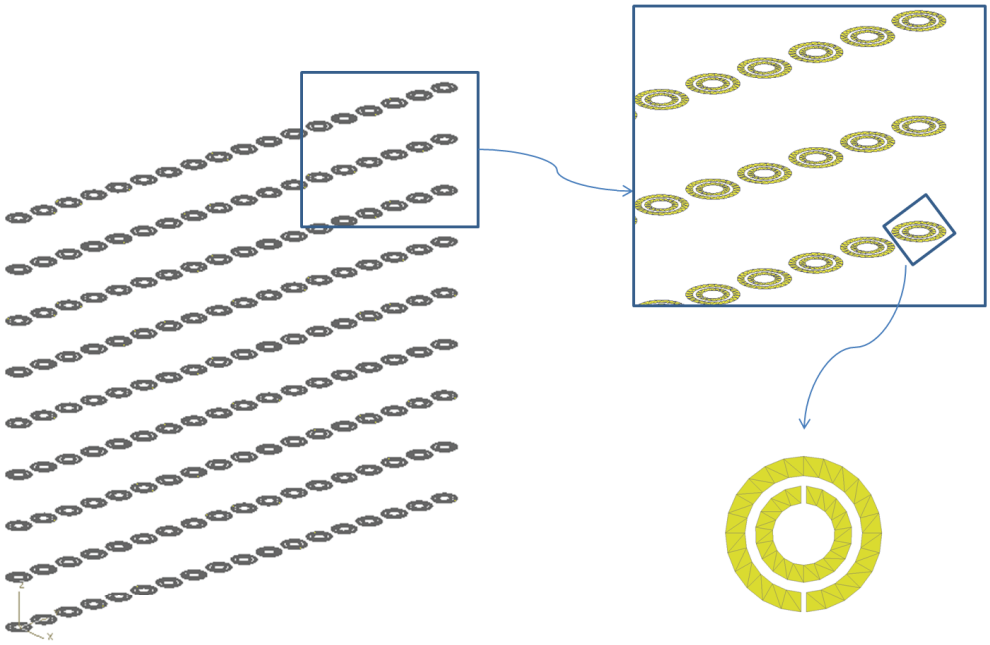

Figure 4.1: Split-ring resonator wall, example of very fine mesh ($\approx \frac{\lambda}{100}$).

equation have been developed. Unfortunately, many of these SIE formulations usually lead to a lower solution accuracy [2].

Another way to improve conditioning of the system matrix is preconditioning. Although effective preconditioners have been developed in recent years [8]-[11], the efficiency of the preconditioner is still problematic. Also, these preconditioners are formulation dependent. It is very difficult to find robust and efficient preconditioner for each problem. Primary source of ill-conditioning is varied physics exist in different regions, such as wave physics and circuit physics. For densely meshed or over-sampled region circuit-physics dominates, but for regular wave problem with homogeneous mesh, wave-physics dominates. For problems involving both regions, results in ill-conditioned matrix equation [37].

In this thesis, we present a novel method, EPA, for solving multi-scale problems in 3-D. EPA is based on DDM and equivalence principle, and it basically decomposes the solution domain into several parts so that the wave and circuit physics can be separated. The main benefit of EPA is that it essentially improves the condition number of the system, so iterative solver converges very fast [2]. Details, properties, and formulation of EPA will be given in the following sections.

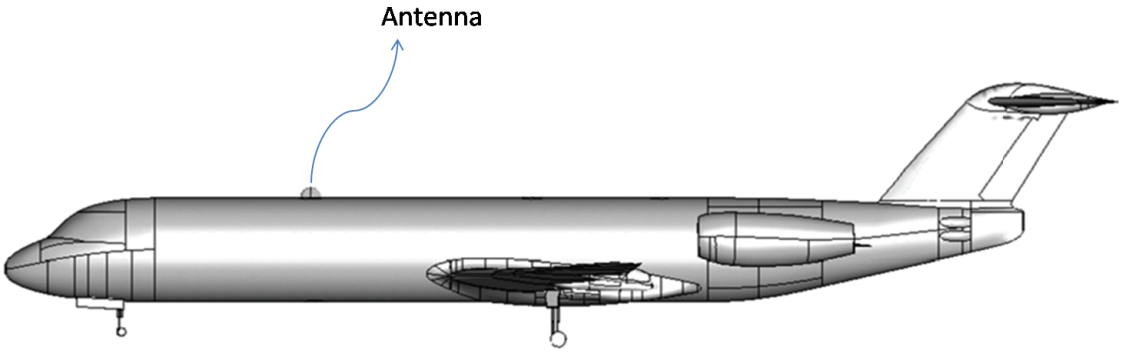

(a)

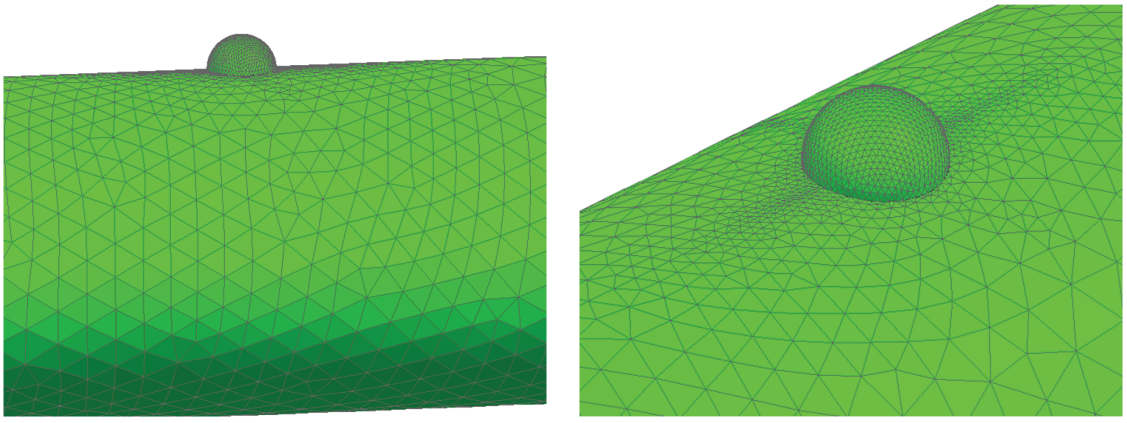

(b) (c)

Figure 4.2: Antenna mounted on a aircraft, example of structure has small details on it: (a) aircraft an antenna, (b) mesh, view-1, and (c) mesh, view-2.

4.1 General Idea of EPA

EPA is based on the equivalence principle, similar to Huygens' principle. According to these principles, the fields inside or outside a closed surface can be determined by the tangential components of the fields on the surface that is depicted in Figure 4.3.

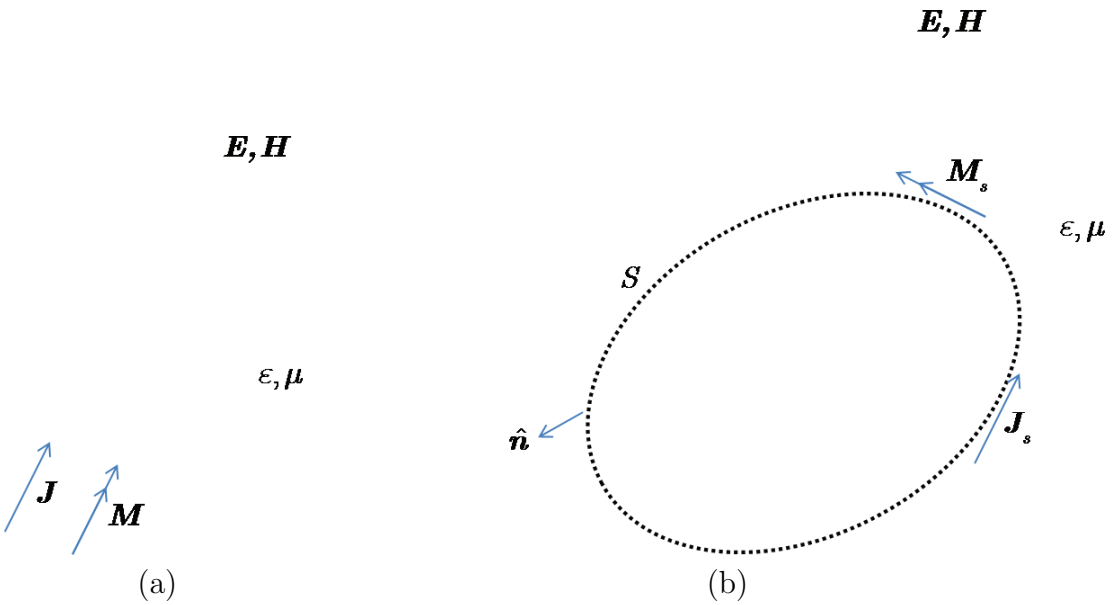

Figure 4.3: Huygens' principle: (a) original problem and (b) tangential components of the fields on the surface.

The EM fields, $\boldsymbol{E}$ and $\boldsymbol{H}$, can be expressed in terms of equivalent electric ($\boldsymbol{J}_s$) and equivalent magnetic ($\boldsymbol{M}_s$) currents as follows:

$$\boldsymbol{E}(\boldsymbol{r}) = \eta\mathcal{T}\{\boldsymbol{J}_s(\boldsymbol{r}')\} - \mathcal{K}\{\boldsymbol{M}_s(\boldsymbol{r}')\} \tag{4.1}$$

$$\boldsymbol{H}(\boldsymbol{r}) = \frac{1}{\eta}\mathcal{T}\{\boldsymbol{M}_s(\boldsymbol{r}')\} + \mathcal{K}\{\boldsymbol{J}_s(\boldsymbol{r}')\}. \tag{4.2}$$

These equations can be expressed in a matrix form as

$$\begin{bmatrix} \boldsymbol{E} \\ \boldsymbol{H} \end{bmatrix} = \begin{bmatrix} \eta\mathcal{T} & -\mathcal{K} \\ \mathcal{K} & \frac{1}{\eta}\mathcal{T} \end{bmatrix} \cdot \begin{bmatrix} \boldsymbol{J}_s \\ \boldsymbol{M}_s \end{bmatrix}, \tag{4.3}$$

(a)

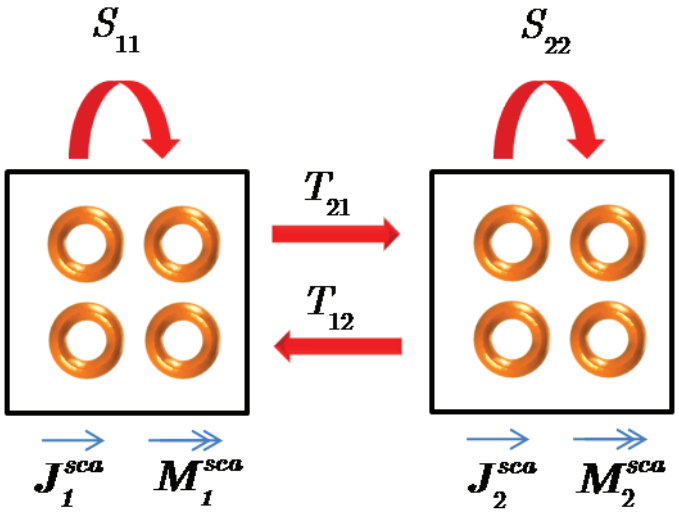

(b)

Figure 4.4: Description of EPA: (a) original problem and (b) decomposed into smaller problems.

where $\eta = \sqrt{\epsilon/\mu}$ is the wave impedance.

$$\boldsymbol{J}_s(\boldsymbol{r}) = \hat{\boldsymbol{n}} \times \boldsymbol{H}(\boldsymbol{r}) \tag{4.4}$$

$$\boldsymbol{M}_s(\boldsymbol{r}) = \boldsymbol{E}(\boldsymbol{r}) \times \hat{\boldsymbol{n}} \tag{4.5}$$

are equivalent electric and magnetic current densities on $\mathcal{S}$ with the unit normal $\hat{\boldsymbol{n}}$ pointing out $\mathcal{S}$. If we can find $\boldsymbol{J}_s$ and $\boldsymbol{M}_s$, then we can calculate EM fields $\boldsymbol{E}$ and $\boldsymbol{H}$ by using (4.1) and (4.2).

The EPA for domain decomposition is derived directly with this theorem for the problems with several regions. EPA starts solving EM problems by separating

a large complex structure into basic parts, which may consist of one or more objects with arbitrary shapes. Each one is enclosed by an ES. Then, the surface equivalence principle operator (EPO) is used to calculate scattering via equivalent surface, and radiation from one ES to another can be captured by using the translation operators (TO). This procedure is depicted in Figure 4.4.

4.2 Using Equivalent Surfaces to Solve the One-Object Scattering Problem

The procedure of solving the one-object scattering problem can be divided into three steps:

- Outside-inside propagation
- Solving for current
- Inside-outside propagation

as shown in Figure 4.5 (b), (c) and (d).

Before starting with the first step of the algorithm, an additional step is required for representing the incident fields in terms of basis functions. From Figure 4.5,

$$\begin{aligned} \boldsymbol{J}^{inc}(\boldsymbol{r}) &= \hat{\boldsymbol{n}} \times (\boldsymbol{0} - \boldsymbol{H}^{inc}(\boldsymbol{r})) \\ &= -\hat{\boldsymbol{n}} \times \boldsymbol{H}^{inc}(\boldsymbol{r}) \end{aligned} \tag{4.6}$$

$$\begin{aligned} \boldsymbol{M}^{inc}(\boldsymbol{r}) &= (\boldsymbol{0} - \boldsymbol{E}^{inc}(\boldsymbol{r})) \times \hat{\boldsymbol{n}} \\ &= \hat{\boldsymbol{n}} \times \boldsymbol{E}^{inc}(\boldsymbol{r}). \end{aligned} \tag{4.7}$$

These equations can be expressed in matrix form as

$$\begin{bmatrix} \bar{\boldsymbol{I}} & 0 \\ 0 & \bar{\boldsymbol{I}} \end{bmatrix} \cdot \begin{bmatrix} \boldsymbol{J}^{inc} \\ \boldsymbol{M}^{inc} \end{bmatrix} = \begin{bmatrix} -\hat{\boldsymbol{n}} \times \boldsymbol{H}^{inc}(\boldsymbol{r}) \\ \hat{\boldsymbol{n}} \times \boldsymbol{E}^{inc}(\boldsymbol{r}) \end{bmatrix}. \tag{4.8}$$

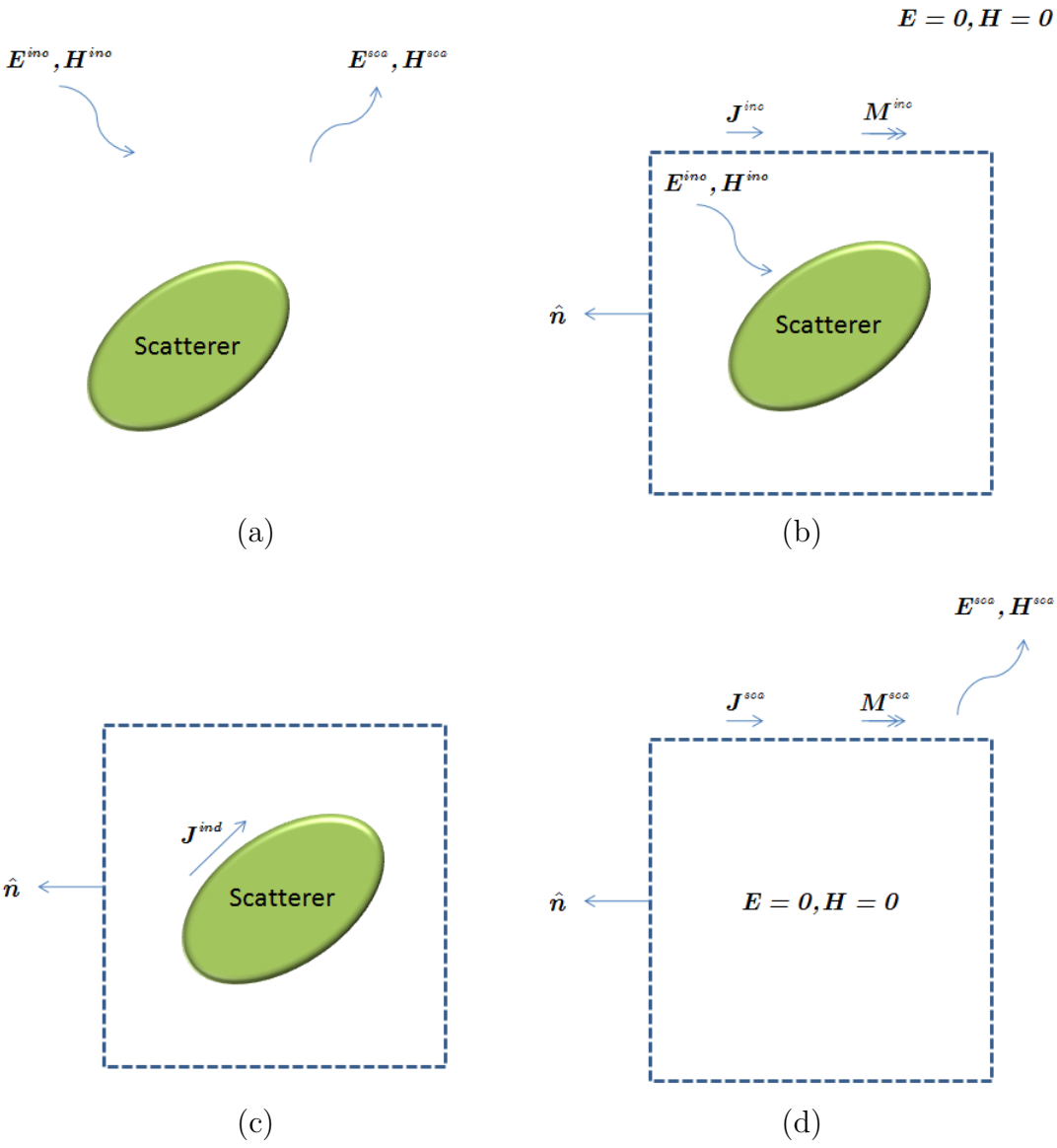

Figure 4.5: One-object scattering problem: (a) original problem, (b) outside-inside propagation, (c) solving for current, and (d) inside-outside propagation.

For the numerical solutions of $\boldsymbol{J}^{inc}$ and $\boldsymbol{M}^{inc}$, we need to discretize the (4.8), as we mentioned before [39],[40]. In (4.8), we need $\boldsymbol{I}_{mn}^{tan}$, $\boldsymbol{v}_m^{E,N}$, and $v_m^{H,N}$. We have derived all these operators in Chapter 3. So by using them directly,

$$\bar{\boldsymbol{I}}^T[n,n,a,b] = \gamma_{nb}\gamma_{na}\frac{l_{nb}l_{na}}{4A_n^2}\Big[I_1 - (x_{nb}+x_{na})I_2 + I_3 - (y_{nb}+y_{na})I_4 + I_5 \\ - (z_{nb}+z_{na})I_6 + (x_{nb}x_{na}+y_{nb}y_{na}+z_{nb}z_{na})I_7\Big], \tag{4.9}$$

where

$$\begin{aligned} I_1 &= \int_{Sn} d\boldsymbol{r}' x^2, & I_5 &= \int_{Sn} d\boldsymbol{r}' z^2, \\ I_2 &= \int_{Sn} d\boldsymbol{r}' x, & I_6 &= \int_{Sn} d\boldsymbol{r}' z, \\ I_3 &= \int_{Sn} d\boldsymbol{r}' y^2, & I_7 &= \int_{Sn} d\boldsymbol{r}'. \\ I_4 &= \int_{Sn} d\boldsymbol{r}' y, \end{aligned} \tag{4.10}$$

$$\boldsymbol{v}^{H,N}[m] = \frac{l_{mb}}{2A_m}\gamma_{ma}\Big[I_1(H_z n_y - H_y n_z) - x_{ma}I_4(H_z n_y - H_y n_z) \\ + I_2(H_x n_z - H_z n_x) - y_{ma}I_4(H_x n_z - H_z n_x) + I_3(H_y n_x - H_x n_y) \\ - z_{ma}I_4(H_y n_x - H_x n_y)\Big], \tag{4.11}$$

and

$$\boldsymbol{v}^{E,N}[m] = \frac{l_{ma}}{2A_m}\gamma_{ma}\Big[I_1(E_z n_y - E_y n_z) - x_{ma}I_4(E_z n_y - E_y n_z) \\ + I_2(E_x n_z - E_z n_x) - y_{ma}I_4(E_x n_z - E_z n_x) + I_3(E_y n_x - E_x n_y) \\ - z_{ma}I_4(E_y n_x - E_x n_y)\Big], \tag{4.12}$$

where

$$I_1 = \int_{Sm} d\boldsymbol{r}' x, \tag{4.13}$$

$$I_2 = \int_{Sm} d\boldsymbol{r}' y, \tag{4.14}$$

$$I_3 = \int_{Sm} d\boldsymbol{r}' z, \tag{4.15}$$

$$I_4 = \int_{Sm} d\boldsymbol{r}' 1. \tag{4.16}$$

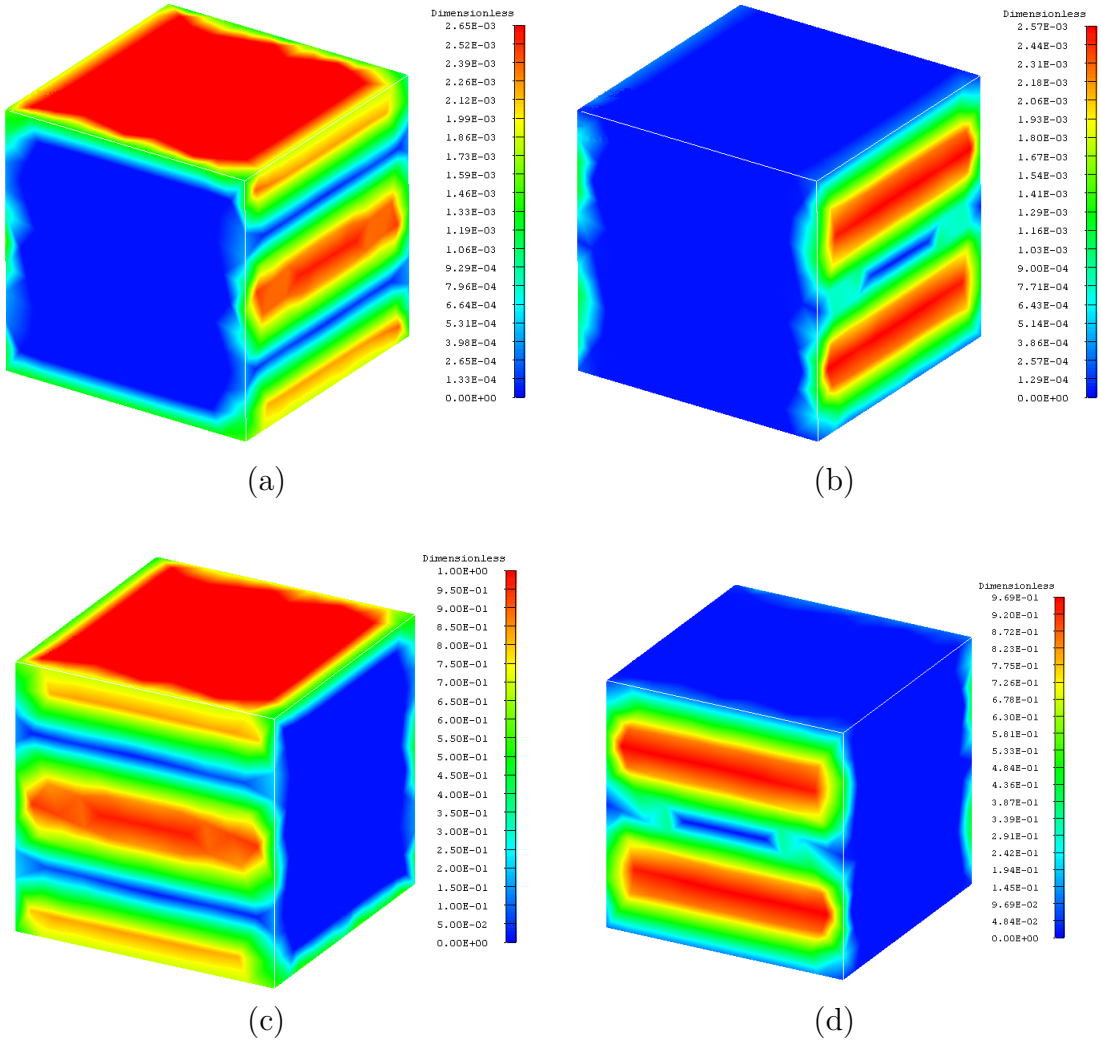

Figure 4.6: Example of incident current on a cube with edge length 1λ: (a) real part of the electric current, (b) imaginary part of the electric current, (c) real part of the magnetic current, and (d) imaginary part of the magnetic current.

By using (4.8), the incident electric and magnetic currents on the ES computed from $\boldsymbol{E}^{inc}$ and $\boldsymbol{H}^{inc}$ replace the source outside the ES. For incident fields, we use the following types of excitations in our numerical simulations.

Planewave

A planewave propagating in the $\hat{\boldsymbol{k}}$ direction with the electric field polarized in the $\hat{\boldsymbol{e}}$ direction ($\hat{\boldsymbol{e}} \perp \hat{\boldsymbol{k}}$) can be written as

$$\boldsymbol{E}^{inc}(\boldsymbol{r}) = \hat{\boldsymbol{e}} E_a \exp\left(ik\hat{\boldsymbol{k}} \cdot \boldsymbol{r}\right) \tag{4.17}$$

$$\boldsymbol{H}^{inc}(\boldsymbol{r}) = \frac{1}{\eta}\hat{\boldsymbol{k}} \times \boldsymbol{E}^{inc}(\boldsymbol{r}) = \hat{\boldsymbol{k}} \times \hat{\boldsymbol{e}} \frac{E_a}{\eta} \exp\left(ik\hat{\boldsymbol{k}} \cdot \boldsymbol{r}\right), \tag{4.18}$$

where E_a is the amplitude of the plane wave.

Hertzian Dipole

Electric and magnetic fields of a Hertzian (ideal) dipole with dipole moment $\boldsymbol{I}_{DM}$ located at $\boldsymbol{r}_d$ can be written as

$$\begin{aligned}\boldsymbol{E}^{inc}(\boldsymbol{r}) = iw\mu \frac{\exp(ik|\boldsymbol{r}-\boldsymbol{r}_d|)}{4\pi|\boldsymbol{r}-\boldsymbol{r}_d|}\Bigg[\boldsymbol{I}_{DM}\left(1 + \frac{i}{k|\boldsymbol{r}-\boldsymbol{r}_d|} - \frac{1}{k^2|\boldsymbol{r}-\boldsymbol{r}_d|^2}\right) \\ - (\boldsymbol{r}-\boldsymbol{r}_d)\frac{\boldsymbol{I}_{DM}\cdot(\boldsymbol{r}-\boldsymbol{r}_d)}{|\boldsymbol{r}-\boldsymbol{r}_d|^2}\left(1 + \frac{3i}{k|\boldsymbol{r}-\boldsymbol{r}_d|} - \frac{3}{k^2|\boldsymbol{r}-\boldsymbol{r}_d|^2}\right)\Bigg]\end{aligned} \tag{4.19}$$

and

$$\boldsymbol{H}^{inc}(\boldsymbol{r}) = \boldsymbol{I}_{DM} \times (\boldsymbol{r}-\boldsymbol{r}_d)\frac{\exp(ik|\boldsymbol{r}-\boldsymbol{r}_d|)}{4\pi|\boldsymbol{r}-\boldsymbol{r}_d|^2}\left(\frac{1}{|\boldsymbol{r}-\boldsymbol{r}_d|} - ik\right), \tag{4.20}$$

respectively. Figure 4.6 shows equivalent currents that are calculated numerically by using 4.8, on a cube with edge length of 1λ. ES is illuminated by a θ polarized plane-wave propagating in the $-\hat{\boldsymbol{z}}$ direction at 300 MHz.

4.2.1 Outside-Inside Propagation

In the first step of the algorithm, incident electric and magnetic currents on the ES are computed. These currents generate original incident fields inside and zero field outside by the extinction theorem [41].

$$\boldsymbol{E}^{inc}(\boldsymbol{r}) = \eta\mathcal{T}\{\boldsymbol{J}^{inc}(\boldsymbol{r}')\} - \mathcal{K}\{\boldsymbol{M}^{inc}(\boldsymbol{r}')\}. \tag{4.21}$$

Since the fields generated in this step only propagate inside, it is named as outside-inside propagation. At this step of the algorithm, we need $\bar{\boldsymbol{T}}^T[m,n,a,b]$ and $\bar{\boldsymbol{K}}^T[m,n,a,b]$. In Chapter 3, we have calculated

$$\begin{aligned}\bar{\boldsymbol{T}}^T[m,n,a,b] = ikC_{nb,ma}\Big[&(x_{nb}x_{ma} + y_{nb}y_{ma} - \frac{4}{k^2})I_1 + I_2 + I_3 - x_{nb}I_4 \\ &- x_{ma}I_5 - y_{nb}I_6 - y_{ma}I_7\Big],\end{aligned} \tag{4.22}$$

where

$$\begin{aligned} I_1 &= \int_{Sm} d\boldsymbol{r}' I_{in1}, & I_5 &= \int_{Sm} d\boldsymbol{r}' I_{in2}, \\ I_2 &= \int_{Sm} d\boldsymbol{r}' x I_{in2}, & I_6 &= \int_{Sm} d\boldsymbol{r}' y I_{in1}, \\ I_3 &= \int_{Sm} d\boldsymbol{r}' y I_{in3}, & I_7 &= \int_{Sm} d\boldsymbol{r}' I_{in3}. \\ I_4 &= \int_{Sm} d\boldsymbol{r}' x I_{in1}, \end{aligned} \tag{4.23}$$

and

$$C_{nb,ma} = \frac{\gamma_{nb} l_{nb} \gamma_{ma} l_{ma}}{4A_b A_a} \tag{4.24}$$

$$I_{in1} = \int_{Sn} d\boldsymbol{r}' g(\boldsymbol{r},\boldsymbol{r}'), \tag{4.25}$$

$$I_{in2} = \int_{Sn} d\boldsymbol{r}' x' g(\boldsymbol{r},\boldsymbol{r}'), \tag{4.26}$$

$$I_{in3} = \int_{Sn} d\boldsymbol{r}' y' g(\boldsymbol{r},\boldsymbol{r}'). \tag{4.27}$$

Also, we have obtained

$$\bar{\boldsymbol{K}}^T[m,n,a,b] = -\frac{\gamma_{nb}\gamma_{ma}}{16\pi A_b A_a}\Big[(y_{nb}-y_{ma})I_1 + z_{ma}I_2 - z_{ma}y_{nb}I_3 + (x_{ma}-x_{nb})I_4 \\ - z_{ma}I_5 + z_{ma}x_{nb}I_6 + (y_{nb}-y_{ma})I_7 + (x_{ma}-x_{nb})I_8 \\ + (y_{ma}x_{nb}-x_{ma}y_{nb})I_9\Big], \tag{4.28}$$

where

$$I_1 = \int_{Sm} d\boldsymbol{r}' z I_{in1}, \qquad I_4 = \int_{Sm} d\boldsymbol{r}' z I_{in2}, \qquad I_7 = \int_{Sm} d\boldsymbol{r}' x I_{in3}, \\ I_2 = \int_{Sm} d\boldsymbol{r}' y I_{in1}, \qquad I_5 = \int_{Sm} d\boldsymbol{r}' x I_{in2}, \qquad I_8 = \int_{Sm} d\boldsymbol{r}' y I_{in3}, \\ I_3 = \int_{Sm} d\boldsymbol{r}' I_{in1}, \qquad I_6 = \int_{Sm} d\boldsymbol{r}' I_{in2}, \qquad I_9 = \int_{Sm} d\boldsymbol{r}' I_{in3}. \tag{4.29}$$

and

$$I_{in1} = \int_{Sn} d\boldsymbol{r}'(x'-x)\frac{e^{ikR}(1-ikR)}{R^3} \tag{4.30}$$

$$I_{in2} = \int_{Sn} d\boldsymbol{r}'(y'-y)\frac{e^{ikR}(1-ikR)}{R^3} \tag{4.31}$$

$$I_{in3} = \int_{Sn} d\boldsymbol{r}'\frac{e^{ikR}(1-ikR)}{R^3}. \tag{4.32}$$

By using these operators and (4.21), outside-inside propagation can be represented in the matrix form as

$$\begin{bmatrix} \text{Outside-Inside} \\ \text{Propagation} \end{bmatrix}_{2m\times n} = \left[\left[\bar{\boldsymbol{T}}^{tan}_{mn}\right]_{m\times n}\left[-\bar{\boldsymbol{K}}^{tan}_{mn}\right]_{m\times n}\right]_{2m\times n}. \tag{4.33}$$

4.2.2 Solving for Current

In this step, the electric current on the PEC object are solved given the incident wave on its surface. Here, we have three choices as current solver. These are EFIE, MFIE and CFIE.

We have derived all the integral equations in Chapter 3. Recalling them,

- EFIE

$$\hat{\boldsymbol{t}} \cdot \eta \mathcal{T}\{\boldsymbol{J}(\boldsymbol{r})\} = -\hat{\boldsymbol{t}} \cdot \boldsymbol{E}^{inc}(\boldsymbol{r}), \tag{4.34}$$

- MFIE

$$\mathcal{I}\{\boldsymbol{J}(\boldsymbol{r})\} - \hat{\boldsymbol{n}} \times \mathcal{K}\{\boldsymbol{J}(\boldsymbol{r})\} = \hat{\boldsymbol{n}} \times \boldsymbol{H}^{inc}(\boldsymbol{r}), \tag{4.35}$$

- CFIE

$$\text{CFIE} = \alpha\text{EFIE} + (1-\alpha)\text{MFIE}. \tag{4.36}$$

We know that, after discretizing these equations with basis functions and testing them with testing functions, we end-up with matrix equations as

$$Z_{mn} a_n = v_m, \tag{4.37}$$

where $\bar{\boldsymbol{Z}}$ is the impedance matrix of the PEC object and, $\boldsymbol{v}$ is the excitation vector, which is constructed by directly using (4.21).

4.2.3 Inside-Outside Propagation

Once the current on the PEC object is known, the equivalent electric and magnetic currents on the ES can be computed. This will generate null field inside and the scattered field outside. Therefore, we call these currents as scattered currents and this step is defined as inside-outside propagation. Induced current, $\boldsymbol{J}^{ind}$, on the PEC object can be radiated by using $\mathcal{T}$ and $\mathcal{K}$ operators directly.

$$\boldsymbol{H}^{sca} = \mathcal{K}\{\boldsymbol{J}^{ind}\} \tag{4.38}$$

$$\boldsymbol{E}^{sca} = \eta \mathcal{T}\{\boldsymbol{J}^{ind}\} \tag{4.39}$$

Then, the fields in (4.38) and (4.39) are projected on the surface by using $\hat{\boldsymbol{n}}$, to obtain scattered currents.

Finally, these three steps, required for one-object scattering problem, can be written as follows,

$$\begin{bmatrix} \boldsymbol{J}_s^{\text{sca}} \\ \frac{1}{\eta}\boldsymbol{M}_s^{\text{sca}} \end{bmatrix} = \begin{bmatrix} \hat{\boldsymbol{n}} \times \mathcal{K} \\ \frac{1}{\eta}\hat{\boldsymbol{n}} \times \mathcal{T} \end{bmatrix} \cdot \begin{bmatrix} \bar{\boldsymbol{Z}} \end{bmatrix}^{-1} \cdot \begin{bmatrix} -\mathcal{T} - \eta\mathcal{K} \end{bmatrix} \cdot \begin{bmatrix} \boldsymbol{J}_s^{\text{inc}} \\ \frac{1}{\eta}\boldsymbol{M}_s^{\text{inc}} \end{bmatrix}, \tag{4.40}$$

where

$$\begin{bmatrix} \hat{\boldsymbol{n}} \times \mathcal{K} \\ \frac{1}{\eta}\hat{\boldsymbol{n}} \times \mathcal{T} \end{bmatrix} \tag{4.41}$$

is the inside-outside propagation operator,

$$\begin{bmatrix} \bar{\boldsymbol{Z}} \end{bmatrix}^{-1} \tag{4.42}$$

is current solver for PEC object, and

$$\begin{bmatrix} -\mathcal{T} - \eta\mathcal{K} \end{bmatrix} \tag{4.43}$$

is the outside-inside propagation operator. We can rewrite (4.40) as

$$\begin{bmatrix} \boldsymbol{J}_s^{\text{sca}} \\ \frac{1}{\eta}\boldsymbol{M}_s^{\text{sca}} \end{bmatrix} = \bar{\boldsymbol{S}} \cdot \begin{bmatrix} \boldsymbol{J}_s^{\text{inc}} \\ \frac{1}{\eta}\boldsymbol{M}_s^{\text{inc}} \end{bmatrix}, \tag{4.44}$$

where we have balanced the equation with $\frac{1}{\eta}$. The scattered field outside the ES can be calculated from scattered currents on ES, which are solved by using (4.44), where we call $\bar{\boldsymbol{S}}$ as a scattering matrix. The unknowns on the PEC object, which is inside the ES, are transferred to the unknowns on its ES with the information of the scatterer embedded in $\bar{\boldsymbol{S}}$. With this method, very complicated structures, with very fine meshes, can be solved easily. Because of the fine meshes, the number of unknowns of the PEC object can be very high. The current distribution on the ES is much smoother than PEC object, so the number of unknowns on the ES can be much less than on the PEC, without losing accuracy. Up to this point, we have solved one object scattering problem by introducing scattering matrix $\bar{\boldsymbol{S}}$. In the next section, we will start to solve multi-object scattering problems.

4.3 Using Equivalent Surfaces to Solve the Multi-Object Scattering Problem

EPA shows its advantages specially in solving the multi-object scattering problems. EPA will help to reduce the memory usage when identical subdomains occur. In this case, for only one EPO, $\bar{\boldsymbol{S}}$ needs to be stored in the memory for those of repeated subdomains. By representing the scatterers with ESs, interac-

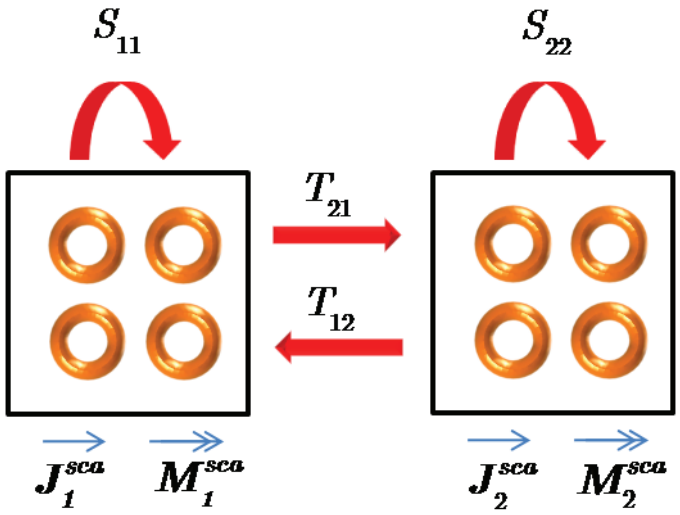

Figure 4.7: Example of the interactions among two ESs.

tion between two objects are substituted with interactions between two equivalent surfaces. The translation operator is used to compute these interactions.

$$\begin{bmatrix} \boldsymbol{J}_2 \\ \frac{1}{\eta}\boldsymbol{M}_2 \end{bmatrix} = \bar{\boldsymbol{T}}_{21} \cdot \begin{bmatrix} \boldsymbol{J}_1 \\ \frac{1}{\eta}\boldsymbol{M}_1 \end{bmatrix}, \tag{4.45}$$

where $\bar{\boldsymbol{T}}_{21}$ is translation operator, and its general form can be written as follows,

$$\bar{\boldsymbol{T}}_{\mathrm{kl}} = \begin{bmatrix} -\hat{\boldsymbol{n}} \times \mathcal{K}_{\mathrm{kl}} & \frac{1}{\eta}\hat{\boldsymbol{n}} \times \mathcal{T}_{\mathrm{kl}} \\ -\frac{1}{\eta}\hat{\boldsymbol{n}} \times \mathcal{T}_{\mathrm{kl}} & -\hat{\boldsymbol{n}} \times \mathcal{K}_{\mathrm{kl}} \end{bmatrix}. \tag{4.46}$$

Here, k and l represent the number of ESs. For example, $\bar{\boldsymbol{T}}_{kl}$ means that, the scattered currents on the ES l is radiated to ES k, and these fields are projected on ES k to obtain scattered currents on the ES k.

By using TOs and EPOs we formulate the simple problem, depicted in Figure 4.7.

$$\begin{bmatrix} \boldsymbol{J}_1^{\mathrm{sca}} \\ \frac{1}{\eta}\boldsymbol{M}_1^{\mathrm{sca}} \end{bmatrix} - \bar{\boldsymbol{S}}_{11} \cdot \bar{\boldsymbol{T}}_{12} \cdot \begin{bmatrix} \boldsymbol{J}_2^{\mathrm{sca}} \\ \frac{1}{\eta}\boldsymbol{M}_2^{\mathrm{sca}} \end{bmatrix} = \bar{\boldsymbol{S}}_{11} \cdot \begin{bmatrix} \boldsymbol{J}_1^{\mathrm{inc}} \\ \frac{1}{\eta}\boldsymbol{M}_1^{\mathrm{inc}} \end{bmatrix} \tag{4.47}$$

$$\begin{bmatrix} \boldsymbol{J}_2^{\mathrm{sca}} \\ \frac{1}{\eta}\boldsymbol{M}_2^{\mathrm{sca}} \end{bmatrix} - \bar{\boldsymbol{S}}_{22} \cdot \bar{\boldsymbol{T}}_{21} \cdot \begin{bmatrix} \boldsymbol{J}_1^{\mathrm{sca}} \\ \frac{1}{\eta}\boldsymbol{M}_1^{\mathrm{sca}} \end{bmatrix} = \bar{\boldsymbol{S}}_{22} \cdot \begin{bmatrix} \boldsymbol{J}_2^{\mathrm{inc}} \\ \frac{1}{\eta}\boldsymbol{M}_2^{\mathrm{inc}} \end{bmatrix} \tag{4.48}$$

By using (4.47) and (4.48), we can obtain matrix equation as

$$\begin{bmatrix} \bar{\boldsymbol{I}} & -\bar{\boldsymbol{S}}_{11} \cdot \bar{\boldsymbol{T}}_{12} \\ -\bar{\boldsymbol{S}}_{22} \cdot \bar{\boldsymbol{T}}_{21} & \bar{\boldsymbol{I}} \end{bmatrix} \cdot \begin{bmatrix} \boldsymbol{C}_1^{sca} \\ \boldsymbol{C}_2^{sca} \end{bmatrix} = \begin{bmatrix} \bar{\boldsymbol{S}}_{11} \cdot \boldsymbol{C}_1^{inc} \\ \bar{\boldsymbol{S}}_{22} \cdot \boldsymbol{C}_2^{inc} \end{bmatrix}. \tag{4.49}$$

Here $\bar{\boldsymbol{I}}$ is the identity operator, and

$$\begin{bmatrix} \boldsymbol{C}_l^{sca} \end{bmatrix} = \begin{bmatrix} \boldsymbol{J}_l^{sca} \\ \frac{1}{\eta}\boldsymbol{M}_l^{sca} \end{bmatrix} \tag{4.50}$$

$$\begin{bmatrix} \boldsymbol{C}_l^{inc} \end{bmatrix} = \begin{bmatrix} \boldsymbol{J}_l^{inc} \\ \frac{1}{\eta}\boldsymbol{M}_l^{inc} \end{bmatrix}, \tag{4.51}$$

where $l = 1, 2$.

By generalizing the algorithm for an arbitrary number of scatterers and ESs, the equivalent scattered currents satisfy

$$\begin{bmatrix} \boldsymbol{J}_l^{\mathrm{sca}} \\ \frac{1}{\eta}\boldsymbol{M}_l^{\mathrm{sca}} \end{bmatrix} = \bar{\boldsymbol{S}}_{ll} \cdot \begin{bmatrix} \boldsymbol{J}_l^{\mathrm{inc}} \\ \frac{1}{\eta}\boldsymbol{M}_l^{\mathrm{inc}} \end{bmatrix} + \bar{\boldsymbol{S}}_{ll} \cdot \left(\sum_{k=l,k\neq l}^{L} \bar{\boldsymbol{T}}lk \cdot \begin{bmatrix} \boldsymbol{J}_k^{\mathrm{sca}} \\ \frac{1}{\eta}\boldsymbol{M}_k^{\mathrm{sca}} \end{bmatrix} \right), \tag{4.52}$$

where

$$\bar{\boldsymbol{S}}_{ll} \begin{bmatrix} \boldsymbol{J}_l^{\mathrm{inc}} \\ \frac{1}{\eta}\boldsymbol{M}_l^{\mathrm{inc}} \end{bmatrix}$$

is the direct scattering of the incident fields, and

$$\sum_{k=l,k\neq l}^{L} \bar{\boldsymbol{T}}_{lk} \cdot \begin{bmatrix} \boldsymbol{J}_k^{\mathrm{sca}} \\ \frac{1}{\eta}\boldsymbol{M}_k^{\mathrm{sca}} \end{bmatrix}$$

represents the secondary scattering effect by using $\bar{\boldsymbol{T}}_{lk}$.

(4.52) can be cast into a matrix equation as follows

$$\begin{bmatrix} \bar{\boldsymbol{I}} & -\bar{\boldsymbol{S}}_{11}\cdot\bar{\boldsymbol{T}}_{12} & \dots & -\bar{\boldsymbol{S}}_{11}\cdot\bar{\boldsymbol{T}}_{1L} \\ -\bar{\boldsymbol{S}}_{22}\cdot\bar{\boldsymbol{T}}_{21} & \bar{\boldsymbol{I}} & & -\bar{\boldsymbol{S}}_{22}\cdot\bar{\boldsymbol{T}}_{2L} \\ \vdots & & \ddots & \vdots \\ \bar{\boldsymbol{S}}_{LL}\cdot\bar{\boldsymbol{T}}_{L1} & \dots & & \bar{\boldsymbol{I}} \end{bmatrix} \cdot \begin{bmatrix} \boldsymbol{C}_1^{sca} \\ \boldsymbol{C}_2^{sca} \\ \vdots \\ \boldsymbol{C}_L^{sca} \end{bmatrix} = \begin{bmatrix} \bar{\boldsymbol{S}}_{11}\cdot\boldsymbol{C}_1^{inc} \\ \bar{\boldsymbol{S}}_{22}\cdot\boldsymbol{C}_2^{inc} \\ \vdots \\ \bar{\boldsymbol{S}}_{LL}\cdot\boldsymbol{C}_L^{inc} \end{bmatrix}. \tag{4.53}$$

Finally, we obtain the system matrix of the EPA. Since all necessary scattering effects are characterized rigorously with surface integral operators, iterative update of the solution can be avoided. As a final example of EPA, we will formulate the problem depicted in Figure 4.8. While solving electromagnetic scattering problems with EPA, it is not necessary to surround all subdomains by ES. Here, PEC_1 and PEC_2 are surrounded by ES, while PEC_3 is not.

$$\begin{bmatrix} \boldsymbol{J}_1^{\mathrm{sca}} \\ \frac{1}{\eta}\boldsymbol{M}_1^{\mathrm{sca}} \end{bmatrix} - \bar{\boldsymbol{S}}_{11}\cdot\bar{\boldsymbol{T}}_{12}\cdot \begin{bmatrix} \boldsymbol{J}_2^{\mathrm{sca}} \\ \frac{1}{\eta}\boldsymbol{M}_2^{\mathrm{sca}} \end{bmatrix} - \bar{\boldsymbol{S}}_{11}\cdot\bar{\boldsymbol{T}}_{13}\cdot\boldsymbol{J}_3 = \bar{\boldsymbol{S}}_{11}\cdot \begin{bmatrix} \boldsymbol{J}_1^{\mathrm{inc}} \\ \frac{1}{\eta}\boldsymbol{M}_1^{\mathrm{inc}} \end{bmatrix} \tag{4.54}$$

$$\begin{bmatrix} \boldsymbol{J}_2^{\mathrm{sca}} \\ \frac{1}{\eta}\boldsymbol{M}_2^{\mathrm{sca}} \end{bmatrix} - \bar{\boldsymbol{S}}_{22}\cdot\bar{\boldsymbol{T}}_{21}\cdot \begin{bmatrix} \boldsymbol{J}_1^{\mathrm{sca}} \\ \frac{1}{\eta}\boldsymbol{M}_1^{\mathrm{sca}} \end{bmatrix} - \bar{\boldsymbol{S}}_{22}\cdot\bar{\boldsymbol{T}}_{23}\cdot\boldsymbol{J}_3 = \bar{\boldsymbol{S}}_{22}\cdot \begin{bmatrix} \boldsymbol{J}_2^{\mathrm{inc}} \\ \frac{1}{\eta}\boldsymbol{M}_2^{\mathrm{inc}} \end{bmatrix} \tag{4.55}$$

$$\bar{\boldsymbol{T}}_{31}\cdot \begin{bmatrix} \boldsymbol{J}_1^{\mathrm{sca}} \\ \frac{1}{\eta}\boldsymbol{M}_1^{\mathrm{sca}} \end{bmatrix} + \bar{\boldsymbol{T}}_{32}\cdot \begin{bmatrix} \boldsymbol{J}_2^{\mathrm{sca}} \\ \frac{1}{\eta}\boldsymbol{M}_2^{\mathrm{sca}} \end{bmatrix} + \bar{\mathcal{T}}_{33}\cdot\boldsymbol{J}_3 = -\boldsymbol{E}_3^{inc} \tag{4.56}$$

Similar equations can be derived for more objects after EPOs and TOs are setup. Note that the unknowns on ES_1 and ES_2 are the scattered currents instead of the total currents. This is because the incident currents on an ES generate zero field outside due to extinction theorem.

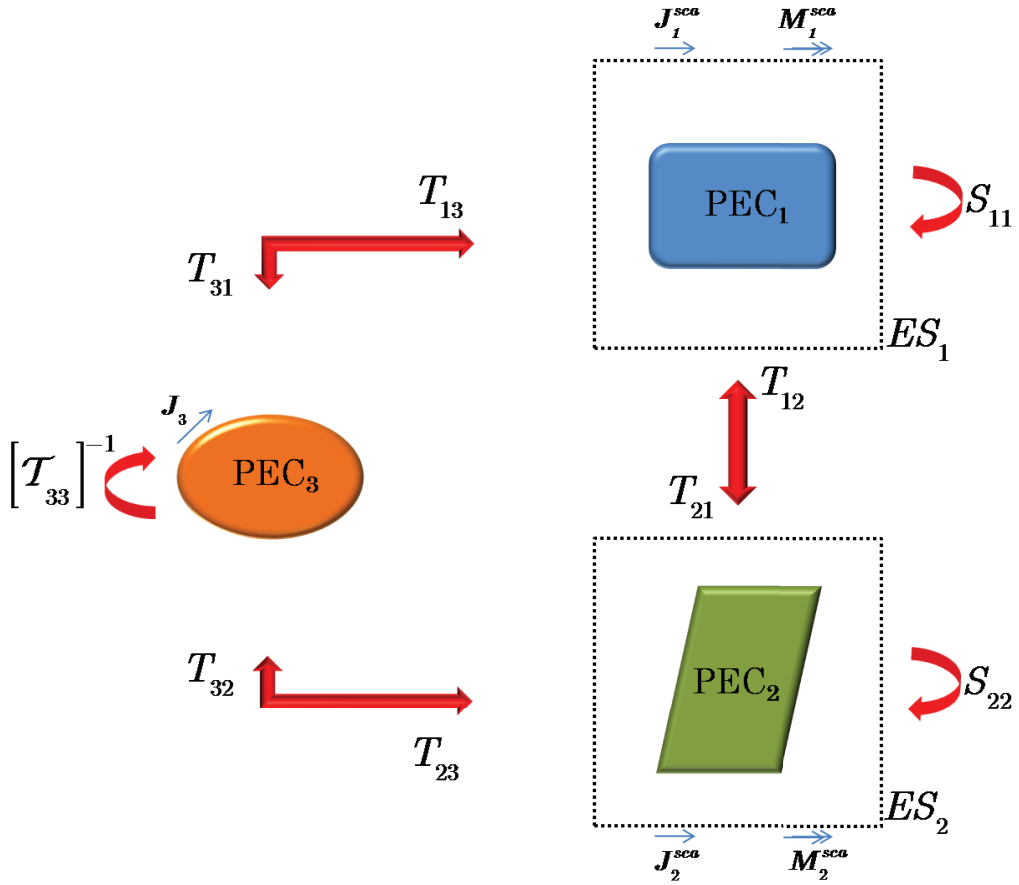

Figure 4.8: Example of the interactions among two ESs and one PEC.

4.4 Numerical Results

To validate the EPA program, the scattered field of a PEC sphere with a radius of 0.5 m. The incident wave, which is a planewave that propagates in $-\hat{z}$ direction illuminates the sphere at 300 MHz. The radar-cross-section (RCS) in different cuts is shown in Figure 4.9. The results are compared with Mie series solutions. ES is selected as sphere with a radius of 0.75λ. This example validates the EPA program for one-object scattering problem.

As a next example, RCS of a PEC cube with edge length of 0.1λ is computed and validated with MLFMA result. In this example, ES is selected as a cube with edge length of 0.2λ. Results are demonstrated in Figure 4.10.

To show the accuracy of EPA for multi-object scattering, we calculate RCS from two PEC cubes. The distance between PEC cubes is 1λ and both of them has edge length of 1λ. ESs are identical and both of them has edge length of 1.5λ. Results of EPA and MLFMA are presented in Figure 4.11. We present the results in three cuts, which are x-y cut, x-z cut, and y-z cut. On x-y cut $\theta = 90^\circ$ and ϕ changes from 0° to 360° as the bistatic angle. For x-z cut $\phi = 0^\circ$ and θ changes from 0° to 180°, while for y-z cut $\phi = 90^\circ$ and θ changes from 0° to 180° as the bistatic angle. By the time, θ is the angle defined from z-axis and ϕ is the angle defined from x-axis.

4.5 Accuracy Tests

While defining the equivalent problem there is no approximation to cause an additional error, so EPA is an accurate method. However, some parameters effect the accuracy of the EPA solution. We will investigate these parameters for both one-object and multi-object scattering problems.

While solving one-object scattering problem, two parameters effect the accuracy of the solution. These are,

- The distance between ES and the PEC object,
- Mesh-size of the ES.

In addition to these parameters, the distance between ESs effect the accuracy of the solution, while solving multi-object scattering problem.

To investigate the first parameter, PEC cube with edge length of 0.1λ is chosen. Then, by using nine ESs, each of which have different edge lengths, we have calculated RCS and compared with MLFMA results. Edge lengths of ESs are

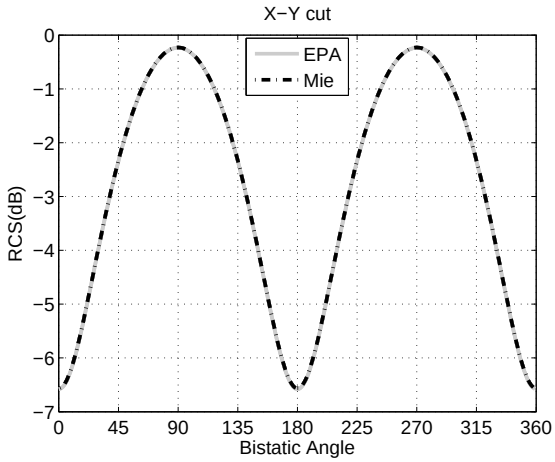

(a)

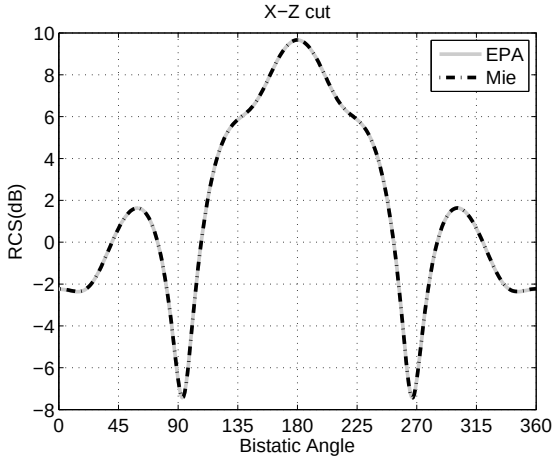

(b)

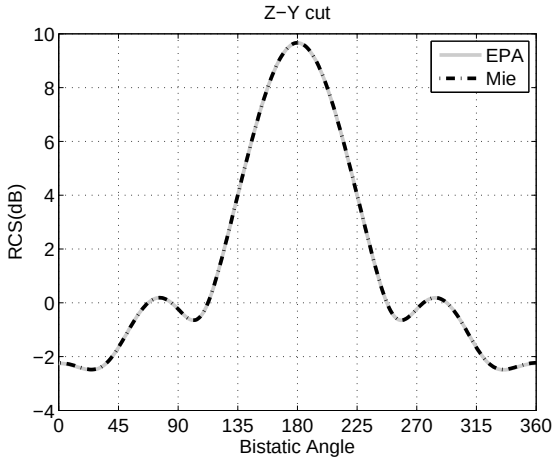

(c)

Figure 4.9: RCS of PEC sphere: (a) x-y cut, (b) x-z cut, and (c) y-z cut.

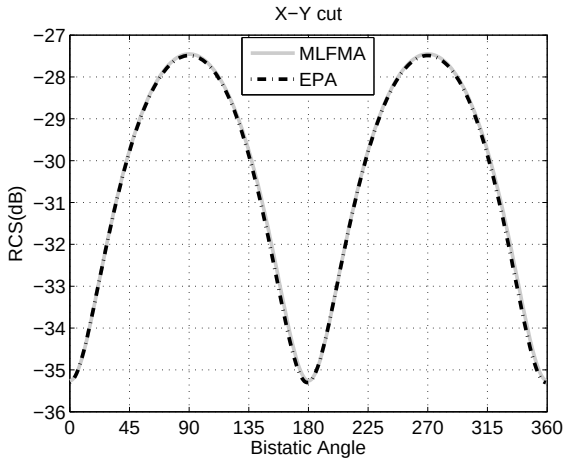

(a)

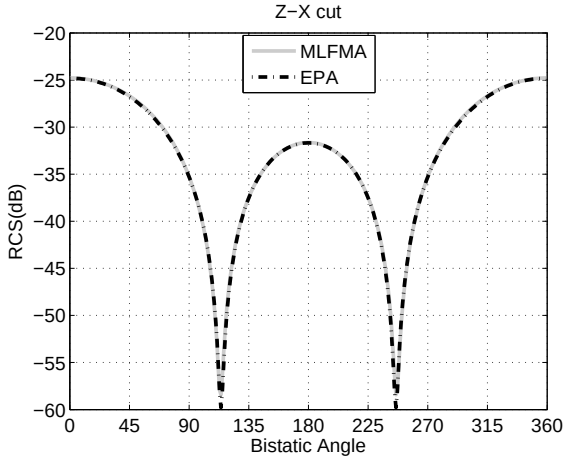

(b)

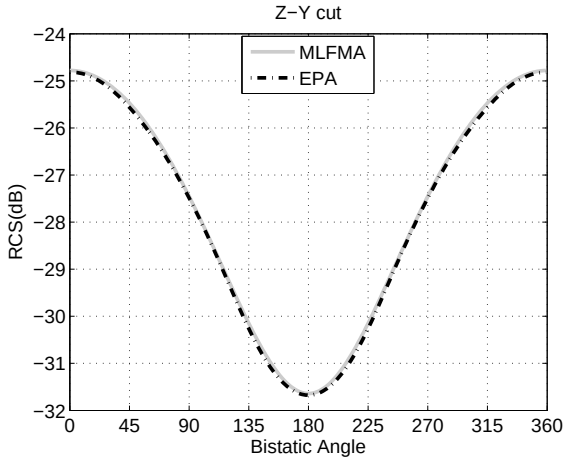

(c)

Figure 4.10: RCS of PEC cube: (a) x-y cut, (b) x-z cut, and (c) y-z cut.

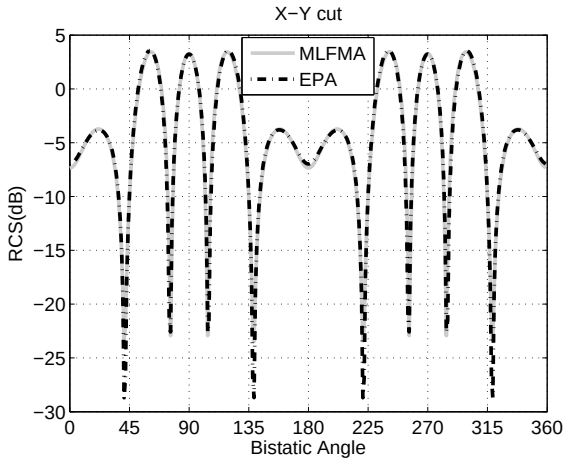

(a)

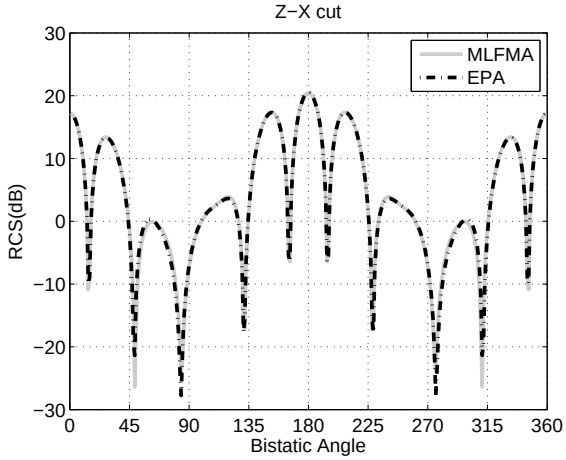

(b)

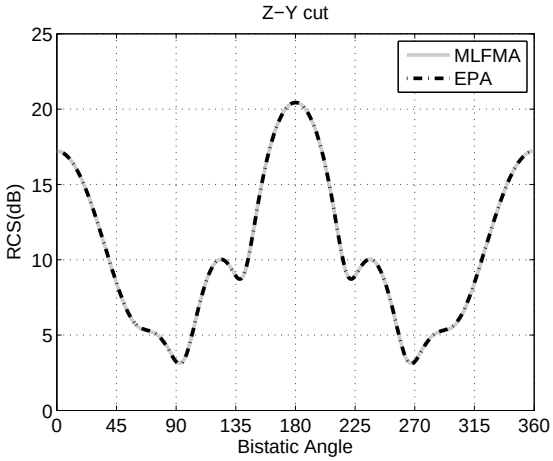

(c)

Figure 4.11: RCS of two PEC cubes: (a) x-y cut, (b) x-z cut, and (c) y-z cut.

chosen as follows: $ES_1 = 0.2\lambda$, $ES_2 = 0.3\lambda$, $ES_3 = 0.4\lambda$, $ES_4 = 0.5\lambda$, $ES_5 = 0.6\lambda$, $ES_6 = 0.7\lambda$, $ES_7 = 0.8\lambda$, $ES_8 = 0.9\lambda$, and $ES_9 = 1.0\lambda$.

The relative error as a function of bistatic angle (θ, ϕ) is defined as

$$\triangle_R(\theta,\phi) = \frac{|\mathrm{RCS}_{\mathrm{ref}}(\theta,\phi) - \mathrm{RCS}_{\mathrm{calc}}(\theta,\phi)|}{\max|\mathrm{RCS}_{\mathrm{ref}}(\theta,\phi)|}, \tag{4.57}$$

where $\mathrm{RCS}_{\mathrm{ref}}$ and $\mathrm{RCS}_{\mathrm{calc}}$ are calculated by using reference solvers (MLFMA, MoM, or Mie series solutions) and by using EPA solver, respectively. As presented in Figures 4.12–4.14, as the distance between ES and the PEC object is increased, accuracy of the solution also increases. For the investigation of the second parameter, edge length of the PEC cube and ES is chosen as 0.2λ and 0.4λ, respectively. Different mesh sizes are applied to ES, such that, $\mathrm{mesh}_1 = \lambda/5$, $\mathrm{mesh}_2 = \lambda/10$, $\mathrm{mesh}_3 = \lambda/20$, and $\mathrm{mesh}_4 = \lambda/40$. As the mesh size on ES is decreased, accuracy of the solution increases. For each of the mesh sizes RCS result are presented in Figures 4.15–4.17.

Finally, to investigate the last parameter, edge length of the PEC cube and ES is chosen as 1.0λ and 1.5λ, respectively. The distance between ESs are chosen to be 0.3λ, 0.4λ, and 0.5λ.

If the distance between ESs is increased, the accuracy of the solution also increases, as shown in Figures 4.18-4.20.

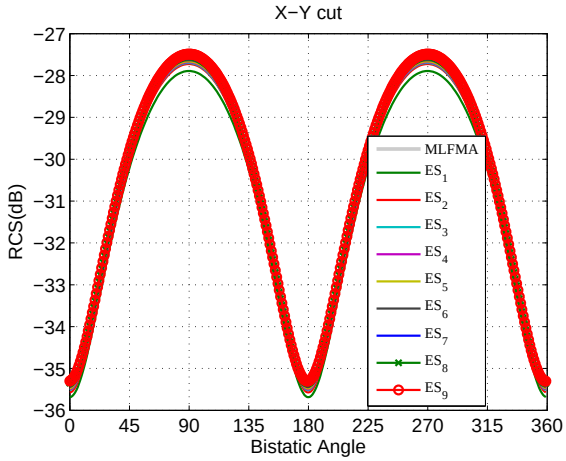

(a)

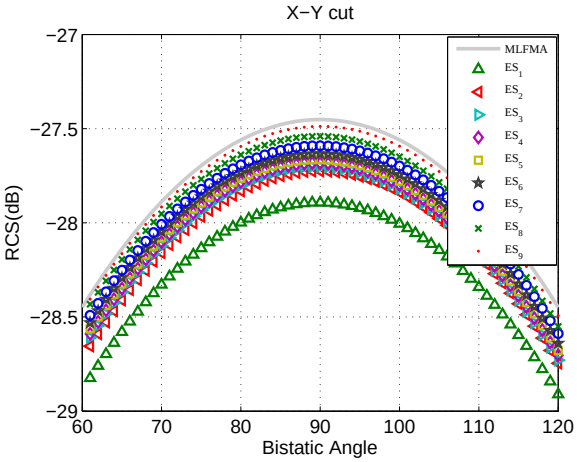

(b)

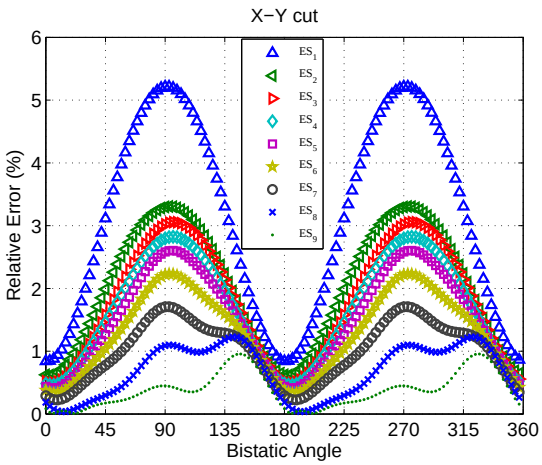

(c)

Figure 4.12: Accuracy test for different size of ESs: (a) RCS (x-y cut) of PEC cube, (b) RCS of PEC cube, and (c) relative error.

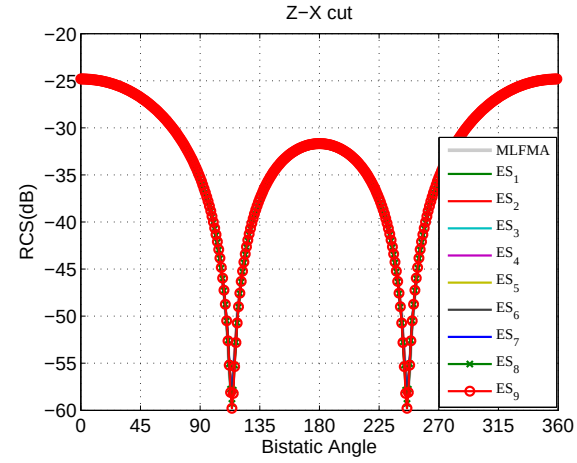

(a)

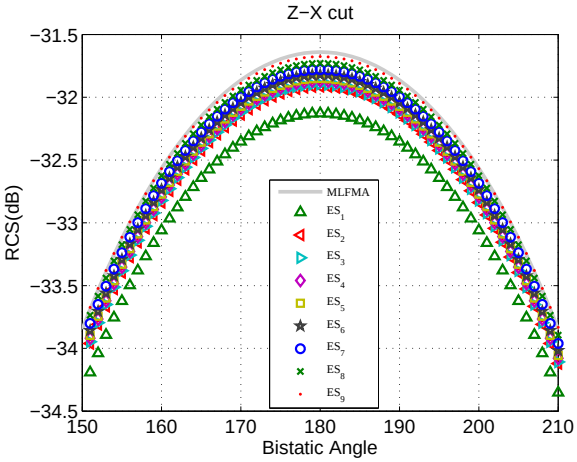

(b)

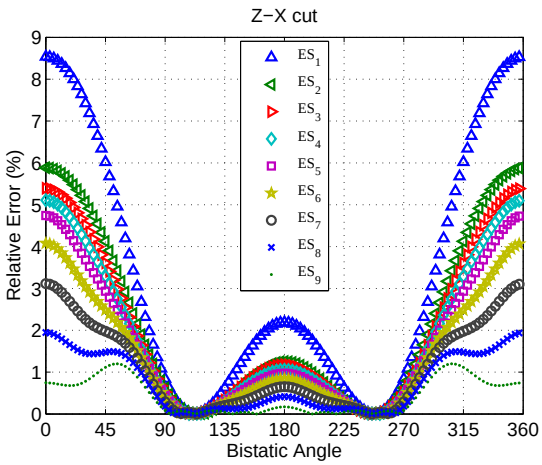

(c)

Figure 4.13: Accuracy test for different size of ESs: (a) RCS of (z-x cut) PEC cube, (b) RCS of PEC cube, and (c) relative error.

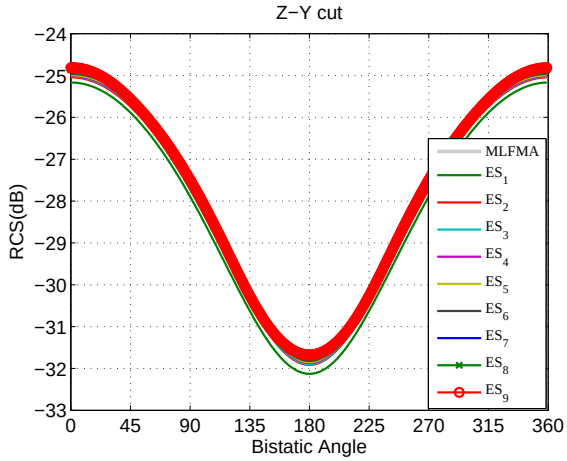

(a)

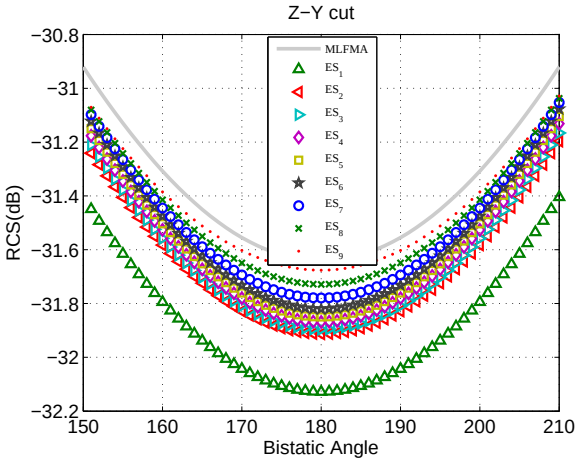

(b)

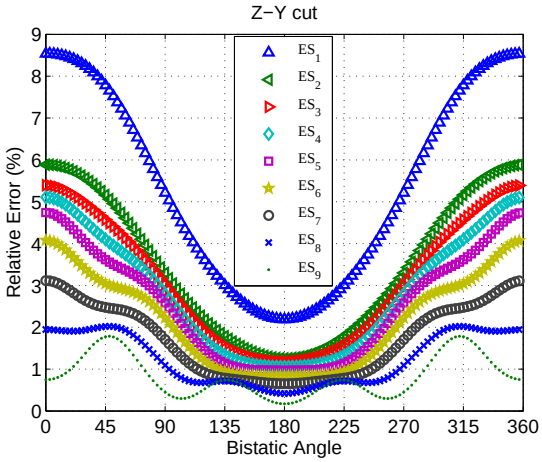

(c)

Figure 4.14: Accuracy test for different size of ESs: (a) RSC of (z-y cut) PEC cube, (b) RCS of PEC cube, and (c) relative error.

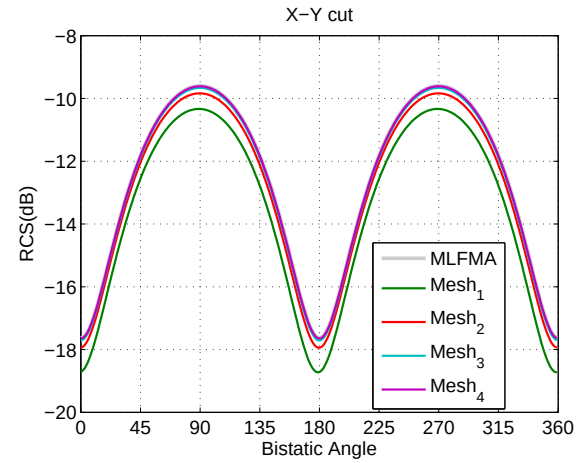

(a)

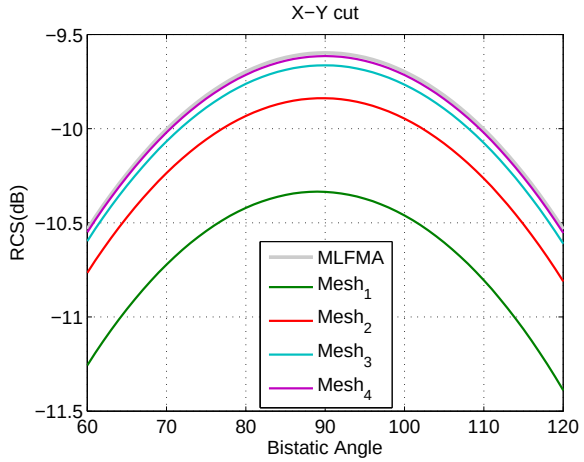

(b)

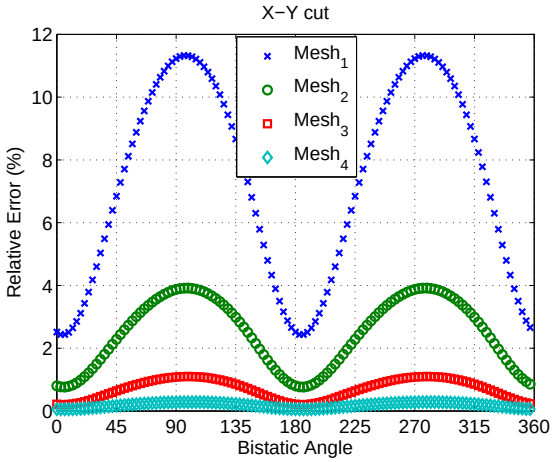

(c)

Figure 4.15: Accuracy test for different mesh size: (a) RCS (x-y cut) of PEC cube, (b) RCS of PEC cube, and (c) relative error.

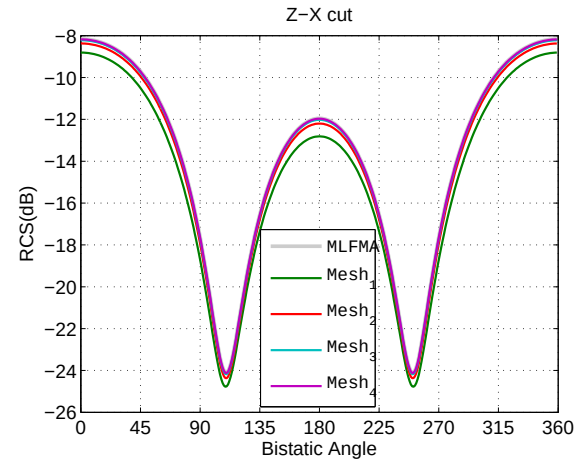

(a)

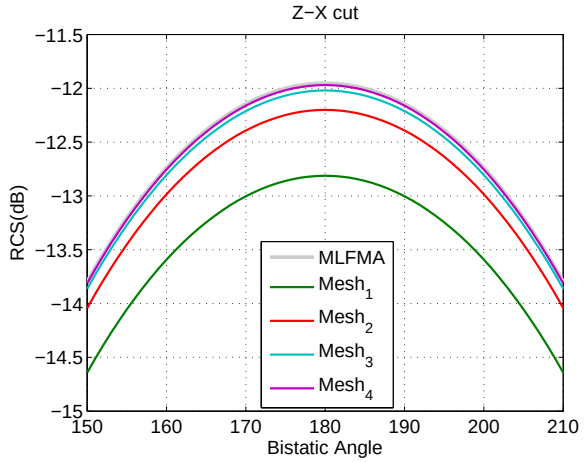

(b)

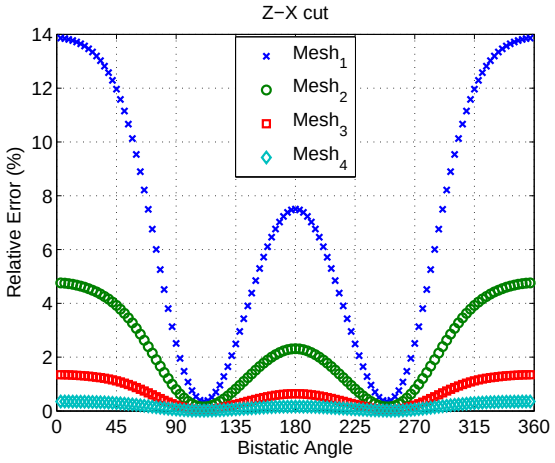

(c)

Figure 4.16: Accuracy test for different mesh size: (a) RCS of (z-x cut) PEC cube, (b) RCS of PEC cube, and (c) relative error.

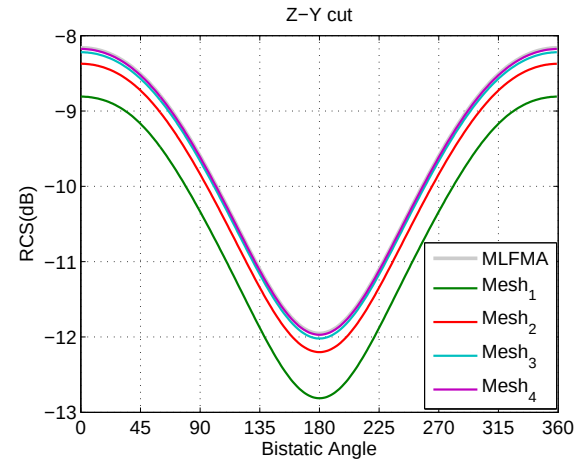

(a)

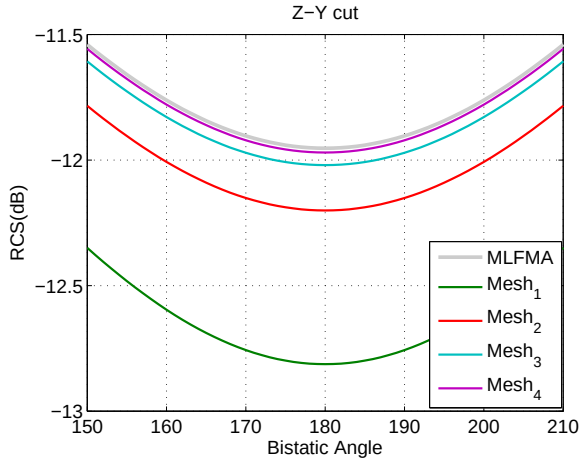

(b)

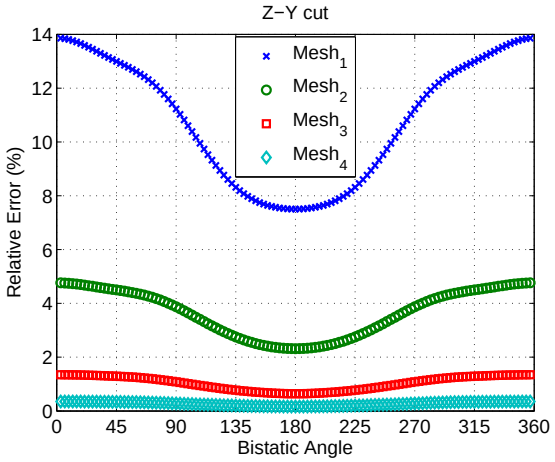

(c)

Figure 4.17: Accuracy test for different mesh size: (a) RSC of (z-y cut) PEC cube, (b) RCS of PEC cube, and (c) relative error.

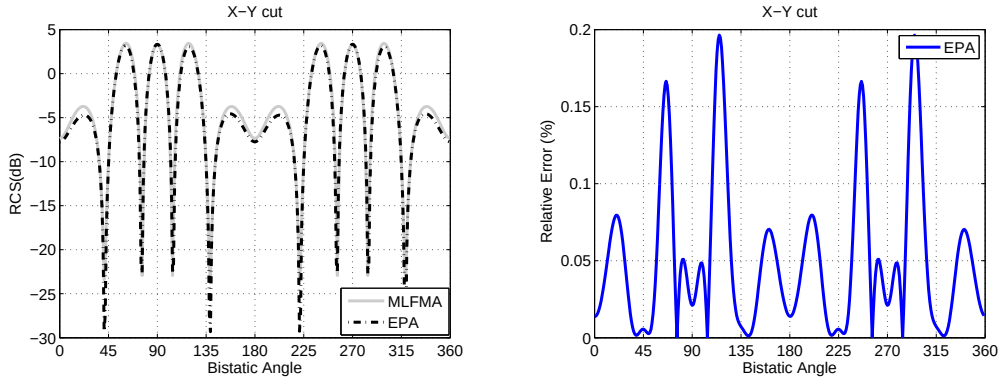

Figure 4.18: RCS results, distances between ESs is 0.5λ: (a) x-y cut, (b) relative error of x-y cut, (c) z-x cut, (d) relative error of z-x cut, (e) z-y cut, and (f) relative error of z-y cut.

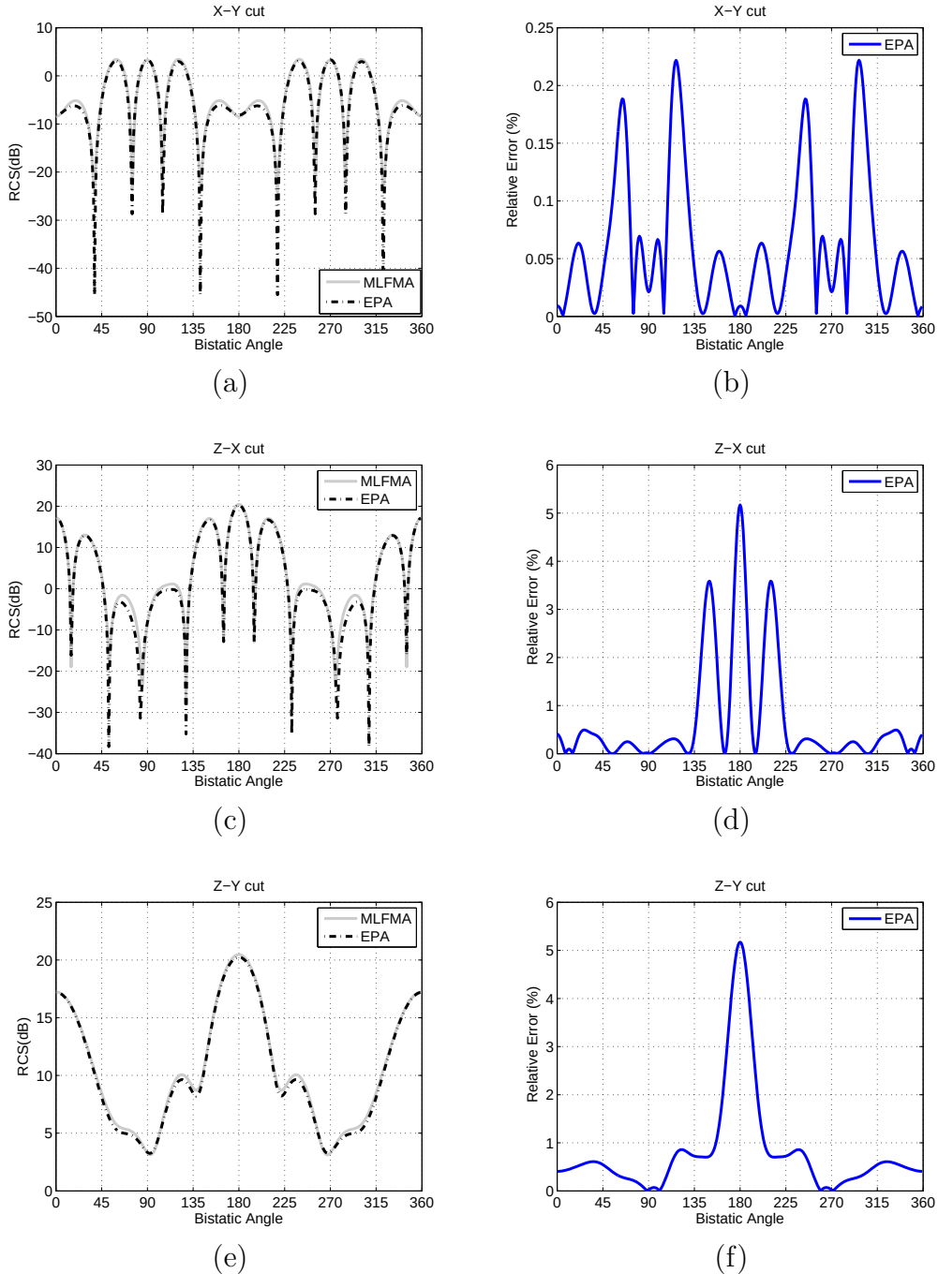

Figure 4.19: RCS results, distances between ESs is 0.4λ: (a) x-y cut, (b) relative error of x-y cut, (c) z-x cut, (d) relative error of z-x cut, (e) z-y cut, and (f) relative error of z-y cut.

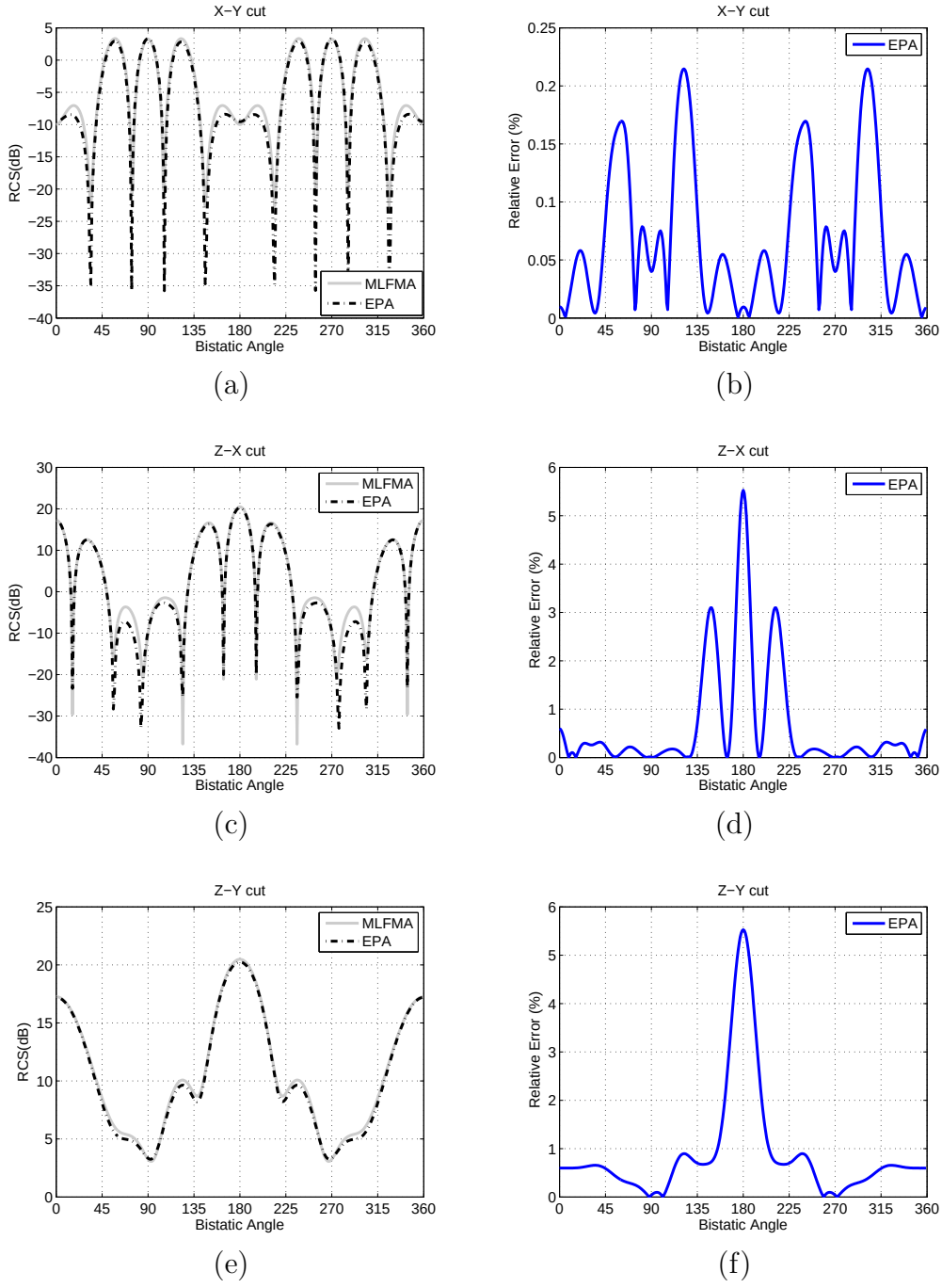

Figure 4.20: RCS results, distances between ESs is 0.3λ: (a) x-y cut, (b) relative error of x-y cut, (c) z-x cut, (d) relative error of z-x cut, (e) z-y cut, and (f) relative error of z-y cut.

Chapter 5

Tangential Equivalence Principle Algorithm

In order to discretize the surface operators, we have used RWG functions and we applied Galerkin method, i.e., using the same set of functions for expanding current densities and for testing boundary conditions. We have employed two types of testing, which are normal and tangential testing. Among these types, $\mathcal{T}$ and $\mathcal{I}$ operators are well-tested with $\boldsymbol{t}_m$. On the other hand, $\mathcal{K}$ operator is well-tested with $\hat{\boldsymbol{n}} \times \boldsymbol{t}_m$ [5].

Surface formulations result in very accurate results if they contain well-tested $\mathcal{T}$ operator. However, tangentially-tested $\mathcal{T}$ operator lead to ill-conditioned matrix equation, since it has a weakly-singular kernel. On the other hand, well-tested $\mathcal{I}$ operator is preferable in terms of efficiency, because it leads to well-conditioned matrix equation that is easy to be solved iteratively [5],[42],[43]. However, discretization of identity operator involves a large numerical error, which contaminates the accuracy of the solution [42],[44].

5.1 Formulation

Formulation of EPA requires well-tested $\mathcal{I}$ operator that contaminates the accuracy of the solution [38]. In the previous chapter, we have tested accuracy of the solution for different cases, and we have seen that accuracy of the solutions decrease for some cases:

- ES is very close to PEC object,
- ESs are very close to each other,
- Mesh size of the ES is not dense enough.

In Chapter 4, we have used (5.1) to discretize the incident currents,

$$\begin{bmatrix} \bar{\boldsymbol{I}} & 0 \\ 0 & \bar{\boldsymbol{I}} \end{bmatrix} \cdot \begin{bmatrix} \boldsymbol{J}^{inc} \\ \boldsymbol{M}^{inc} \end{bmatrix} = \begin{bmatrix} -\hat{\boldsymbol{n}} \times \boldsymbol{H}^{inc}(\boldsymbol{r}) \\ \hat{\boldsymbol{n}} \times \boldsymbol{E}^{inc}(\boldsymbol{r}) \end{bmatrix}. \tag{5.1}$$

The solution of (5.1) usually requires negligible time; however, as we told above, use of discretized identity operators deteriorate the accuracy of the results. For improving the accuracy of certain SIE formulations in the case of very low contrast objects, an alternative field projection was developed. The idea is to represent the fields with the surface integral representations by utilizing integro-differential operators [40] as,

$$\begin{bmatrix} \eta\bar{\boldsymbol{T}}_{tan} & -\bar{\boldsymbol{K}}_{tan} \\ \bar{\boldsymbol{K}}_{tan} & \eta^{-1}\bar{\boldsymbol{T}}_{tan} \end{bmatrix} \cdot \begin{bmatrix} \boldsymbol{J}^{inc} \\ \boldsymbol{M}^{inc} \end{bmatrix} = -0.5 \begin{bmatrix} \hat{\boldsymbol{n}} \times \boldsymbol{E}^{i}(\boldsymbol{r}) \\ \hat{\boldsymbol{n}} \times \boldsymbol{H}^{i}(\boldsymbol{r}) \end{bmatrix}. \tag{5.2}$$

Using (5.2) and reformulating EPA results in a new algorithm, called tangential EPA (T-EPA). The idea of T-EPA is to use (5.2) instead of (5.1) for representing the incident field and the fields defined by the scattering and translation operators, in terms of the basis functions. This formulation is completely free of identity operators. On the other hand, the improved accuracy comes at the cost of reduced efficiency since it is necessary to solve an additional matrix equation rather than an extremely sparse matrix as expressed in (5.1).

After some modifications, formulation for EPA becomes valid for T-EPA. The inside-outside propagation operator and translation operator are modified as

$$\text{inside-outside operator} : \left[\begin{array}{cc} \eta\mathcal{T}_{tan} & \mathcal{K}_{tan} \end{array} \right], \tag{5.3}$$

$$\text{translation operator} : \left[\begin{array}{cc} \eta\mathcal{T}_{tan} & -\mathcal{K}_{tan} \\ \mathcal{K}_{tan} & \eta^{-1}\mathcal{T}_{tan} \end{array} \right], \tag{5.4}$$

and the outside-inside operator remains unchanged.

5.2 Solution Accuracy

In order to validate T-EPA, we will consider the geometry depicted in Figure 5.1. The mesh on the PEC cubes contains ten subsections per edge and on the ES the

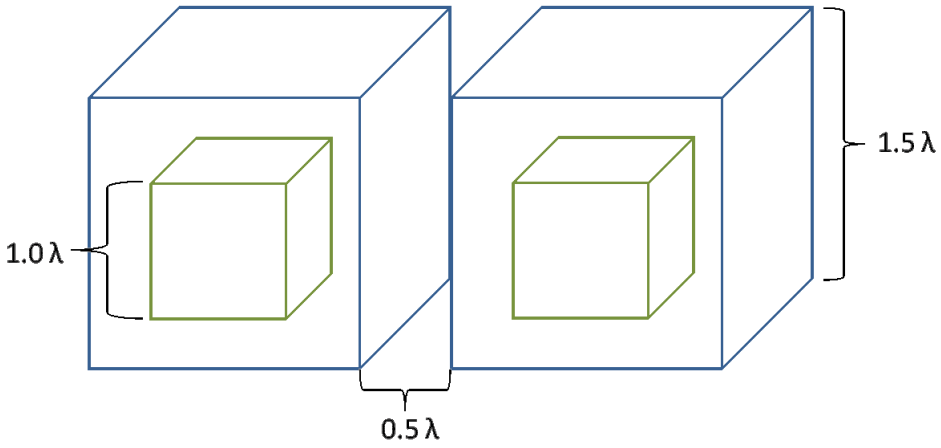

Figure 5.1: Example of the interactions among two ESs.

number of subsections is varied from three to ten. Figure 5.2 shows the forward scattered RCS calculated with MoM, EPA and T-EPA. From Figure 5.2 it can be concluded that EPA can lead to a significant loss of accuracy if the mesh on the ES is not dense enough.

As we did for EPA, we can investigate three parameters for T-EPA and compare the results with EPA. To investigate the first parameter, PEC cube with edge

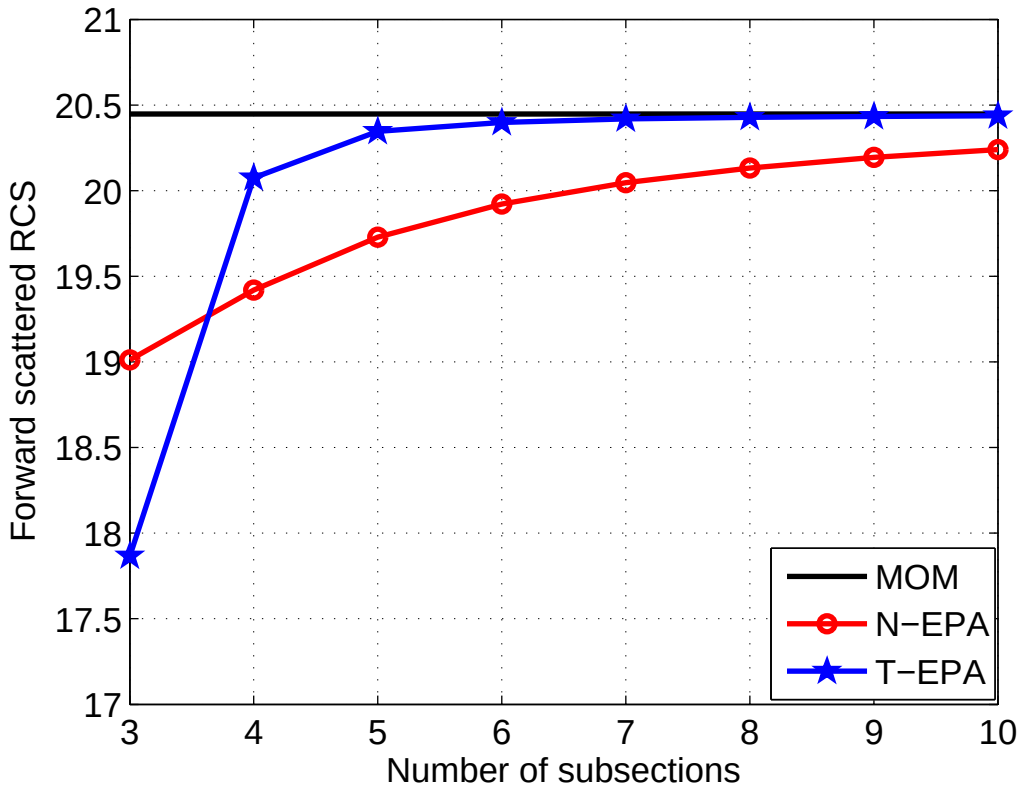

Figure 5.2: Forward scattered RCS for two PEC cubes as a function of subsections per the sides of ESs.

length of 0.1λ are chosen. Then, by using three ESs, each of which have different edge lengths, we have calculated RCS and compared results with MLFMA solutions. Edge length of these ESs are chosen as follows: $\mathrm{ES}_1 = 0.2\lambda$, $\mathrm{ES}_2 = 0.5\lambda$, and $\mathrm{ES}_3 = 1.0\lambda$.

As presented in Figures 5.3–5.5, accuracy of the solution decreases, as the distance between ES and PEC object is decreased. This is because when the ES and the PEC object get close to each other, near field of the cubes require finer sampling.

From Figure 5.3, it is seen that the average relative error for EPA is 3.11%, 3.21%, and 5.34% for x-y cut, z-x cut, and z-y cut, respectively. On the other

hand, for T-EPA the relative error is 0.33%, 0.35%, and 0.52% for x-y cut, z-x cut, and z-y cut, respectively. Also, the number of unknowns on the PEC object is 450, while the number of unknowns on ES is only 144. In the original problem, the size of the system matrix is 450×450, whereas EPA and T-EPA reduced the system matrix to the size of 144×144. Hence, the reduction in the system matrix is 90%. This means that we can solve the same problem by using with T-EPA, by using 90% less unknowns without losing accuracy.

Similarly, from Figure 5.4 it is seen that the average relative error for EPA is 1.67%, 1.79%, and 2.82% for x-y cut, z-x cut, and z-y cut, respectively. On the other hand, for T-EPA relative error is obtained as 0.07%, 0.07%, and 0.12% for x-y cut, z-x cut, and z-y cut, respectively.

Next, from Figure 5.5 it is obtained that the average relative error for EPA is 0.37%, in x-y cut, 0.42% in z-x cut, and 0.83% in z-y cut obtained. On the other hand, it is 0.03%, in x-y cut, 0.02%, in z-x cut and 0.04% in z-y cut.

Again, to investigate the second parameter, edge length of the PEC cube and ES is chosen 0.2λ and 0.4λ, respectively. Different mesh sizes are applied to ES, such that, $\text{mesh}_1 = \lambda/5$, $\text{mesh}_2 = \lambda/10$, $\text{mesh}_3 = \lambda/20$, and $\text{mesh}_4 = \lambda/40$.

As the mesh size on ES is decreased, accuracy of the solution increases as illustrated in Figures 5.6-5.8. Finally, to investigate the last parameter, edge length of the PEC cube and ES are chosen as 1.0λ and 1.5λ, respectively, and the distance between ESs are 0.3λ, 0.4λ, and 0.5λ.

Another observation from the results is that the accuracy of the solution increases if the distance between ESs is increased, as presented in Figures 5.9-5.14.

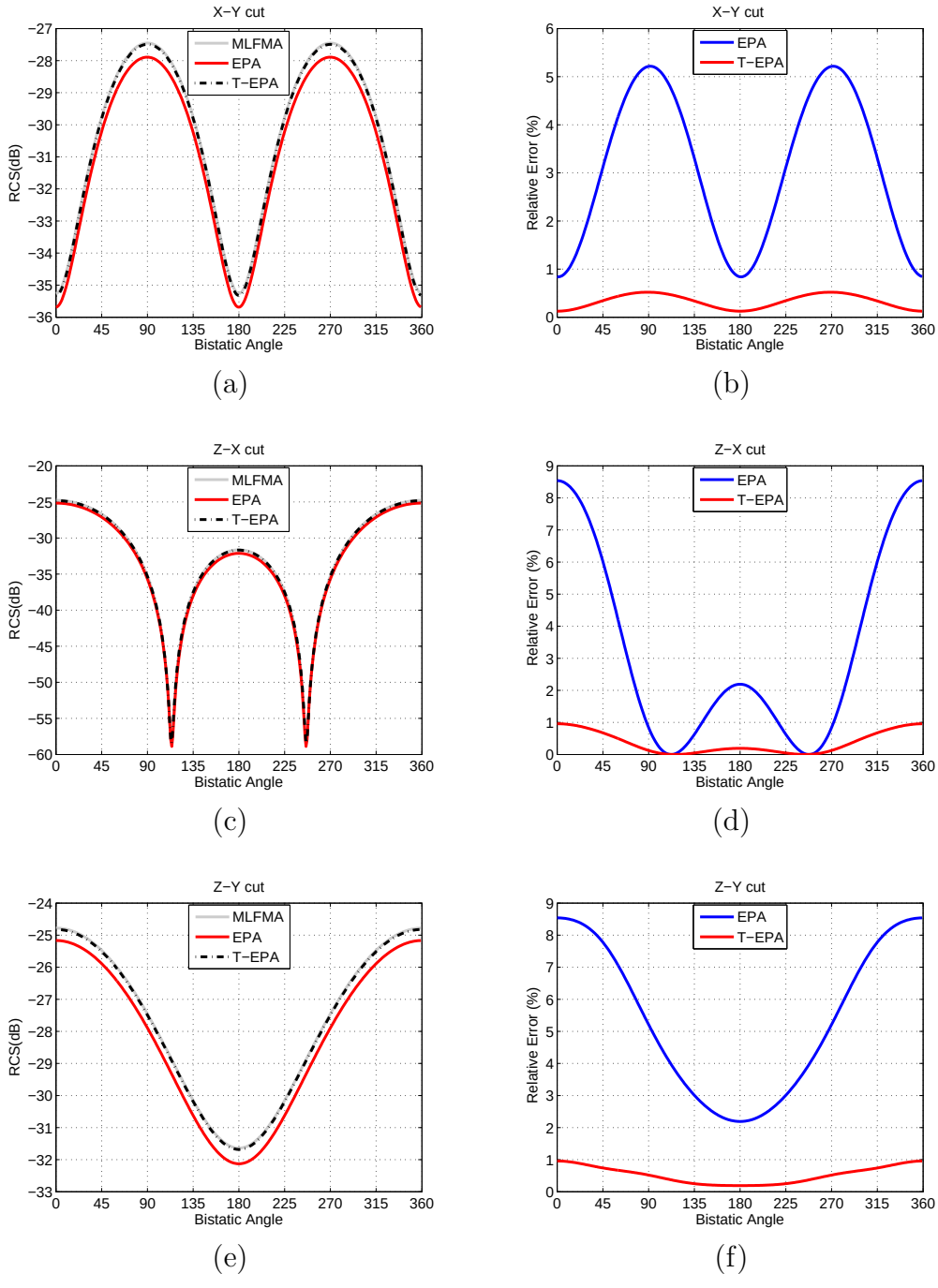

Figure 5.3: RCS results, when ES is 0.2λ: (a) x-y cut, (b) relative error of x-y cut, (c) z-x cut, (d) relative error of z-x cut, (e) z-y cut, and (f) relative error of z-y cut.

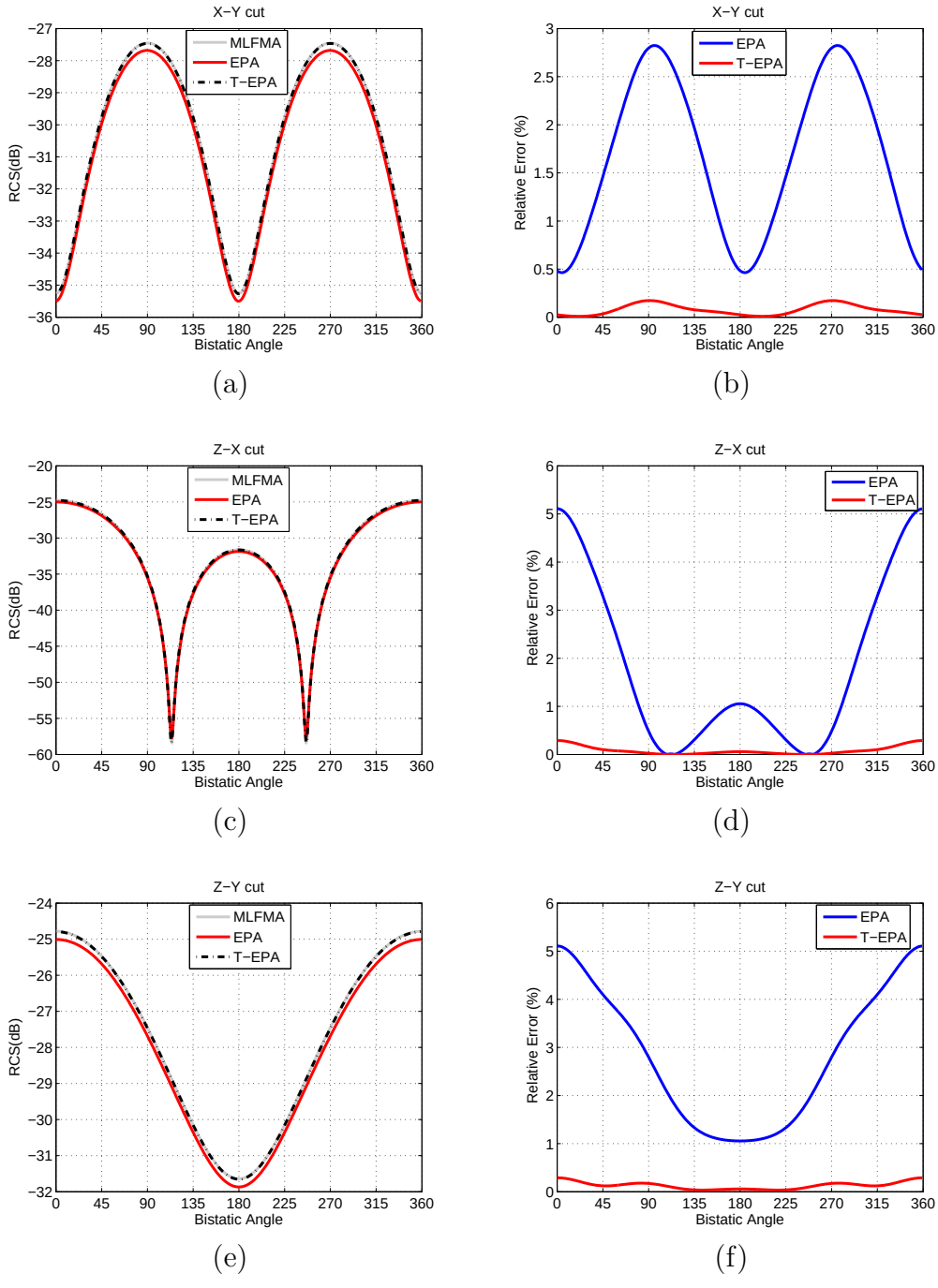

Figure 5.4: RCS results, when ES is 0.5λ: (a) x-y cut, (b) relative error of x-y cut, (c) z-x cut, (d) relative error of z-x cut, (e) z-y cut, and (f) relative error of z-y cut.

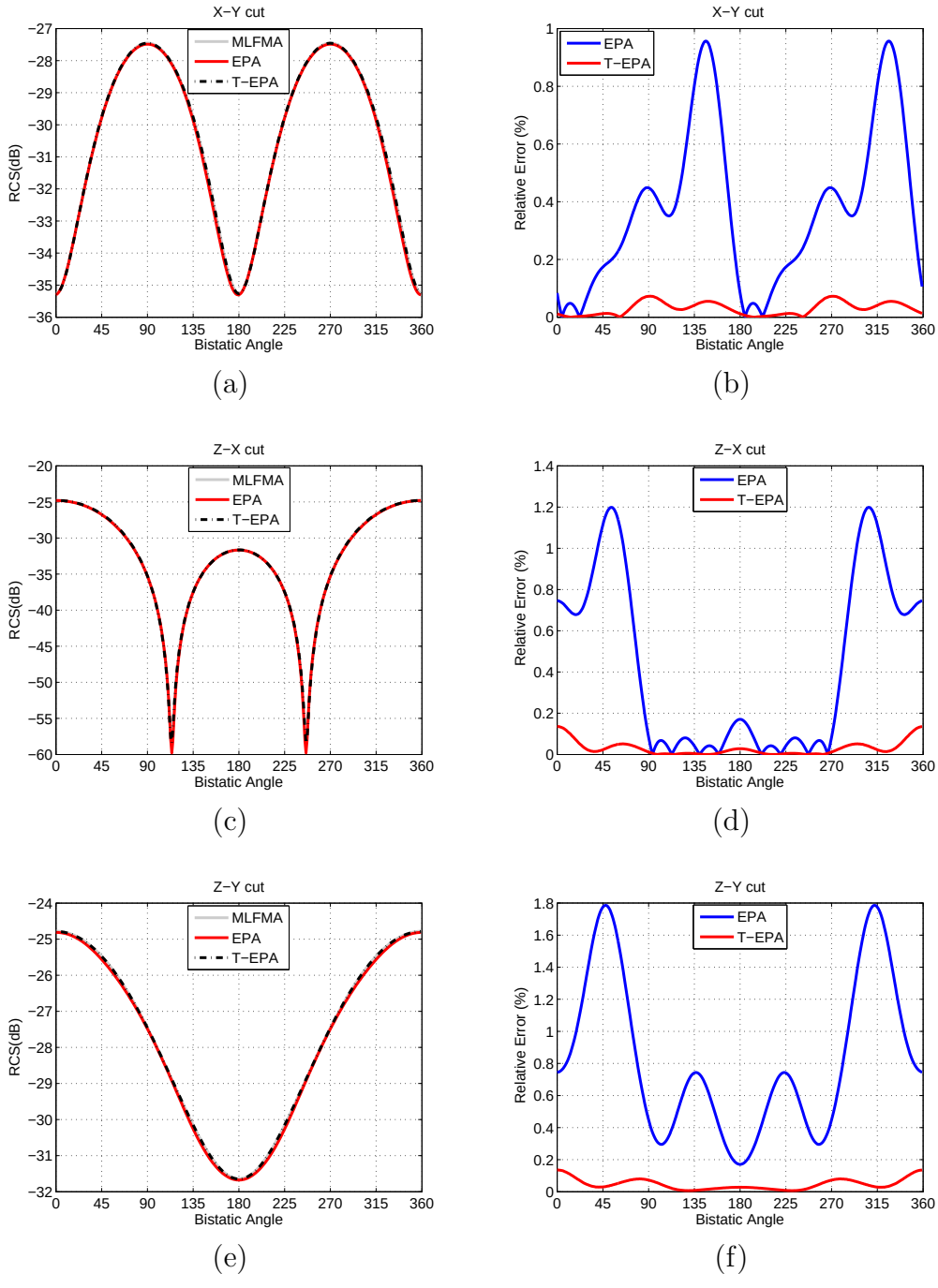

Figure 5.5: RCS results, when ES is 1.0λ: (a) x-y cut, (b) relative error of x-y cut, (c) z-x cut, (d) relative error of z-x cut, (e) z-y cut, and (f) relative error of z-y cut.

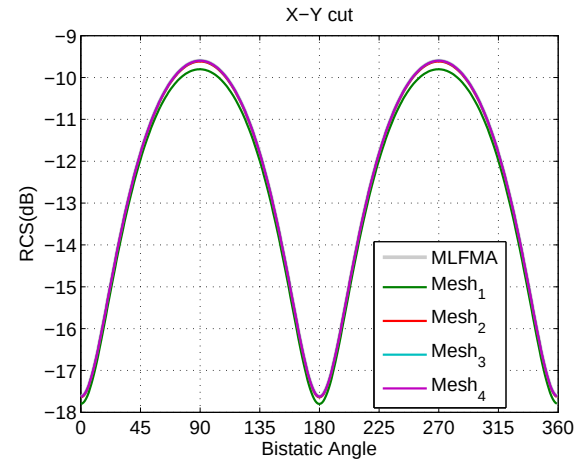

(a)

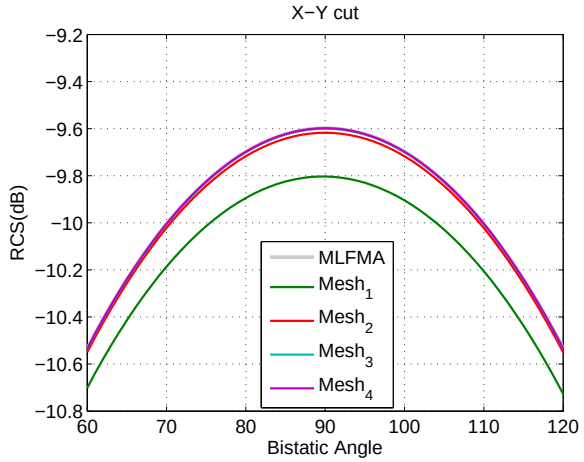

(b)

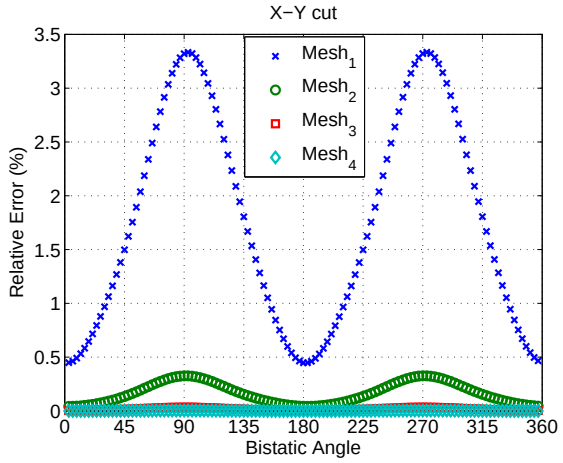

(c)

Figure 5.6: Accuracy test for different mesh size: (a) RCS (x-y cut) of PEC cube, (b) RCS of PEC cube, and (c) relative error.

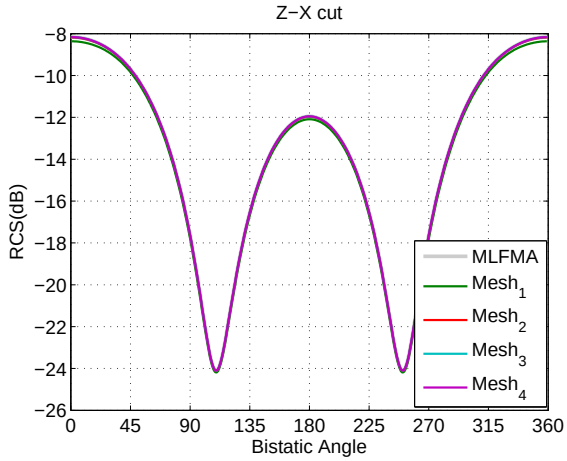

(a)

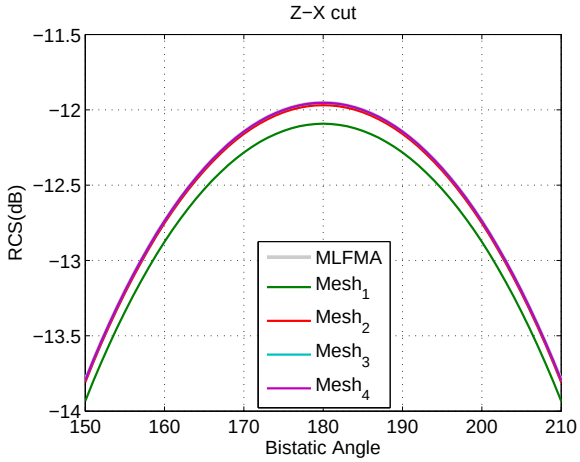

(b)

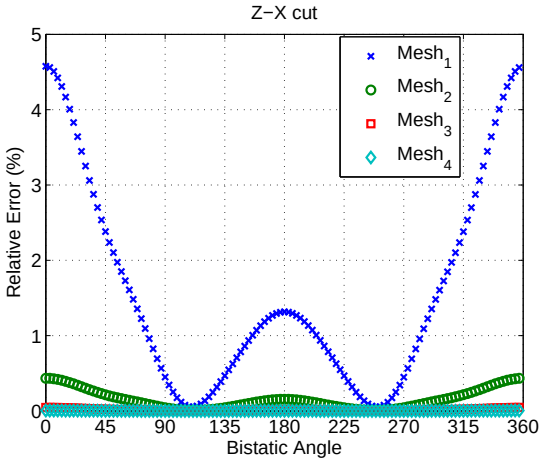

(c)

Figure 5.7: Accuracy test for different mesh size: (a) RCS (z-x cut) of PEC cube, (b) RCS of PEC cube, and (c) relative error.

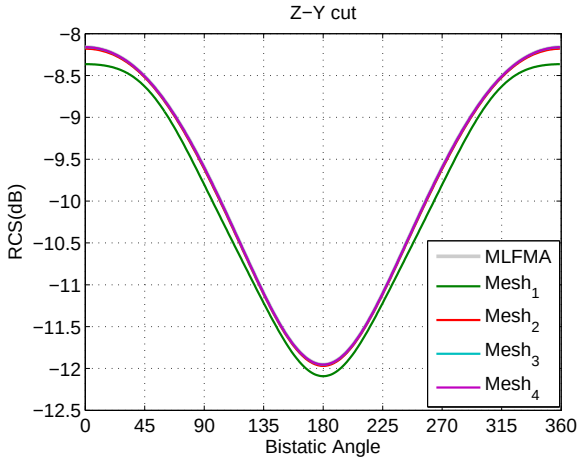

(a)

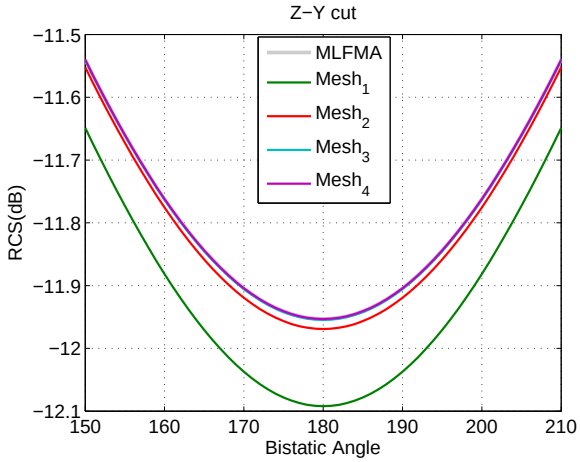

(b)

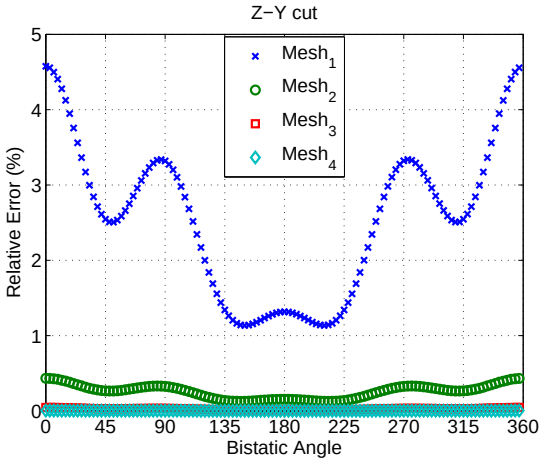

(c)

Figure 5.8: Accuracy test for different mesh size: (a) RCS (z-y cut) of PEC cube, (b) RCS of PEC cube, and (c) relative error.

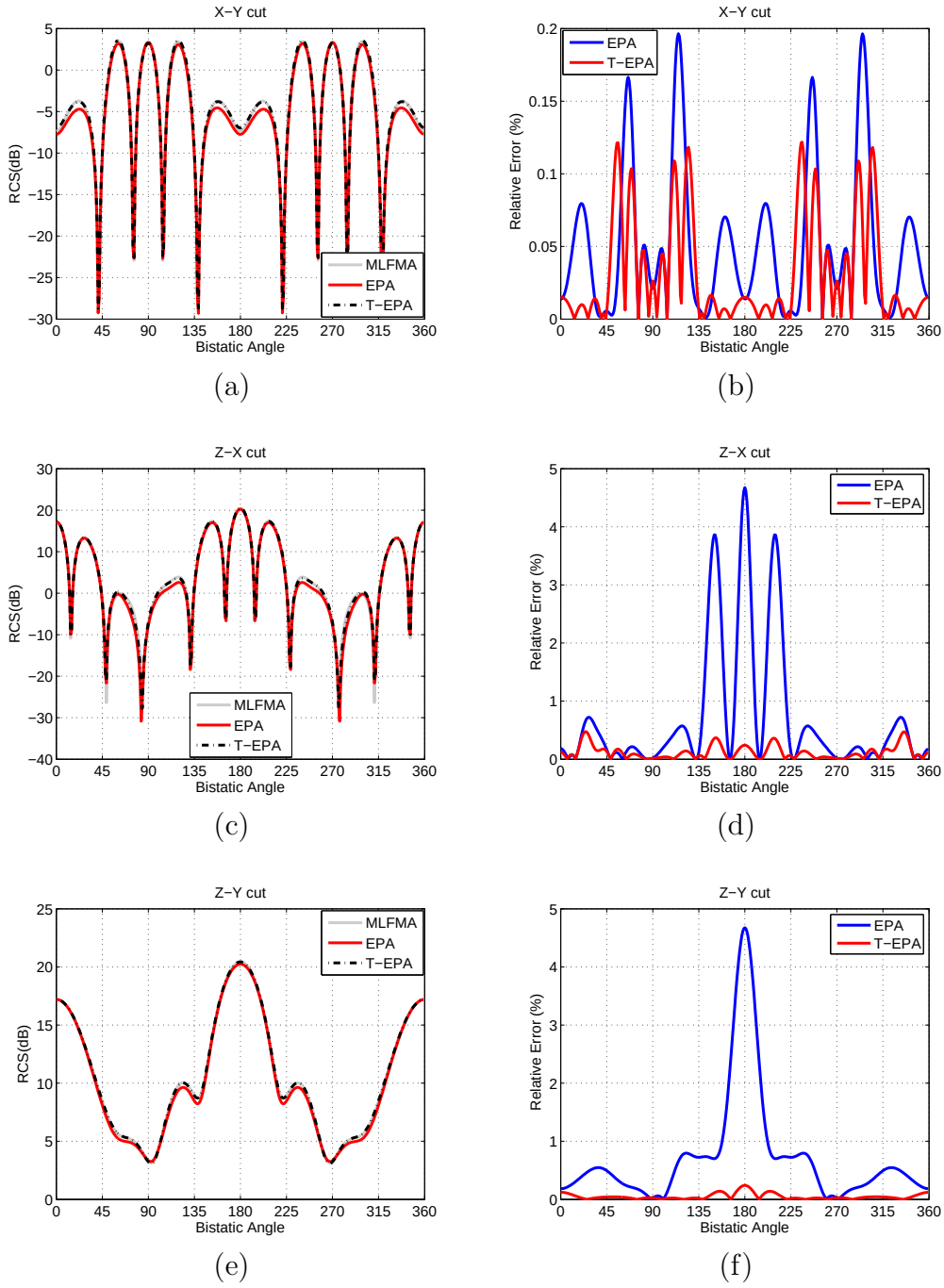

Figure 5.9: RCS results, distances between ESs is 0.5λ: (a) x-y cut, (b) relative error of x-y cut, (c) z-x cut, (d) relative error of z-x cut, (e) z-y cut, and (f) relative error of z-y cut.

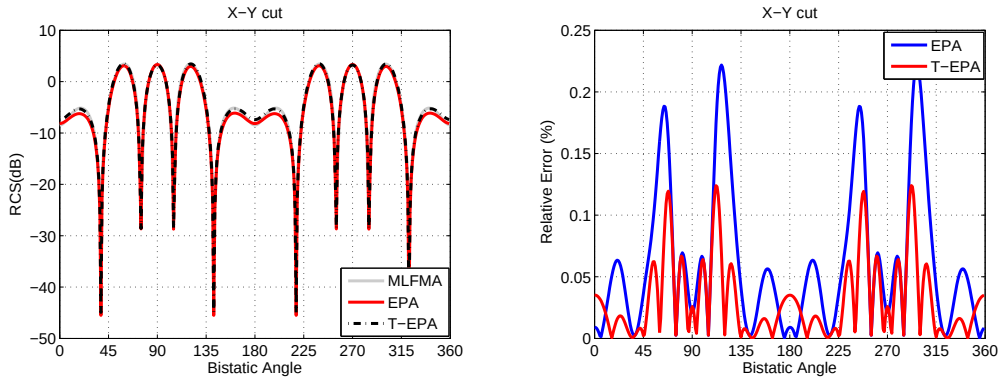

(a)

(b)

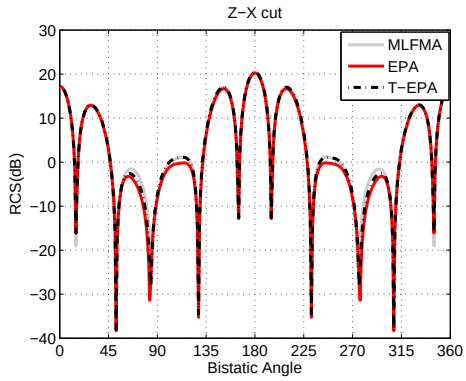

(c)

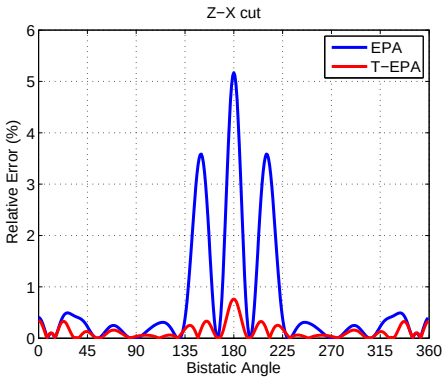

(d)

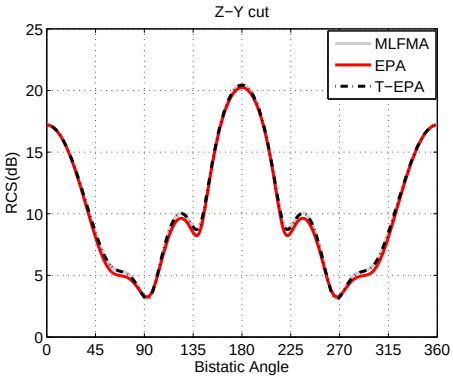

(e)

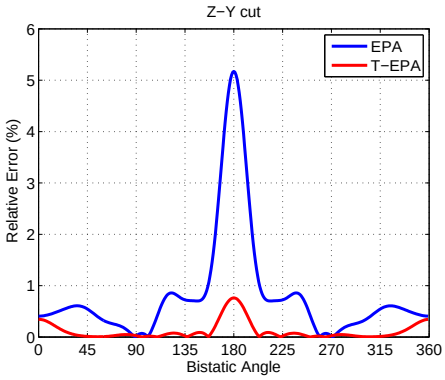

(f)

Figure 5.10: RCS results, distances between ESs is 0.4λ: (a) x-y cut, (b) relative error of x-y cut, (c) z-x cut, (d) relative error of z-x cut, (e) z-y cut, and (f) relative error of z-y cut.

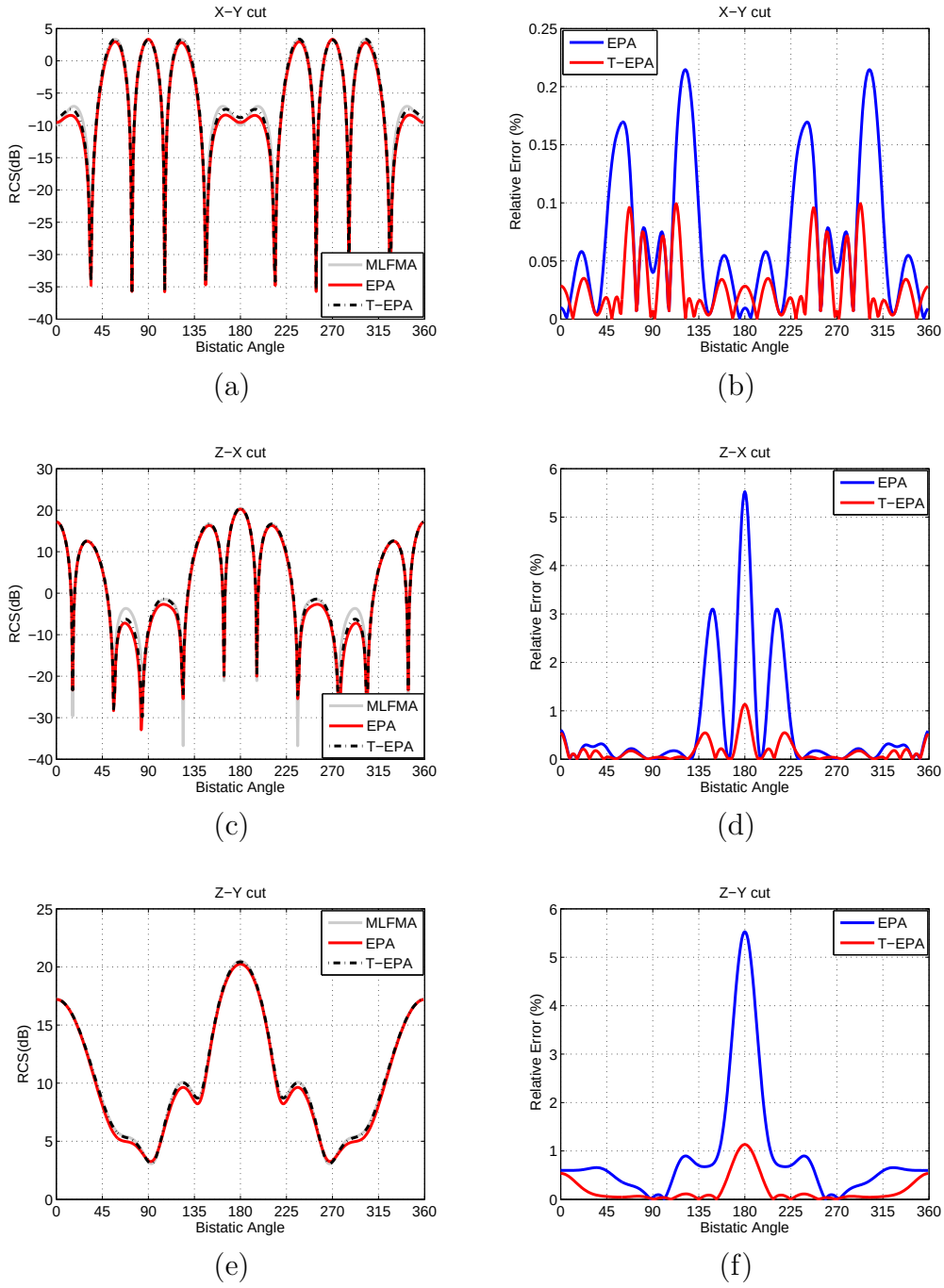

Figure 5.11: RCS results, distances between ESs is 0.3λ: (a) x-y cut, (b) relative error of x-y cut, (c) z-x cut, (d) relative error of z-x cut, (e) z-y cut, and (f) relative error of z-y cut.

The following numerical examples investigated in this research are related with metamaterials (MMs). There are two major difficulties encountered in solving MMs with conventional fast solvers. The first one is, MMs exhibit resonances, leading to ill-conditioned matrices that are difficult to solve. And the second problem is, MMs usually involve small geometric details with respect to wavelength, whereas their overall sizes are in the orders of the wavelength. When we used MLFMA to solve MMs, convergence is not achieved, especially at resonance frequencies. So, the efficiency of the algorithm may deteriorate significantly.

The first example presents the power transmission properties of split-ring resonators (SRRs), which are shown in Figure 4.1. The scattering problem is formulated with T-EPA, and EFIE is used to the solve current on the SRRs. Dimensions of a single SRR is as follows: the smaller ring has 43 μm inner radius and 67.2 μm outer radius, the larger ring has 80.7 μm inner radius and 107.5 μm outer radius, and the gap width is 7 μm. The SRR arrays are obtained by arranging SRRs with periodicities of 262.7 μm in the y direction, and 450 μm in the z direction. The structures are embedded into homogeneous host medium with a relative permittivity of 4.8. The incident field is generated by a Hertzian dipole located at $x = 1.2$ mm. Details of the first problem is depicted in Figure 5.12, more details can be found in [45].

Figure 5.13 presents power transmission of single SRR geometry. Result of T-EPA is compared with the MLFMA. Then, the relative error is plotted in Figure 5.13(b). Next, in Figure 5.14 power transmission of single SRR is demonstrated for different frequencies, by calculating at different points in the z=0 plane. As shown in the Figure 5.13(a), transmission drops at 97 GHz, significantly.

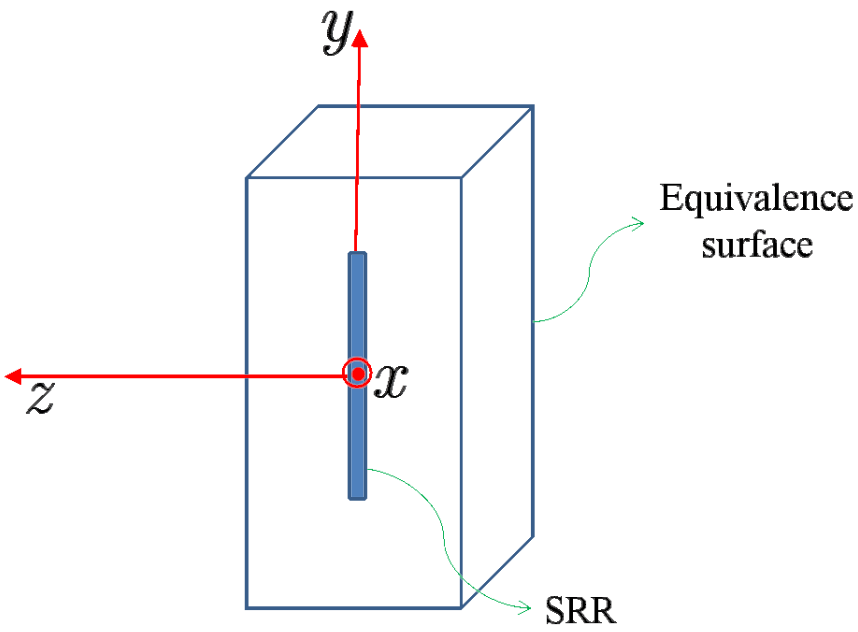

(a)

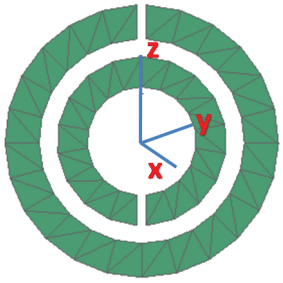

(b)

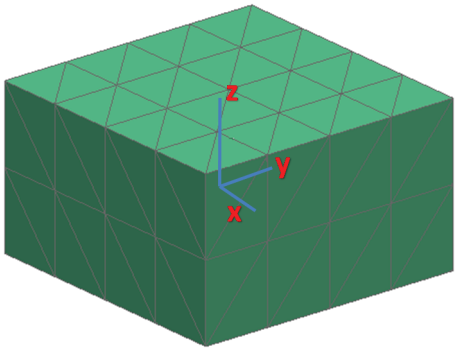

(c)

Figure 5.12: Details of the single SRR problem: (a) problem set-up, (b) SRR, and (c) equivalent surface.

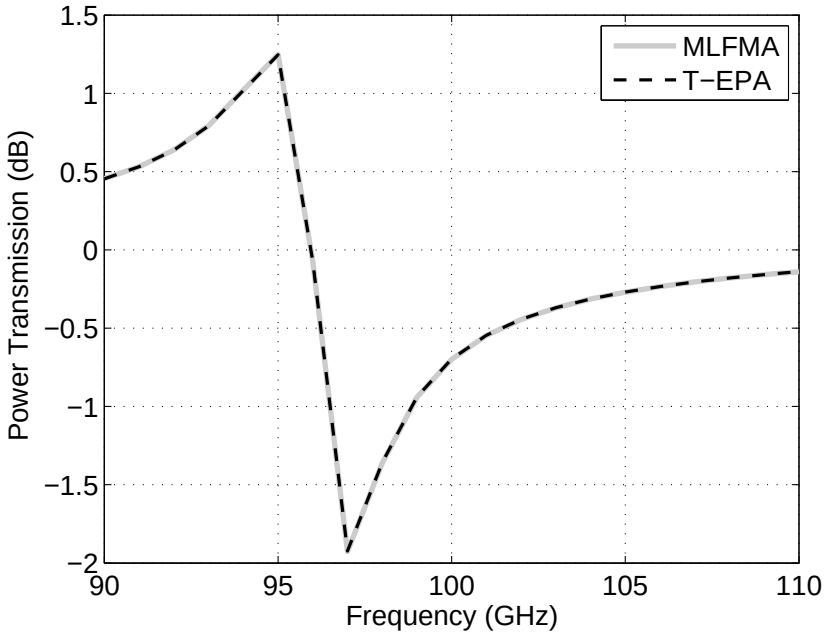

(a)

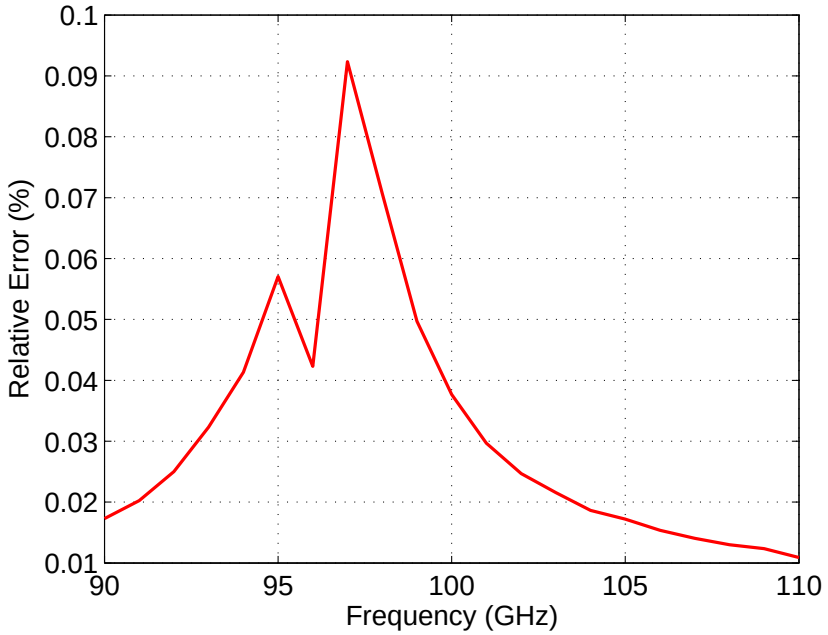

(b)

Figure 5.13: Power transmission of single SRR at $x = -1.2$ mm: (a) power transmission and (b) relative error.

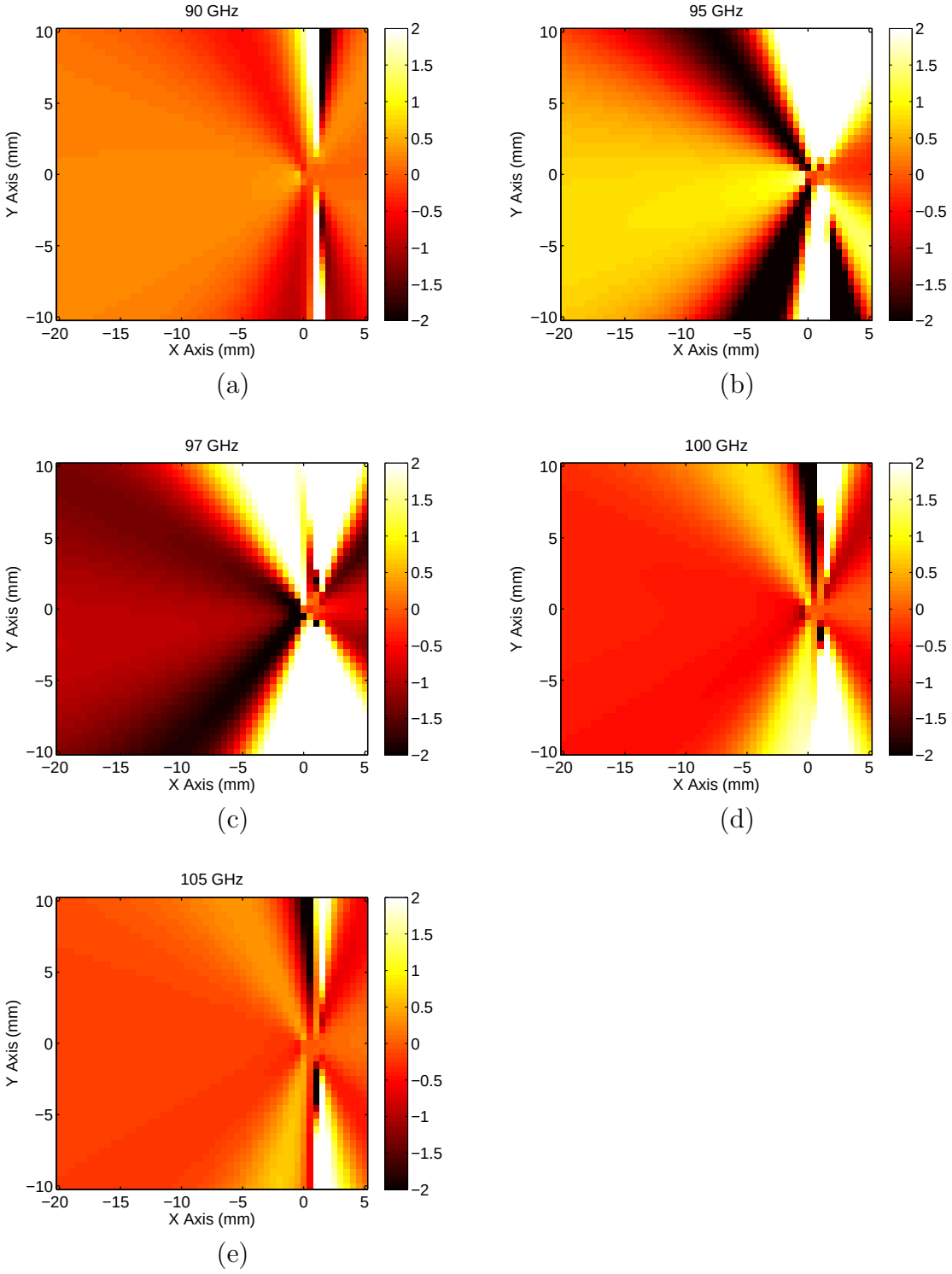

Figure 5.14: Power transmission of single SRR problem calculated at $z = 0$ plane for different frequencies: (a) 90 GHz, (b) 95 GHz, (c) 97 GHz, (d) 100 GHz, and (e) 105 GHz.

After solving single SRR problem accurately, problems that contain multiple SRRs are solved. First, 2×2 SRR wall is solved by using two ES, each of which contains two SRRs. Setup of the problem is shown in the Figure 5.15 and the result of power transmission is demonstrated in Figure 5.16.

Then, 6×6 and 10×10 SRR wall problems are solved. To solve 6×6 SRR problem, geometry is divided into three parts, so three ESs are used. Each of the ESs contain 2×6 SRR in it. Setup of the problem is illustrated in the Figure 5.17 and the result of power transmission is presented in Figure 5.18. Finally, to solve 10×10 SRR problem, geometry is divided into five parts, so five ESs are used. Each one contains 2×10 SRR in it. Figure 5.19 shows the setup of the problem, while the result of power transmission is presented in Figure 5.20.

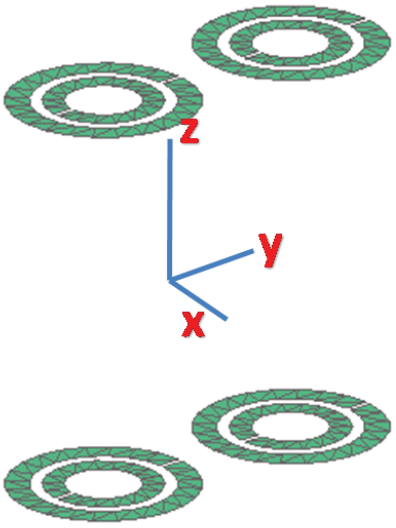

(a)

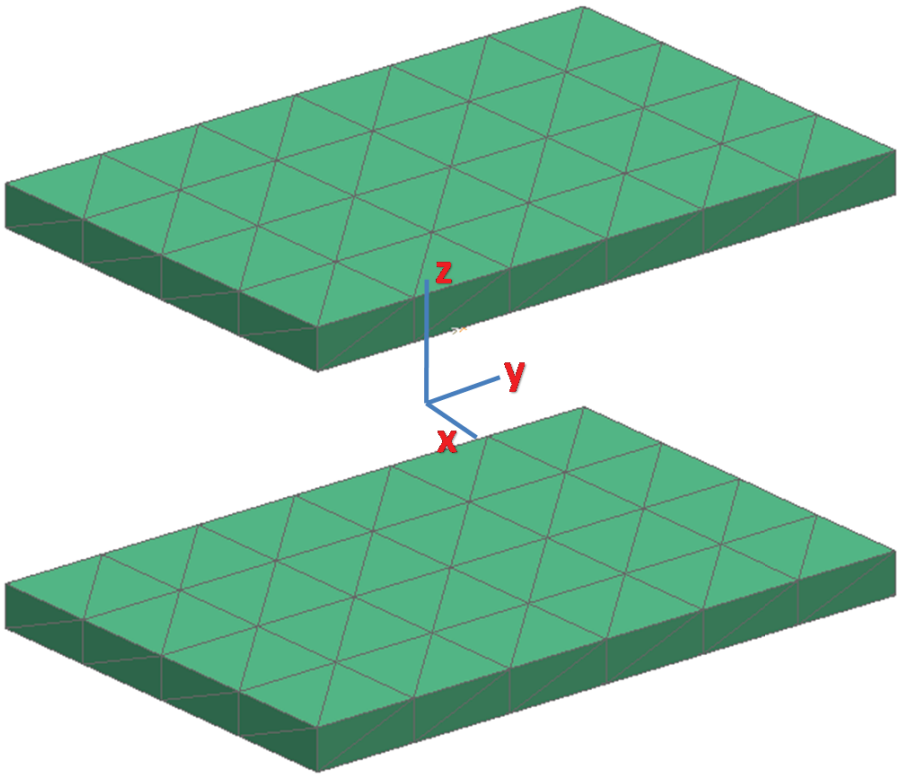

(b)

Figure 5.15: 2×2 SRR wall problem: (a) SRR wall and (b) equivalent surfaces.

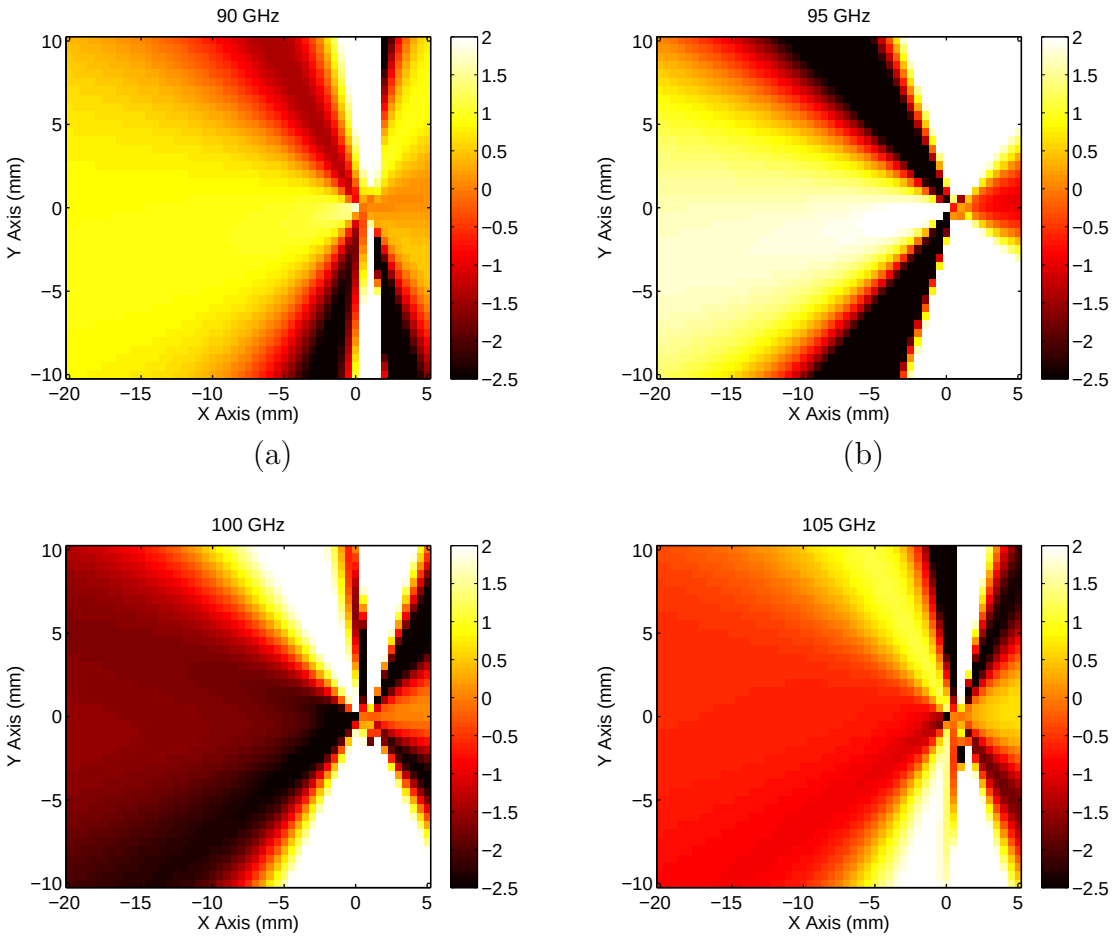

Figure 5.16: Power transmission of 2×2 SRR problem calculated at $z = 0$ plane for different frequencies: (a) 90 GHz, (b) 95 GHz, (c) 100 GHz, and (d) 105 GHz.

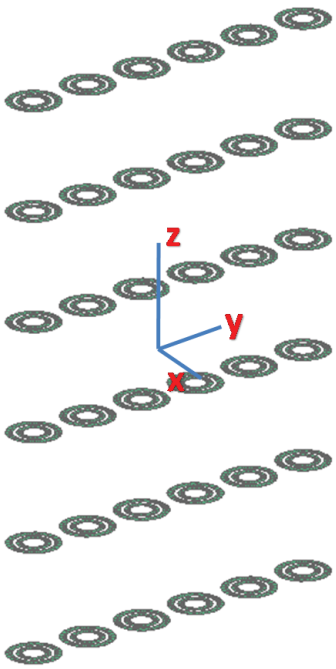

(a)

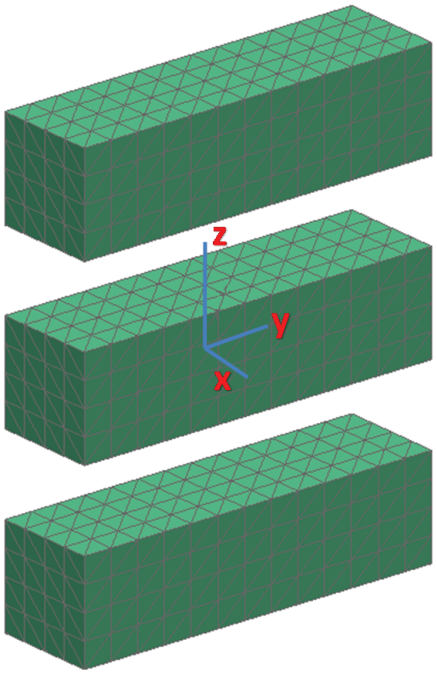

(b)

Figure 5.17: 6×6 SRR wall problem: (a) SRR wall and (b) equivalent surfaces.

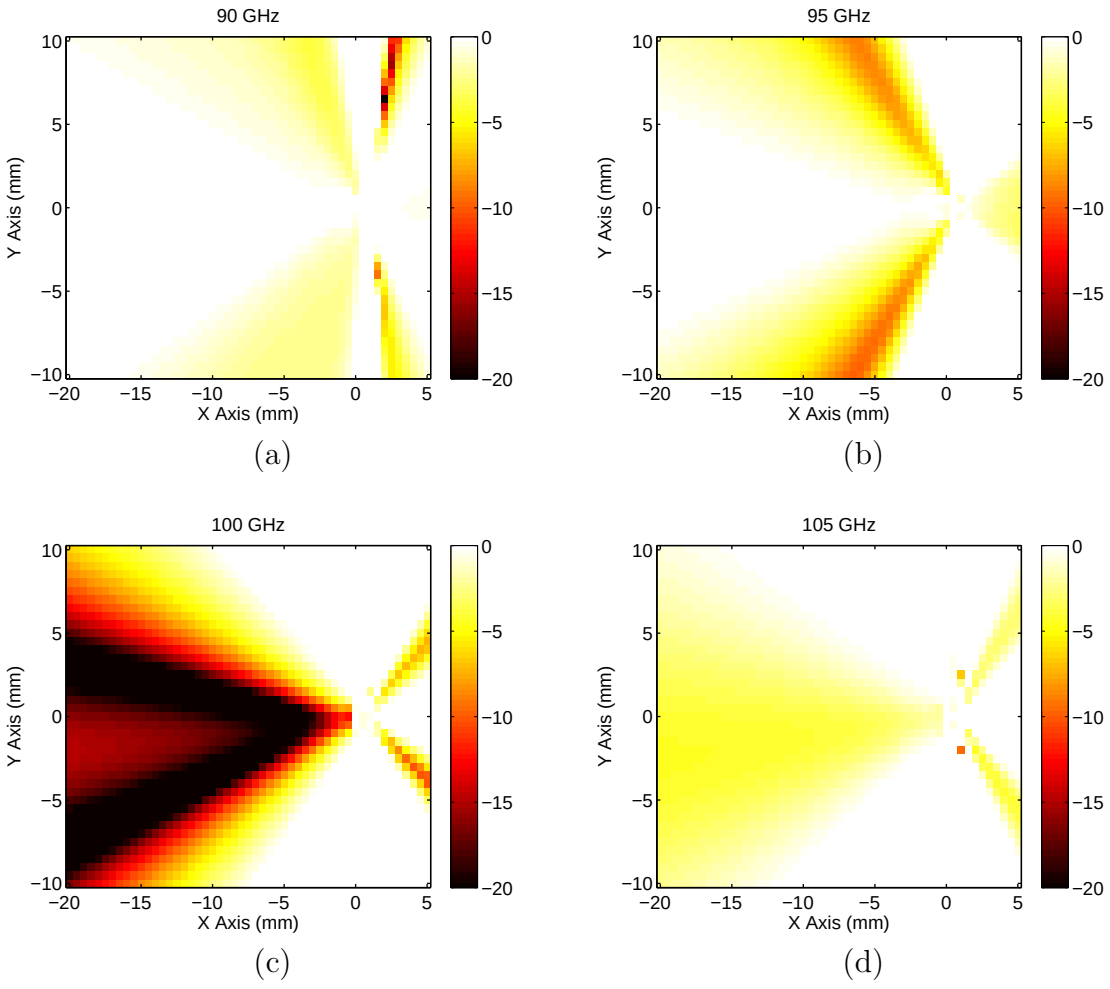

Figure 5.18: Power transmission of 6×6 SRR problem calculated at $z = 0$ plane for different frequencies: (a) 90 GHz, (b) 95 GHz, (c) 100 GHz, and (d) 105 GHz.

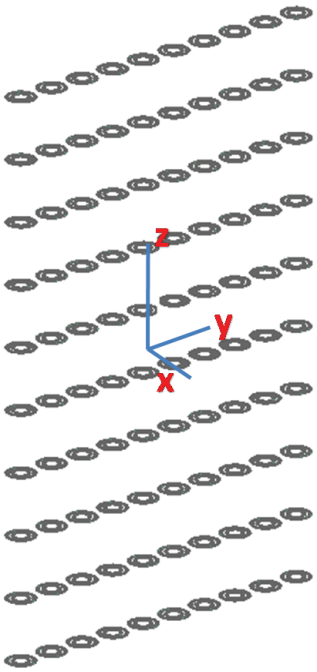

(a)

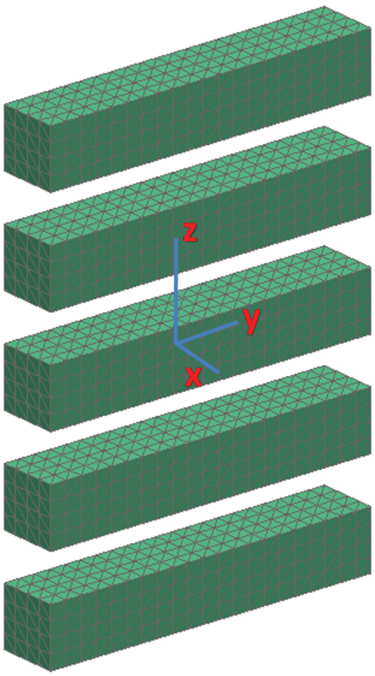

(b)

Figure 5.19: 10×10 SRR wall problem: (a) SRR wall and (b) equivalent surfaces.

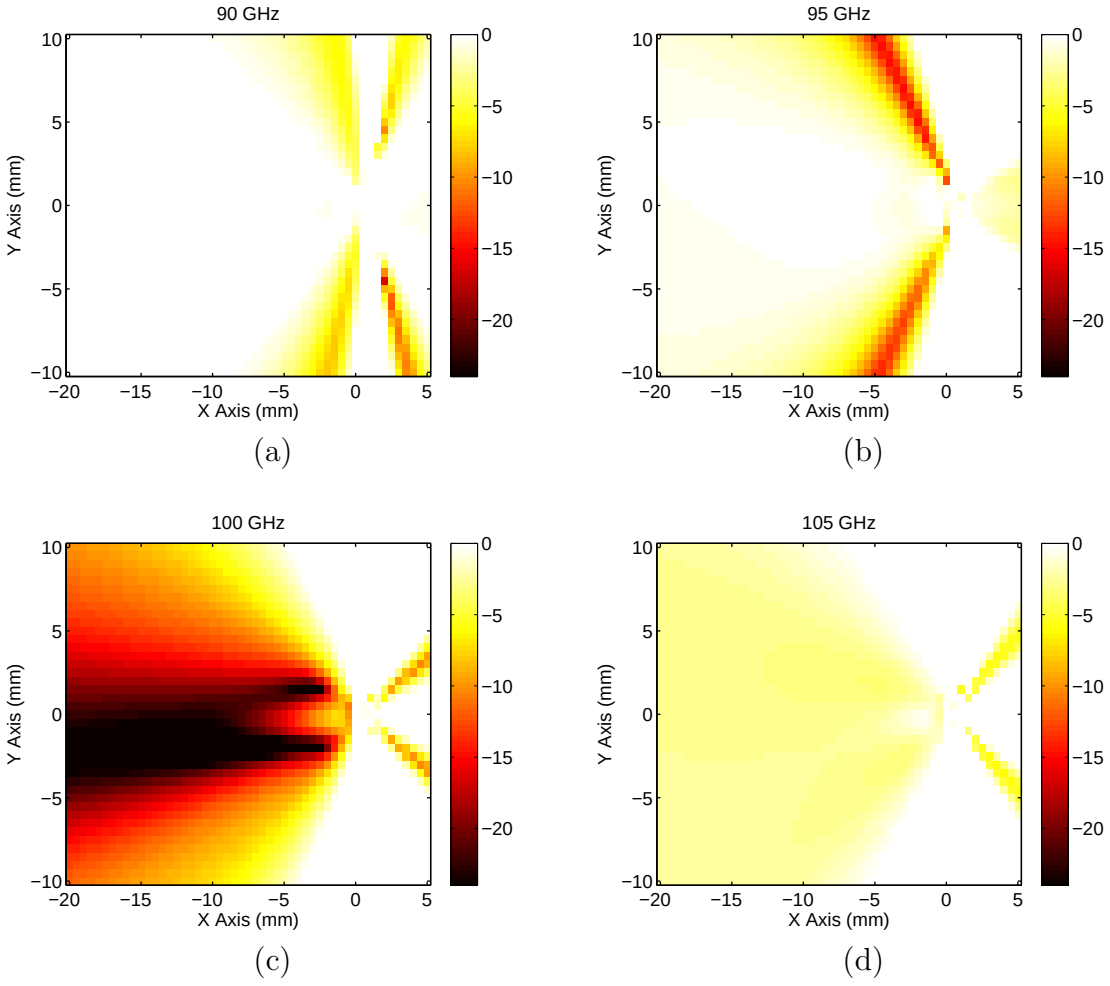

Figure 5.20: Power transmission of 10×10 SRR problem calculated at $z = 0$ plane for different frequencies: (a) 90 GHz, (b) 95 GHz, (c) 100 GHz, and (d) 105 GHz.

Next, we have investigated the solution efficiency of the algorithm. For this purpose, 3×9 SRR wall problem is solved by using three ESs. The number of iterations and the solution time of the problem for different frequencies are plotted in Figure 5.21. For the iterative solutions of the problem, we have considered preconditioners based on sparse approximate inverse (SAI) and block diagonal preconditioner (BDP) to obtain quick convergences of MLFMA. In Figure 5.21(a), number of iterations for T-EPA is compared with that of MLFMA, MLFMA-SAI, and MLFMA-BDP. It is seen that, number of iterations with MLFMA is very high. Moreover, The results show a similar increase on the number of iteration near 95 GHz as reported earlier in [46]. When we have applied BDP to MLFMA, iterations are dropped for some frequencies. However, they are still very high. As another alternative, we have applied SAI preconditioner to MLFMA. Then, the iterations dropped significantly. On the other hand, T-EPA is used to solve the same problem without preconditioning. We can see in Figure 5.21(a) that the number of iterations is very low, since T-EPA replaces the original ill-conditioned problems with the new well-conditioned ones.

T-EPA requires additional meshing, and composed of several surface operators, TO and EPO. Therefore, matrix system solved in T-EPA is much more complicated than those of MLFMA. The total processing time of T-EPA depend much on the construction of ESs. For example, by increasing the number of ESs both the solution accuracy and convergence of iterative solution decreases. Further, in Figure 5.21(b), it is shown that, T-EPA requires the minimum solution time among the presented results.

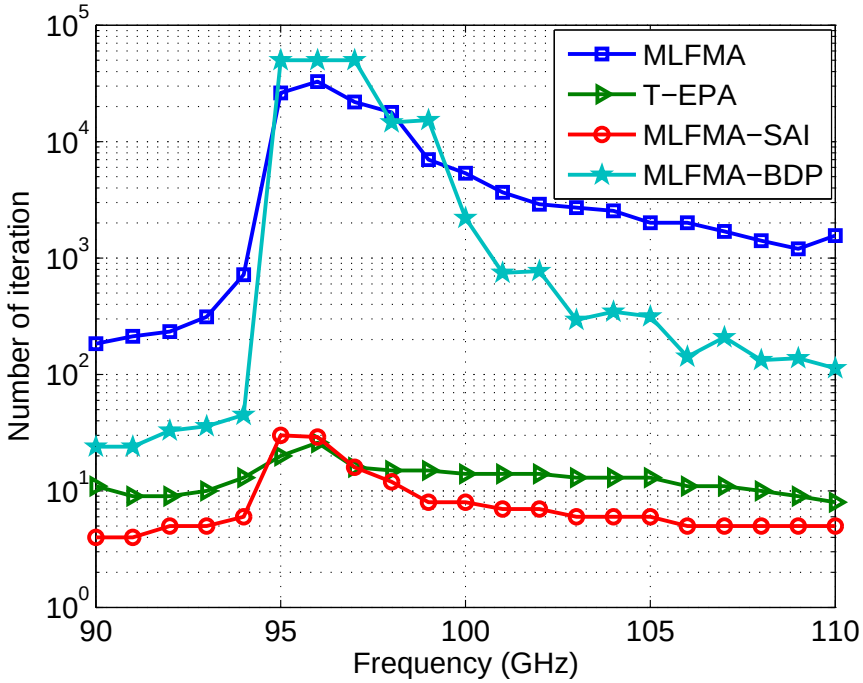

(a)

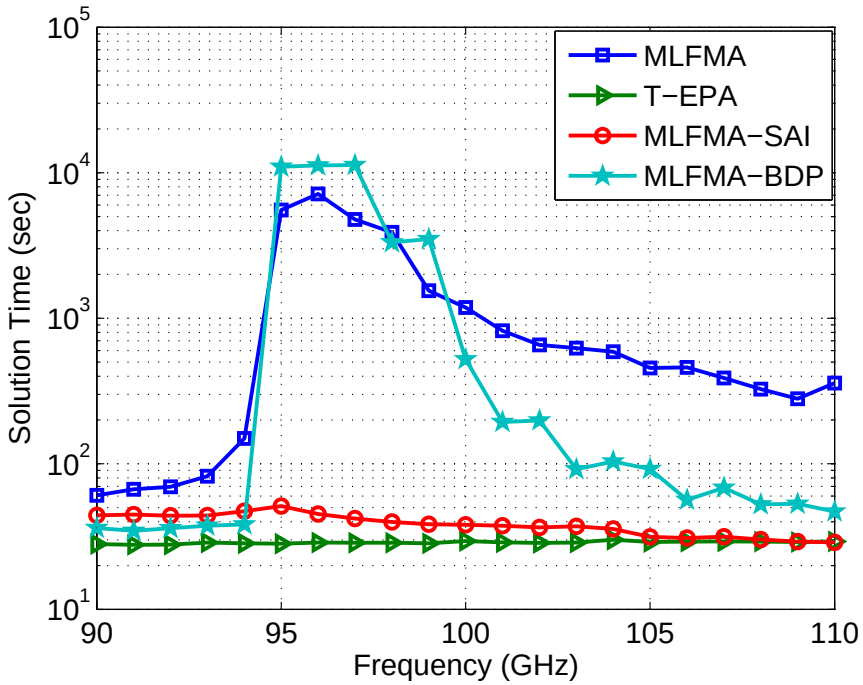

(b)

Figure 5.21: Efficiency of the algorithm: (a) number of iterations versus frequency and (b) solution time versus frequency.

Chapter 6

Conclusion

In this thesis, EPA and T-EPA are applied to solve EM scattering problems that contain PEC objects with arbitrary shapes. Properties of the algorithms are investigated and discussed in details. Numerical examples show that EPA leads to significant improvement on the conditioning of the matrix equation. Also, EPA loses its accuracy if ESs are very close to each other, or if an ES is very close to the PEC object. This problem is due to the presence of the identity operator in representing the surface currents in terms of the basis functions. As a remedy of this problem, tangential-EPA (T-EPA) is introduced. As a result, properties of both algorithms can be summarized as follows:

- The equivalent surfaces of EPA and T-EPA can be arbitrarily shaped,
- The scatterers that are enclosed by ES can be arbitrarily shaped,
- The scattering operator that electromagnetically characterizes a scattering domain encompasses the scattered field for all possible excitations,
- The interactions between ESs are mediated by transfer operators that depend only on the shape and relative position of ESs. Thus, they may be computed only once for a given spatial distribution,

- EPA and T-EPA are suitable for parallel computing, since the calculation of the transfer matrices involves just pairs of ESs at a time,
- EPA and T-EPA divides original problem into smaller subproblems by transforming the unknowns onto the ES. Since the current on the ES is usually much smoother than the currents on the surfaces of encapsulated parts, the number of unknowns on the final matrix equation can be lower than the original one,
- The method is well-suited and efficient for periodic structures with identical subproblems where the same scattering and translation operators can be used without recalculating them,
- By casting the equations into a single matrix equation, all interactions and scattering effects of the regions are taken into account simultaneously and hence iterative update of the solutions is not required,
- The method essentially improves the matrix conditioning compared to the straightforward MOM and MLFMA formulations,
- EPA and T-EPA are error controllable since the desired accuracy can be obtained by adjusting some parameters that are mentioned in Chapters 4 and 5.

Bibliography

[1] W. C. Chew, J.-M. Jin, E. Michielssen, and J. Song, *Fast and Efficient Algorithms in Computational Electromagnetics*. Boston: Artech House, 2001.

[2] P. Ylä-Oijala and M. Taskinen, "Electromagnetic scattering by large and complex structures with surface equivalence principle algorithm," *Waves in Random and Complex Media.*, vol. 19, no. 1, pp. 105–125, Feb. 2009.

[3] J. M. Song and W. C. Chew, "Multilevel fast multipole algorithm for solving combined field integral equations of electromagnetic scattering," *Microw. Opt. Technol. Lett.*, no. 10, pp. 14–19, 1995.

[4] J. M. Song, C. C. Lu, and W. C. Chew, "Multilevel fast multipole algorithm for electromagnetic scattering by large complex objects," *IEEE Trans. Antennas Propagat.*, no. 45, pp. 1488-1493, 1997.

[5] P. Ylä-Oijala, M. Taskinen and S. Järvenpä, "Surface integral equation formulations for solving electromagnetic scattering problems with iterative methods," *Radio Sci.*, 40, 2005. doi: 10.1029/2004RS003169.

[6] T. W. Lloyd, J. M. Song, G. Kang, and C.-C. Lu, "Numerical study of surface integral formulations for low-contrast objects, *IEEE Antennas Wireless Propag. Letters*, vol. 4, pp. 482–485, 2005.

[7] Ö. Ergül and L. Gürel, "Comparison of integral-equation formulations for the fast and accurate solution of scattering problems involving dielectric objects with the multilevel fast multipole algorithm," *IEEE Trans. Antennas Propagat.*, vol. 57, no. 1, pp. 176–187, Jan. 2009.

[8] K. Sertel and J. L. Volakis, "Incomplete LU preconditioner for FMM implementation," *Microwave Opt. Tech. Lett.*, vol. 26, no. 4, pp. 265–267, 2000.

[9] J. Lee, J. Zhang, and C. C. Lu, "Incomplete LU preconditioning for large scale dense complex linear systems from electromagnetic wave scattering problems," *J. Comput. Phys.*, vol. 185, pp. 158–175, 2003.

[10] B. Carpentieri, "Fast iterative solution methods in electromagnetic scattering," *Progress In Electromagnetics Research*, vol. 79, 151–178, 2008.

[11] T. Malas, Ö. Ergül, and L. Gürel, "Effective preconditioners for large integral-equation problems," *European Conference on Antennas and Propagation (EuCAP 2007)*, Edinburgh, UK, Nov. 2007.

[12] T. Malas and L. Gürel, "Incomplete LU preconditioning with multilevel fast multipole algorithm for electromagnetic scattering," *SIAM J. Scientific Computing*, vol. 29, no. 4, 1476–1494, 2007.

[13] R. Kornhuber, Ed., Domain Decomposition Methods in Science and Engineering, ser. Lecture notes in computational science and engineering. Berlin, Germany: Springer, vol. 40, 2005.

[14] B. Butrylo, F. Musy, L. Nicolas, R. Perrussel, R. Scorretti, and C. Vollaire, "A survey of parallel solvers for the finite element method in computational electromagnetics," *COMPEL*, vol. 23, no. 2, pp. 531–546, 2004.

[15] Y. Lu and C. Y. Shen, "A domain decomposition finite-difference method for parallel numerical implementation of time-dependent Maxwell's equations," *IEEE Trans. Antennas Propag.*, vol. 45, no. 3, pp. 556–562, Mar. 1997.

[16] B. Stupfel and M. Mognot, "A domain decomposition method for the vector wave equation," *IEEE Trans. Antennas Propag.*, vol. 48, no. 5, pp. 653–660, May 2000.

[17] M. N. Vouvakis and J. F. Lee, "A finite element domain decomposition technique for the analysis of large electromagnetic problems," in *Proc. Antennas and Propagation Society Int. Symp.*, vol. 1A, pp. 168–171, Jul. 2005.

[18] H. Rogier, D. D. Zutter, and F. Olyslager, "Rigorous analysis of frequency selective surfaces of finite extent using a hybrid finite difference time domain-boundary integral equation technique," *Radio Sci.*, vol. 35, no. 2, pp. 483–494, Apr. 2000.

[19] S. A. Schelkunoff, "Some equivalence theorems of electromagnetics and their application to radiation problems," *Bell System Tech. J.*, vol. 15, pp. 92–112, 1936.

[20] C. Huygens, *Traite de la Lumiere*, Leyeden, 1690. Translated into English by S. P. Thompson and reprinted by the University of Chicago Press, London, 1912.

[21] J. D. Kraus and K. R. Carver, *Electromagnetics*, Second Edition, McGraw-Hill, New York, pp. 464–467, 1973.

[22] R. F. Harrington, *Time-Harmonic Electromagnetic Fields*, McGraw-Hill, New York, 1961.

[23] N. Morita, N. Kumagai, and J. R. Mautz, *Integral Equation Methods for Electromagnetics.* Boston: Artech House, 1990.

[24] A. J. Poggio and E. K. Miller, "Integral equation solutions of three-dimensional scattering problems," in *Computer Techniques for Electromagnetics*, R. Mittra, Ed. Oxford: Pergamon Press, Chap. 4, 1973.

[25] J. R. Mautz and R. F. Harrington, "H-field, E-field, and combined field solutions for conducting bodies of revolution," *AEÜ*, vol. 32, no. 4, pp. 157–164, Apr. 1978.

[26] L. Gürel, K. Sertel, and İ. K. Şendur, "On the choice of basis functions to model surface electric current densities in computational electromagnetics," *Radio Sci.*, vol. 34, no. 6, pp. 1373–1387, Nov.-Dec. 1999.

[27] R. F. Harrington, *Field Computation by Moment Methods*. New York: Macmillan, 1968.

[28] L. Gürel and Ö. Ergül, "Comparisons of FMM implementations employing different formulations and iterative solvers," in *Proc. IEEE Antennas and Propagation Soc. Int. Symp.*, vol. 1, pp. 19–22, 2003.

[29] Ö. S. Ergül, Fast multipole method for the solution of electromagnetic scattering problems, M. S. Thesis, Bilkent University, Ankara, Turkey, Jun. 2003.

[30] S. M. Rao, D. R. Wilton, and A. W. Glisson, "Electromagnetic scattering by surfaces of arbitrary shape," *IEEE Trans. Antennas Propag.*, vol. 30, no. 3, pp. 409–418, May 1982.

[31] L. Gürel and Ö. Ergül, "Singularity of the magnetic-field integral equation and its extraction," *IEEE Antennas Wireless Propag. Lett.*, vol. 4, pp. 229-232, 2005.

[32] R. D. Graglia, "On the numerical integration of the linear shape functions times the 3-D Green's function or its gradient on a plane triangle," *IEEE Trans. Antennas Propag.*, vol. 41, no. 10, pp. 1448–1455, Oct. 1993.

[33] P. Ylä-Oijala and M. Taskinen, "Calculation of CFIE impedance matrix elements with RWG and $\hat{\boldsymbol{n}}\times$RWG functions," *IEEE Trans. Antennas Propag.*, vol. 51, no. 8, pp. 1837–1846, Aug. 2003.

[34] D. A. Dunavant, "High degree efficient symmetrical Gaussian quadrature rules for the triangle," *Int. J. Numer. Meth. Eng.*, vol. 21, pp. 1129–1148, 1985.

[35] J. R. Mautz and R. F. Harrington, "An E-field solution for a conducting surface small or comparable to the wavelength," *IEEE Trans. Antennas Propag.*, vol. 32, no. 4, pp. 330–339, Apr. 1984.

[36] J.-S. Zhao and W. C. Chew, "Integral equation solution of Maxwells equations from zero frequency to microwave frequencies," *IEEE Trans. Antennas Propag.*, vol. 48, no. 10, pp. 330–339, Oct. 2000.

[37] M-K. Li and W. C. Chew, "Multiscale simulation of complex structures using equivalence principle algorithm with high-order field point sampling scheme," *IEEE Trans. Antenn. Propag.*, vol. 56, pp. 2389–2397, 2008.

[38] Ö. Ergül and L. Gürel, "Contamination of the accuracy of the surface integral equations with the discretization error of the identity operator," *in Proc. Int. Workshop on Electromagnetic Wave Scattering (EWS)*, pp. 6.16.12, 2008.

[39] M. K. Li, W. C. Chew, and L. J. Jiang, "A domain decomposition scheme based on equivalence theorem, *Microw. Opt. Technol. Lett.*, vol. 48, issue 9, pp. 1863–1857, Sept. 2006.

[40] Ö. Ergül and L. Gürel, "Stabilization of integral-equation formulations for the accurate solution of scattering problems involving low-contrast dielectric objects," *IEEE Trans. Antennas Propagat.*, vol. 56, pp. 799–805, 2008.

[41] W.C. Chew, *Waves and Fields in Inhomogeneous Media*, IEEE Press, New York, 1995.

[42] P. Ylä-Oijala, M. Taskinen, and S. Järvenpää, "Analysis of surface integral equations in electromagnetic scattering and radiation problems," *Eng. Anal. Boundary Elem.*, vol. 32, no. 3, pp. 196–209, Mar. 2008.

[43] D. R. Wilton and J. E. Wheeler III, "Comparison of convergence rates of the conjugate gradient method applied to various integral equation formulations," *Prog. Electromagn. Res.*, pp. 131–158, 1991.

[44] C. P. Davis and K. F. Warnick, "High-order convergence with a low-order discretization of the 2-D MFIE," *IEEE Antennas Wireless Propag. Lett.*, vol. 3, pp. 355–358, 2004.

[45] L. Gürel, Ö. Ergül, A. Ünal, and T. Malas, "Fast and accurate analysis of large metamaterial structures using the multilevel fast multipole algorithm," *Prog. Electromagn. Res.*, PIER 95, pp. 179–198, 2009.

[46] Ö. Ergül, A. Ünal, and L. Gürel, "Accurate modeling of metamaterials with MLFMA," *European Conference on Antennas and Propagation (EuCAP 2006)*, Nice, France, Nov. 2006.